

Alma Mater Studiorum – Università di Bologna

DOTTORATO DI

RICERCA IN CHIMICA

Ciclo XXXV

Settore Concorsuale: 03/A1 Chimica Analitica

Settore Scientifico disciplinare: CHIM/01 Chimica Analitica

***Development of effect-based bio-chemiluminescent
cell bioassays for nutraceutical and biomedical
applications***

Presentata da: Angela Punzo

Coordinatore Dottorato:

Prof. Luca Prodi

Supervisore:

Prof.ssa Barbara Roda

Co-Supervisore:

Prof.ssa Cristiana Caliceti

**Esame finale
anno 2023**

Abstract

Health monitoring using whole-cell bioassays has recently fascinated public interest and the scientific community. Several whole cell-based biosensors have been described in the literature for the last 20 years and these reports have revealed great potential for their use in different areas such as nutraceuticals and biomedical diagnostics. Moreover, the use of human cells as sensing elements offers unique features, providing more predictive information about human effects (e.g., detection of unclassified compounds and synergistic effects, information about the bioavailable concentration).

The activity carried out during my Ph.D. was mainly focused on the development and optimization of effect-based bio-chemiluminescent cell bioassays for biomedical and nutraceutical applications. In particular, a rapid and simple all-in-one effect-based chemiluminescent bioassay which relies on an adamantylidene - 1,2 - dioxetane probe for the selective detection of intracellular H_2O_2 in human living cells was developed. H_2O_2 is an unavoidable by-product of cell metabolism and when its production is not properly balanced it can lead to chronic pathologies. The use of the conventional chemiluminescent system based on luminol-HRP with even higher detectability allow to not selectively detect intracellular H_2O_2 but in the cell cultures supernatant, thus limiting the analytical information and in addition requiring several steps. For this reason, the extreme simplicity of our method, its high selectivity, low detection limit, and ability to cross cell membranes make the probe suitable to be employed for the quantification of intracellular H_2O_2 in different living human cell type exposed to different pro-oxidant stimuli. The final goal of the bioassay developed during the first two years of my Ph.D. was its application for the screening of antioxidant activity of nutraceuticals and for monitoring the intracellular H_2O_2 production in peripheral blood mononuclear cells (PBMCs) from hypercholesterolemic subjects before and after two months treatment with Evolocumab, a new generation LDL-cholesterol lowering drug.

Moreover, a recombinant bioluminescent protein was developed during the last year using the Baculovirus expression system in insect cells. In particular,

the protein combines the extracellular domain (ECD) of the Notch high affinity mutated form of one of the selective Notch ligands defined as Jagged 1 (Jag1) with a red emitting firefly luciferase since a pivotal role of “aberrant” Notch signaling activation in colorectal cancer (CRC) was reported. The probe was validated and characterized in terms of analytical performance and through imaging experiments, in order to understand if Jagged1-FLuc binding correlates with a Notch signaling overexpression and activation in CRC progression.

Index

CHAPTER ONE

<i>Introduction</i>	11
1.1 Whole cell-based biosensors	12
1.2 Recombinant DNA technology and protein expression	15
1.2.1 Recombinant fusion proteins	18
1.2.2 Baculovirus expression system	20
1.3 Chemical luminescence as the detection strategy	21
1.3.1 Bioluminescence	22
1.3.2 Chemiluminescence	26
1.3.3 Chemiluminescent systems for the evaluation of living cells intracellular biomarkers.....	29
1.4 References	33

CHAPTER TWO

<i>Aim of the Thesis</i>	45
---------------------------------------	----

CHAPTER THREE

Selective chemiluminescent TURN-ON quantitative bioassay and imaging of intracellular hydrogen peroxide in human living cells

3.1 Introduction	50
3.2 Material and Methods	53
3.2.1 Chemicals	53
3.2.2 Plant material.....	54

3.2.3 Cell cultures	54
3.2.4 Cytotoxicity assay	55
3.3 Bioassay Procedure	55
3.3.1 Principle of the bioassay	55
3.3.2 Calibration curve for quantification of H ₂ O ₂	56
3.3.3 Quantification of intracellular H ₂ O ₂ in human living cells.....	57
3.3.4 Method validation.....	57
3.3.5 Assay for antioxidant activity in human living cells	57
3.3.6 Chemiluminescence imaging experiments.....	58
3.3.7 Data analysis	58
3.4 Results and Discussion	59
3.4.1 Quantitative detection of H ₂ O ₂ in cell-free system	59
3.4.2 Quantification of intracellular H ₂ O ₂ in human living cells.....	60
3.4.3 Method validation.....	64
3.4.4 Cell-based assay for antioxidant activity	65
3.5 Conclusions	67
3.6 Acknowledgments	68
3.7 References	69
3.8 Supplementary Material	74
3.8.1 Extracts of Brassicaceae	74
3.8.2 Glucosinolate and isothiocyanate analysis	74
3.8.3 Bioassay procedure in Caco-2 cells in the presence of a NOS inhibitor	75
3.8.4 Results.....	75
3.8.4.1 Characterization of plant extracts	75

3.8.4.2 Quantification of intracellular H ₂ O ₂ in Caco-2 human living cells in the presence of a NOS inhibitor.....	76
3.8.5 References.....	78

CHAPTER FOUR

Grape pomace for topical application: Green NaDES sustainable extraction, skin permeation studies, antioxidant and anti-inflammatory activities characterization in 3D human keratinocytes

4.1 Introduction	80
4.2 Material and Methods.....	82
4.2.1 Chemicals	82
4.2.2 Red pomace materials and extracts	83
4.2.3 HPLC-ESI-MS/MS method	83
4.2.4 <i>Ex Vivo</i> permeation study by Franz diffusion cells.....	84
4.2.5 3D Keratinocyte cell model	85
4.2.6 Quantification of intracellular H ₂ O ₂ in 3D HaCaT cells.....	86
4.2.7 Antioxidant activity of red pomace extracts in HaCaT spheroids	86
4.2.8 Cell cytotoxicity: lactate dehydrogenase release	87
4.2.9 Spectrophotometric cell viability bioassay.....	87
4.2.10 Protein release.....	88
4.2.11 Statistical analysis.....	88
4.3 Results and Discussion.....	89
4.3.1 Extraction and characterization of anthocyanins in NaDES extracts	89

4.3.2 Skin permeation of anthocyanins derived from NaDES extracts.....	91
4.3.3 Safety of NaDES extracts <i>in vitro</i> in human 3D keratinocytes	92
4.3.4 Evaluation of intracellular H ₂ O ₂ production in human 3D keratinocytes	94
4.3.5 Antioxidant activity of NaDES extracts toward human HaCaT spheroids	95
4.3.6 Protective effects of NaDES extracts on HaCat spheroids in the presence of the cytotoxic agent menadione.....	96
4.4 Conclusions.....	98
4.5 Acknowledgments	99
4.6 References.....	100
4.7 Supplementary Material.....	105

CHAPTER FIVE

Fermentation of Vaccinium floribundum berries with Lactiplantibacillus plantarum reduces oxidative stress in endothelial cells and modulates macrophages function

5.1 Introduction	107
5.2 Material and Methods.....	109
5.2.1 Reagents	109
5.2.2 Pushgay berries fermentation	110
5.2.3 Preparation of Pushgay berries solutions	111
5.2.4 Evaluation of total phenolic content	111
5.2.5 HPLC-ESI-MS/MS analysis	111
5.2.6 Cell culture.....	112
5.2.7 Cell viability and proliferation assays	113

5.2.8 Cytotoxicity	114
5.2.9 RNA extraction.....	114
5.2.10 Reverse Transcriptase-Quantitative PCR	114
5.2.11 Antioxidant activity of berries solution	115
5.2.12 Preparation of cell lysates for enzymatic assay	116
5.2.13 Glutathione Reductase (GR) activity assay	116
5.2.14 Glutathione Peroxidase (Gpx) activity assay	116
5.2.15 Catalase (CAT) activity assay.....	117
5.2.16 Superoxide Dismutase (SOD) activity assay	117
5.2.17 Statistical analysis.....	117
5.3 Results	117
5.3.1 Content of polyphenols in berries solutions	117
5.3.2 Cytotoxicity of berries solutions in HUVECs	119
5.3.3 Effect of the fermentation of Pushgay Berries on antioxidant activity in HUVECs	120
5.3.4 Effect of fermentation of Pushgay berries on H ₂ O ₂ -Induced cell mortality in HUVECs	121
5.3.5 Effect of fermentation of Pushgay berries on HO-1 expression in H ₂ O ₂ - treated HUVECs	122
5.3.6 Effect of treatment with fermented Pushgay berries on glutathione reductase activity in HUVECs.....	122
5.3.7 Effect of treatment with Pushgay berries on RAW264.7 cells proliferation	123
5.3.8 Effect of fermentation of Pushgay berries on RAW264.7 cells growth	124
5.3.9 Effects of Pushgay berries on the expression of iNOS and TNF α in	

RAW264.7 cells	125
5.4 Discussion	126
5.5 Conclusions.....	130
5.6 Acknowledgments	130
5.7 References.....	131

CHAPTER SIX

Treatment with PCSK9 inhibitor Evolocumab improves vascular oxidative stress and arterial stiffness in hypercholesterolemic patients with high cardiovascular risk

6.1 Introduction	142
6.2 Material and Methods.....	145
6.2.1 Chemicals	145
6.2.2 Study population	145
6.2.3 Treatment	146
6.2.4 Assessments	146
6.2.4.1 Clinical Assessments.....	146
6.2.4.2 Clinical chemistry analyses	146
6.2.4.3 Blood pressure measurements.....	146
6.2.4.4 Non-invasive vascular tests.....	147
6.2.5 H ₂ O ₂ bioassay procedure.....	148
6.2.5.1 PBMCs collection	148
6.2.5.2 Quantification of intracellular H ₂ O ₂ in PBMCs	148
6.2.6 Cell viability assay.....	149

6.2.7 Data analysis	149
6.3 Results and Discussion	150
6.3.1 Evolocumab treatment decreases intracellular H ₂ O ₂ production in PBMCs	151
6.3.2 Arterial stiffness improvement in Evolocumab- treated patients in association with Ezetimibe and Ezetimibe+ statin	153
6.3.3 H ₂ O ₂ decrease correlates with arterial stiffness improvement	155
6.4 Conclusions.....	156
6.5 Acknowledgements	157
6.6 References.....	158
6.6 Supplementary Material.....	165

CHAPTER SEVEN

Jagged1-Fluc: a bioluminescent recombinant protein as potential diagnostic tool for the high- throughput screening of colorectal cancer

7.1 Introduction	167
7.2 Material and Methods.....	169
7.2.1 Reagents and kits	169
7.2.2 Fusion gene design, transformation, and protein expression.....	170
7.2.3 Study population	170
7.2.4 Insect cell culture	171
7.2.5 Human cell culture	172
7.2.6 Calibration curve of Jag1-Fluc in a cell-free system	172

7.2.7 Cell-based calibration curve of Jag1-Fluc in fixed and living human colorectal adenocarcinoma cells (Caco-2).....	173
7.2.8 Jag1-Fluc selectivity vs Notch receptors in fixed cells	173
7.2.9 <i>In vitro</i> Cell-based imaging	174
7.2.10 Bioluminescence imaging (BLI) on <i>ex-vivo</i> human biopsies	174
7.2.11 Data analysis	175
7.3 Results and Discussion	175
7.3.1 Characterization of Jag1-Fluc light output in a cell-free system.....	175
7.3.2 Evaluation of Jag1-Fluc BL emission in fixed and living human colorectal adenocarcinoma cells (Caco-2)	176
7.3.3 Human soluble Jagged 1 chimera as competitor of Notch receptors in Caco-2 and MCF-7.....	177
7.3.4 BL imaging on fixed Caco-2 cells.....	178
7.3.5 <i>Ex vivo</i> BLI: Jag1-Fluc binding on human tissue	179
7.4 Conclusion	180
7.5 References	181
7.5 Supplementary Material	185

1

Introduction

1.1 Whole cell-based biosensors

A biosensor is an analytical device able to specifically detect analytes in many biological fluids including cells or tissues, combining biological recognition elements such as antibodies, enzymes, or engineered cells, with a physical transducer in contact with the recognition element. In this way, we can achieve the analytical signal using a compact and portable device.

(Fig.1.1) [1]. Due to the cross-disciplinary nature of their development, several fields of research such as biology, chemistry, physics, and information science are usually involved [2,3]. Whole-cell biosensors, relying on living cells as sensing elements, can quantitatively detect information concerning the status of a given biological structure such as 'living cells' status, by converting signals that are part of their homeostasis, into electrical or optical outputs [4]. Biosensors have rapidly expanded taking advantage of novel nano-microfabrication and immobilization techniques, and these recent changes have provided these types of whole-cell bioassays with unique and unexploited advantages compared to conventional biosensors [5]. Some of the major advantages of whole-cell-based biosensors are [6]:

- versatility (cells can be genetically engineered to express a specific biorecognition element for various analytes classes);
- measurement of bioavailable fraction (only specific signaling pathways are activated by the analyte fraction able to enter into living cells);
- provide functional information about general toxicity, synergic effects, pharmacology, and physiology;
- rapidity and high sensitivity;
- high predictability about human effects.

Several cell-based bioassays have been reported over the years, but few of them can be considered true biosensors according to the IUPAC definition as "integrated receptor-transducer devices, which are able to provide selective quantitative or semi-quantitative analytical information using a biological recognition element" [7]. Indeed, sometimes whole cell biosensors are not stand-alone integrated receptor-transducer devices due to the need for checking cell

growth, sterility, and particular storage conditions.

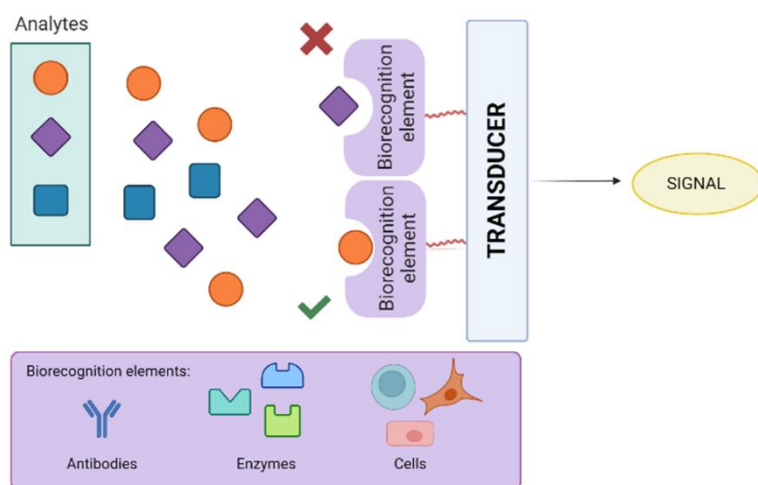


Figure 1.1: Schematic representation of a biosensor with some examples of the most adopted biorecognition elements (e.g., antibodies, enzymes, and cells).

Yeast, bacteria, and mammalian cell lines have been widely adopted for whole-cell bioassays application. The bioluminescent microorganism *Aliivibrio fischeri* was first described as part of a whole-cell biosensor because of its easy cultivation and integration with a transducer [8]. Biosensors based on yeast cells present the same advantages as bacterial biosensors but with an increased predictivity, due to the similarities of cellular processes and molecular pathways with human cells [9]. However, mammalian cells are the best choice when predictive information about bioactivity or toxicity to humans is required [10]. The main issues regarding the performance of a whole-cell biosensor are related to their limited stability and shelf-life due to the complexities of keeping cells alive and responsive for a long time. The production of cells in a ready-to-use format is the final goal in this research field. Particularly, the possibility of storing cells for a long period of time, under monitored conditions, and activating them at the time needed are important problems to solve in the near future [11].

Appropriately designed, the *in vitro* whole-cell bioassays can help to predict the effects *in vivo* and can provide significant biochemical and pharmacological insights that are not possible in a whole animal study. The evident advantages of whole cell-based bioassays have led to their successful application in many fields such as food analysis, environmental monitoring, drug screening, and medical

diagnostics [12,13]. The new biomedical sensor technologies development at molecular and cellular levels has become important for the diagnosis of several diseases, ranging from pathogen detection to precise molecular tools used in early-stage cancer and genetic diseases diagnosis. Indeed, cellular receptors, ion channels, enzymes, or other intracellular molecules can be used as targets for biological analytes [14]. Thus, whole cell-based biosensors can measure functional information and the effects of the analyte on the physiological function of living cells. Parameters can include the determination of the impact of a compound or drug composition on the physiological system, the inhibition or promotion effect relative to a given receptor, and other influences that the analyte might have on the cell's metabolism (such as secondary messengers and their enzymes), the toxicity and the side effects of the tested substances on cells [10]. Whole cell-based biosensors have consequently emerged as a dynamic tool for qualitative and quantitative analysis of different analytes for clinical diagnosis.

In this context, 3D cell-based biosensors have gained increased interest thanks to the possibility to achieve more physiologically relevant information, and more predictive data for *in vivo* tests to better mimic cell interactions [15]. Cells grown in 3D culture can be combined with a biosensor either by direct attachment into a biotic or abiotic substrate surface or by indirect attachment via entrapment in a biocompatible material [16]. The versatility of 3D cell culture systems gives them a plethora of possible biomedical and bioanalytical applications, including early detection and chronic management of illness, cancer cell biology and tissue engineering, pathogen testing, toxicology assays, and drug screening [17,18]. Nowadays, 3D cell cultures should be considered as the necessary step between the conventional two-dimensional (2D) monolayer cell culture and animal models. Given their simplicity, rapidity, and cost-effectiveness, 2D cell-based assays allow to avoid large-scale and cost-intensive animal testing and are one of the most attractive bioanalytical tools for the drug discovery procedure. Indeed, due to different morphology and functionality, 2D cell assays may sometimes provide a distorted and non-predictive reaction to drugs and misleading information about *in vivo* response. For these reasons, this kind of test must be necessarily integrated with more predictive tests on animals [19,20]. 3D cell models due to their

improved cell-cell interactions, the variety of cell populations, and structures that resemble or mimic the *in vivo tissue* architecture, are capable of bridging the gap between 2D cell culture models and whole-animal systems [21].

The principle at the basis of 3D structured spheroids formation is self-assembly [22]. Cell cultures with this structure exhibit improved cell viability and stable morphology [23]. For biosensor applications, the selection of a proper matrix is crucial due to the variety of cell lines. Indeed, advances in synthetic-biologic matrices allowed to design of various natural or synthetic hydrogels in order to obtain different 3D cell models (**Fig. 1.2**) [24].

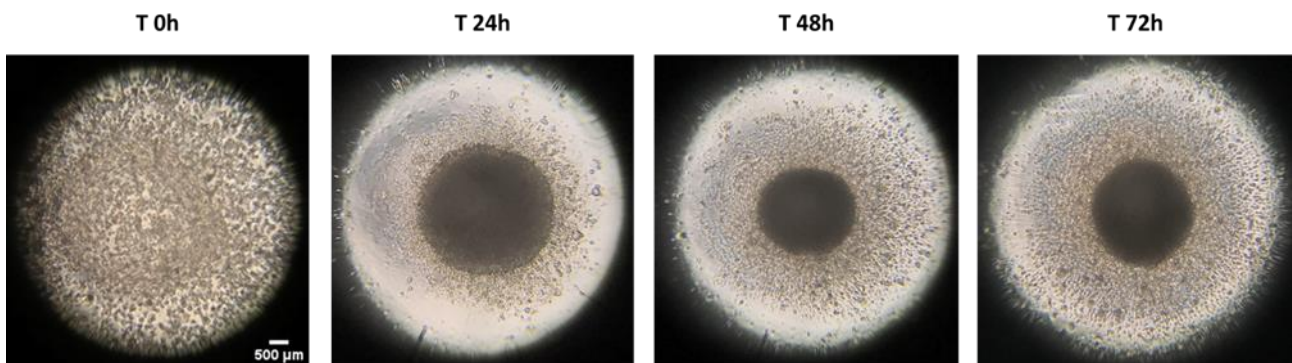


Figure 1.2: *HaCaT* cells (human keratinocytes cell line) seeded into a 96-well black microtiter plate made of a hydrophilic and neutrally charged hydrogel coating covalently bound with polystyrene surfaces, imaged at time 0 or after 24 h, 48 h, and 72 h overnight incubation.

1.2 Recombinant DNA technology and protein expression

In the early 1970s, HindIII [25] and EcoRI [26] restriction enzymes discovery led to significant innovation in the development of recombinant DNA technology and protein expression, thus promoting the first cloning experiments with DNA fragments transmission from one bacterial strain to another, using a plasmid as a carrier [27]. Thanks to this technology, a gene or multiple genes can be identified, cut, and introduced into another organism's genome. Recombinant proteins, as a result of this technique, are foreign proteins coded by a manipulated gene (recombinant gene), generated by a specific host recombinant expression system

(**Fig. 1.3**) [28]. The recombinant gene is the result of a new genetic combination where one or more DNA segments or whole genes are inserted from different DNA molecules. Thus, when the plasmid containing the recombinant gene is introduced into a host expression system, the protein synthesis pathways of the host will then result in the expression of the protein of interest [29].

Recombinant DNA technology is based on the use of three main tools:

- enzymes (e.g., bacterial restriction enzymes, polymerases, and ligases);
- vectors (e.g., plasmids, bacteriophages, and baculoviruses)
- host organism (e.g., mammalian, insect, yeast, and bacterial cells).

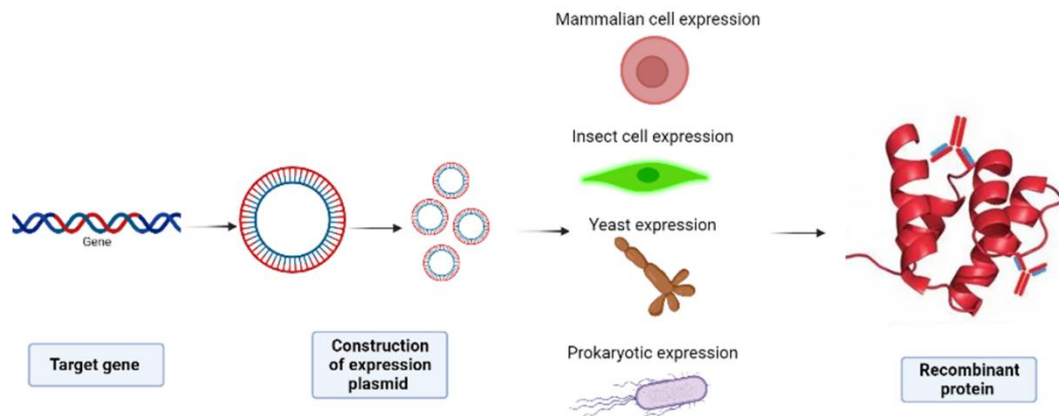


Figure 1.3: Schematic representation of recombinant protein production with some examples of the most used host expression systems (e.g. mammalian, insect, yeast, and bacterial cells).

The cut, synthesis, and binding of DNA are promoted by restriction enzymes, polymerases, and ligases respectively. Each component plays an important role. Restriction enzymes cut at a specific site within the DNA molecule (restriction site), thus producing sticky ends in the DNA sequence where the desired gene will specifically bind [30]. After the gene integration, the vector, carrying the gene of interest, enters the host organism, where the recombinant DNA is introduced. Although several types of vectors have been developed, the most adopted vectors are bacteriophages, plasmids, and baculoviruses [31]. The vector must contain the same restriction sites that are present within the gene of choice to mediate the

gene integration.

Generally, the recombinant DNA technology presents five steps (**Fig. 1.4**):

- cut of the desired DNA where restriction sites are present, through restriction enzymes;
- amplification of the gene copies through polymerase chain reaction (PCR);
- insertion of the desired gene into the vector;
- the vector entry into the host organism;
- obtaining the products of the recombinant gene (e.g., proteins);

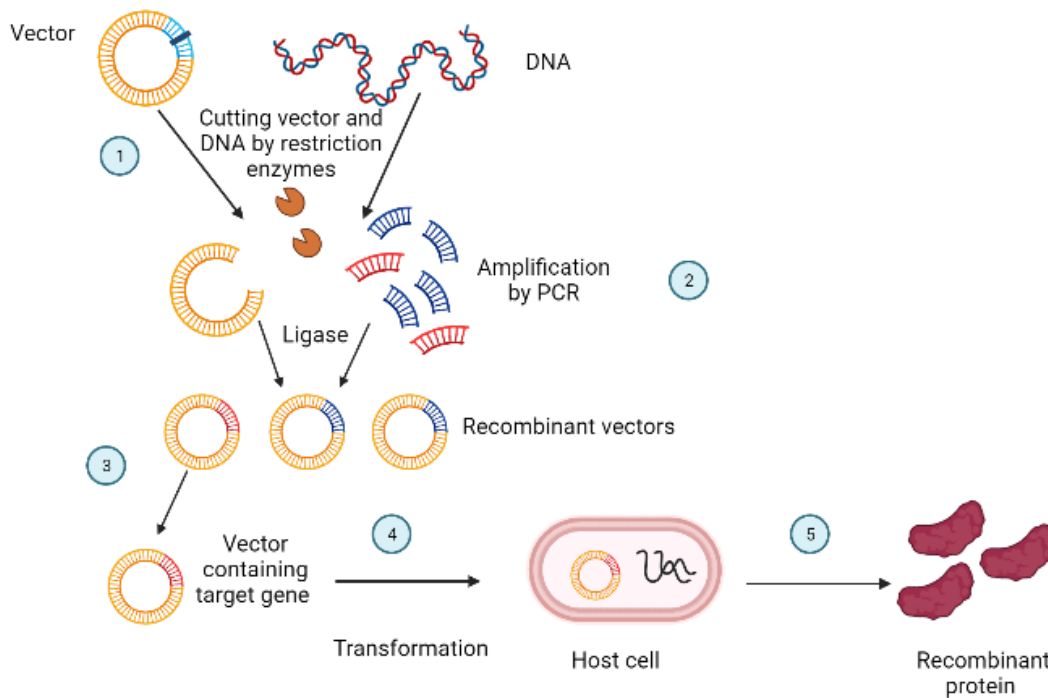


Figure 1.4: Steps of recombinant DNA technology: 1) cut of the desired DNA by restriction enzymes, 2) amplification of the gene copies by PCR, 3) gene insertion into the vector, 4) vectors transfer into the host organism, and 5) products of recombinant genes (e.g., recombinant protein).

Each system of protein expression presents its own advantages and disadvantages such as production costs, feasibility, glycosylation state, and other aspects which influence the choice according to the application [32]. Compared with natural proteins, recombinant proteins can be produced in large amounts with relative simplicity. Recombinant protein technology, thanks to their variety, found

a wide range of applications, from medical diagnostic reagents in human healthcare such as vaccines, drugs, or antibodies, to biochemical analysis (e.g., imaging, protein research). Prokaryotic and eukaryotic expression hosts systems, such as *Escherichia coli*, yeast, insect, and mammalian cell cultures have been established as production platforms, according to their use [33]. Particularly, expression systems using bacteria as hosts offer rapid production in large quantities [28]. Among these different hosts, mammalian cell lines are often used to produce approved recombinant biopharmaceuticals, due to the presence of the glycosylation machinery within these systems, and the fact that today monoclonal antibodies represent most of new therapeutic candidates for many diseases treatment, being safe from off-target side effects [34]. The first human recombinant protein used to treat disease was recombinant human insulin developed in 1982 [35]. Since then, the recombinant protein industry has rapidly grown and actually, there are many types of therapeutic recombinant proteins forming a comprehensive system of recombinant human proteins. Over 180 recombinant proteins are in use as therapeutic agents today [36]. Therapeutic recombinant proteins are an important class of medicines serving patients who need novel therapies. In clinical practice, the recombinant proteins include recombinant hormones, interferons, tumour necrosis factors, growth factors, interleukins, blood clotting factors, thrombolytic drugs, and enzymes for treating major diseases such as diabetes, myocardial infarction, dwarfism, congestive heart failure, multiple sclerosis, neutropenia, cerebral apoplexy, anaemia, thrombocytopenia, hepatitis, rheumatoid arthritis, asthma, Crohn's disease, and cancers therapies [29].

1.2.1 Recombinant fusion proteins

One of the most common techniques of genetic engineering reported for biological study and protein functions research is represented by recombinant fusion protein, or fusion protein for short [37]. A fusion protein is a protein containing at least two domains that are encoded by separate genes that have been combined into a single fusion gene which is transcribed and translated as a single unit, generating a polypeptide [38]. Fusion proteins are principally used as:

- aids in the purification of cloned genes;
- expression level reporters;
- histochemical “tags” to enable visualization of the location of proteins in a cell, tissue, or organism;
- chimeric protein drug.

There are essentially two types of fusion proteins (**Fig. 1.5**). In the first one two proteins or protein subunits are fused end-to-end and usually linked by a linker [37]. The two components present different features, for example, the first peptide may contribute to recognition, binding, and toxicity, while its fused partner may aid stability and targeting of the chimeric polypeptide. Indeed, the tag presence simplifies affinity-based purification [39].

In the second type of fusion or chimeric protein, the sequences of two similar proteins are combined in a tangled way to provide a novel protein, often with gained innovative activity. This type of fusion protein typically contains only a single type of novel activity rather than two separate activities as noted above for the first type of fusion protein.

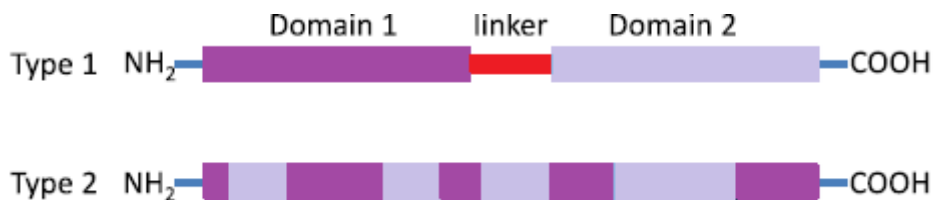


Figure 1.5: *Two types of fusion proteins: the first one involves two proteins or protein subunits fused end-to-end and typically connected by a linker, and the second, in which amino acids from both givers are mixed in the fusion protein product.*

The increasing number of sequenced genes and genomes, in combination with the use of polymerase chain reaction (PCR) to recover intact genes, provides many combinations for the possible fusion of structural genes from various sources. Protein purification is usually performed through affinity chromatography, where a protein that can be easily and conveniently purified is linked to a protein of interest [39]. The almost endless number of possible arrangements of fusion

partners have turned this technique into a versatile and valuable tool within many research areas such as biochemistry and biotechnology [40]. Indeed, protein fusion technology can be used to produce proteins containing molecules with visible or assayable reporter proteins for monitoring gene expression and protein localization. Several different types of gene expression reporter systems have been used, including luciferase, β -galactosidase, β -lactamase, chloramphenicol acetyltransferase (CAT), alkaline phosphatase (AP), and natural or engineered bioluminescent and fluorescent proteins. GFP and luciferase are the two most frequently used reporter proteins, for *in vivo* and *in vitro* expression and localization studies [41,42].

1.2.2 Baculovirus expression system

One of the most used expressing host methods to produce high-quality recombinant protein is the baculovirus-insect cell system (BEVS-IC) [43]. The system exploits a virus that naturally infects arthropods and insects as a vector: the baculovirus. The virus belongs to the *Baculoviridae* family and has a double-stranded, circular DNA genome. Baculovirus gene promoters can drive hyper-expression of external genes in host insect cells, which can provide for high levels of production of a protein with complex glycosylation and other post-translational modifications to better mimic human proteins [40]. First described in the early 1980s the baculovirus expression vector system, has been successfully proven for mediated foreign gene expression and stimulated great interest in the scientific field of recombinant protein production [44]. Since then, BEVS has been extensively used in biotechnology and biomedicine areas for vaccine production, stem cell transduction, tissue engineering, viral vector production, gene therapy, cancer therapy, and other fields [45]. The first BEVS-IC-derived product for humans was the vaccine Cervarix™, now widely used to protect against cervical cancer caused by human papillomavirus (HPV). Eleven BEVS products have been approved by Food and Drug Administration (FDA), including four human vaccines for the prevention of cervical cancer, seasonal influenza, and coronavirus disease 2019 (COVID-19). In addition to two human therapeutics for prostate cancer and hereditary lipoprotein lipase deficiency (LPLD), and five

veterinary vaccines [46].

The production of proteins via BEVS is a two-step process. First, the insect cells are grown to a desired concentration. In the second step, the cells are infected with the baculovirus. Like other viruses, the baculovirus takes control of the gene expression machinery of the host cell and triggers responses that lead to the production of the target product [45]. During this process, the virus replicates itself using the metabolic machinery of the host. The recombinant virus can be used to infect cultured insect cells or larvae (caterpillars), leading to high-level transcription of the foreign cDNA during the very late phase of infection. The resulting mRNA then can be translated to produce the protein of interest [44]. The potential for high-level recombinant protein production is one of the major advantages of the BEVS, with “high-level” defined as ≥ 100 mg of recombinant protein per liter of infected insect cell culture [43]. In addition, BEVS eukaryotic protein processing capabilities, which include the ability to provide post-translational protein modifications such as phosphorylation and glycosylation make it a powerful tool for a wide variety of biotechnology applications [47].

1.3 Chemical luminescence as the detection strategy

Chemical luminescence is a physical phenomenon that consists of light production through a chemical reaction [48]. Different subtypes can be distinguished according to the kind of stimulus able to trigger the reaction. Mixing the reagents triggers the chemical production of light of chemiluminescence (CL) and bioluminescence (BL), the latter exploiting photoproteins and enzymes isolated from living organisms [49]. Releasing of excited state molecules produced during an electron-transfer reaction that occurs on an electrode is typical of electrogenerated luminescence (ECL) [50], while the light emission characteristic of thermochemiluminescence (TCL) is induced by the decomposition of a thermodynamically relative unstable molecule when heated above a threshold temperature [51]. The ability to produce photons without the need for photoexcitation, as required for fluorescence, to avoid problems resulting from light scattering, background fluorescence, or light source instability are only some of the major advantages of chemical luminescence detection techniques, thus

attracting the analytical interest during the past years [48]. Since no external excitation source is required, the instrumentation for chemical luminescence measurements is very simple. Moreover, when imaging detection systems, such as charge-coupled device (CCD) or complementary metal-oxide semiconductor (CMOS) cameras, are coupled with chemical luminescence detection, flexible configurations of the reading cell are possible (e.g., the spatial distribution of microarray spots on a functionalized surface).

1.3.1 Bioluminescence

Bioluminescence (BL) is a characteristic phenomenon of some organisms that emit light through a chemical reaction that involves specific endogenous enzymes (e.g., luciferases) or photoproteins [52]. The peculiar photo-physical property of BL, with respect to CL, is that the light emission derives from an enzyme-singlet excited state product complex [48].

A large variety of marine and terrestrial organisms (e.g., bacteria, fungi, fish, insects, worms) express bioluminescent proteins and consequently, many bioluminescent proteins have been identified and characterized about their different biological origins, evolutionary functions, corresponding reaction mechanisms, and specific substrates, observing that the bioluminescent properties significantly vary, according to the species and the protein itself (**Fig. 1.6**). Remarkably, the BL emission spectra of naturally occurring bioluminescent systems cover all the visible range between 400 nm and 650 nm, while all bioluminescent substrates studied until now share the peroxide bond $-O-O-$ as the same luminophore [53]. In nature, the most common biological functions of BL are counterillumination camouflage, defense, attraction, warning, and interaction. Naturally bioluminescent systems can be classified into two major categories: distinct luciferase enzymes and luciferin (substrate) moieties, and photoproteins in which the light-emitting chromophore is part of the protein itself and light emission is triggered by changes in the protein's environment [54].

For example, photoprotein aequorin isolated from the jellyfish *Aequorea victoria* is a calcium-regulated protein in which light emission is initiated upon calcium binding [55].

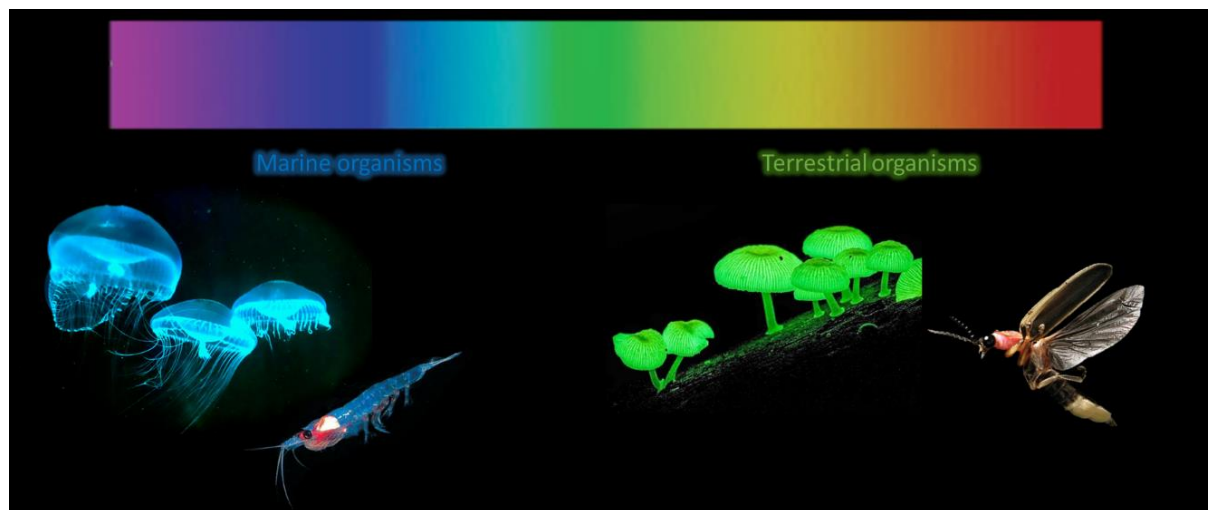


Figure 1.6: Examples of naturally bioluminescent emitting organisms. From left to right: *Aequorea victoria*, *Euphasia superba*, *Agaricus gardneri* and *Photinus pyralis*.

Among all the bioluminescent organisms, fireflies are the most studied and well-characterized such as the North American firefly, *Photinus pyralis* (Order: Coleoptera, Family: *Lampyridae*) and more recently the Italia firefly (*Luciola italica*) [56, 57]. Because of its high bioluminescence efficiency and ready availability, the *P. pyralis* firefly luciferase system is used in molecular biology, analytical, biosensors, biomedical, pharmaceutical, and diagnostic applications. The accepted name for the *P.pyralis* luciferase enzyme is Photinus-luciferin 4-monooxygenase, but it is commonly designated as firefly luciferase or simply luciferase (Luc). Determination of ATP, gene reporter, microbial detection, immunoassays, nucleic acid assays, nucleotide analysis, biosensing detection of protein–protein interactions, and high-throughput screening in drug discovery and *in vivo* and *in vitro* imaging of tumors as well as infections are some of the common applications of FLuc [58].

P. pyralis luciferase is a 61-kDa monomeric protein that does not require any post-translational modifications, not showing any toxicity to cells even at high concentrations and thus being suitable for heterologous expression in both prokaryotic and eukaryotic systems [59]. Luciferase substrate is firefly luciferin (LH₂), and the reaction requires adenosine-5'-triphosphate (ATP), molecular oxygen (O₂), and a metallic cation (Mg²⁺).

The total bioluminescent chemical reaction catalyzed by Luc is:



Luciferin can be found in _D or _L optical isomers, but only the _D isomer reacts promptly through the bioluminescent pathway. As shown in **figure 1.7**, the adenylation of luciferin is followed by cyclization, and decarboxylation of the adenylation-luciferin complex, resulting in the emission of CO₂ and light [60]. The reaction takes place in two steps. In the first step, in the presence of ATP, D-luciferin is converted into luciferyl adenylate, the central intermediate of the BL reaction. In the second step, thanks to the presence of molecular oxygen, around 80% of adenylate is oxidized via a single electron-transfer mechanism into peroxide which ultimately leads to the production of oxyluciferin and emission of light [58].

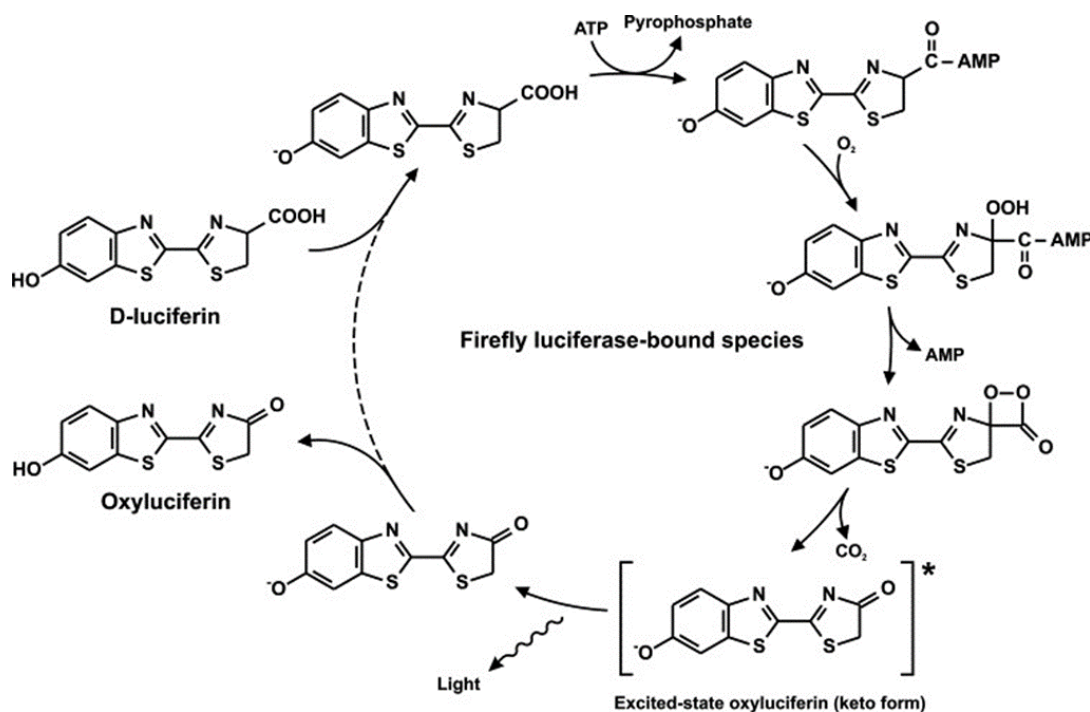


Figure 1.7: Mechanism of firefly bioluminescence.

The light generation from LH₂ is highly efficient, providing great sensitivity for detecting the luciferase protein using available light-measuring technology [61].

The light intensity of the luciferase reaction depends on luciferin concentration, and the concentration of the enzyme does not affect the bioluminescence intensity. The typical emission spectrum for firefly luciferase is in the yellow-green region ($\lambda_{em} = 550\text{--}570\text{ nm}$), with a peak at 562 nm at basic media (pH 7.5 - 7.8). It presents glow-type kinetics and a broad emission band [62].

Firefly luciferin and other modified luciferins, among others, easily crosses through the biological membranes including cell membranes, the blood-brain barrier, and the blood-placenta barrier. Interestingly, cell membranes crossing is increased at low pH (e.g., 100 mM Na-citrate, pH 5.2) due to the protonation of the carboxyl group of D-luciferin [63,64]. In the presence of protease inhibitors, the half-life of firefly luciferase expressed in mammalian cells was calculated to be in the range of 1 to 4 hours. Luciferase is a pH-sensitive enzyme, and acid media (pH 5-6) can shift the emission to red (maximum at 620 nm), as well as high temperatures and heavy metal cations. It is believed that conformational changes, which influence the active site microenvironment, are also responsible for the different color emissions [65]. To better adapt to research needs, the different luciferases discovered have undergone significant cloning and mutagenesis manipulation to the improvement of thermostability, altered spectral emission, and increased quantum yield emission. Indeed, various firefly luciferases have been mutated to shift their emission wavelengths toward the red region of the spectrum ($\lambda_{em} = 615\text{ nm}$), such as red-emitting firefly luciferases. Red light is transmitted through live tissue more efficiently than other wavelengths of visible light [66]. For example, in bioluminescence imaging (BLI) of animal tissues, the range of light peak emission is important since blue light is more absorbed by host tissues than red-shifted [67,68]. For this reason, there is a great interest in modifying both Luc and LH₂ to obtain red-shifted emission spectra for BL imaging applications. In 1966, White et al. [69] reported that NH₂-LH₂, which was the result of the substitution of the 60-hydroxyl group of D-LH₂ with the electron-donating amino group, could generate a red-shift BL signal of 590 nm in the presence of Fluc in the cells, and the near-infrared photon flux is 10 times higher than that of D-LH₂, thus opening the way for the production of novel luciferins [70], [71]. Also, luciferases can be modified through amino-acids

substitution thus obtaining chimeric luciferases [72]. The development of mutant luciferase-luciferin pairs with red-shift emission spectra increased the sensitivity of BL imaging driving its application in deep-tissue imaging. Thus, red shifting the emission spectrum of luciferases enhance their efficacy for *in vivo* or *in vitro* monitoring of biological processes. In this context, since photoproteins or enzymes that emit at different wavelengths exist or can be created, it may be possible to provide a multicolor functional assay able to coordinately analyze and monitor multiple functions in processes in *ex vivo* samples, living cells, and living animals using spectrally resolved imaging methods [73].

1.3.2 Chemiluminescence

Chemiluminescence (CL) is a phenomenon where light is generated through chemiexcitation during a chemical reaction [74]. Usually, two reagents are needed: a substrate and an oxidant which react to form a product or an intermediate, sometimes in the presence of a catalyst or enhancer (e.g., substituted phenols and boronic acids, indophenols, and N-alkyl phenothiazines). Then the singlet excited intermediate, with high energy, emits light returning to the ground state [49].

To have the best conditions for light production through a chemical reaction the following requirements are needed:

- The free energy necessary requirements to populate the electronically excited state (singlet) must be sufficiently exergonic and satisfy the following relationship:

$$-\Delta G \geq \frac{hc}{\lambda_{ex}} = \frac{28600}{\lambda_{ex}}$$

Therefore, in the visible range (400–750 nm) about 40–70 kcal mol⁻¹ are required by a chemiluminescence reaction to produce photons.

- This electronically excited state must be accessible on the reaction coordinate.

- From the excited state to the ground state the photon emission of the species involved must be a favorable energy release route.

This implies that either the product of the reaction must be fluorescent or – if by energy transfer – an excited state can be populated (this energy transfer can occur intra- or intermolecularly).

The chemical luminescence quantum yield is defined as the number of photons emitted for each reacting molecule, and can be calculated as shown below:

$$\Phi_{\text{CL}} = \Phi_{\text{R}} \Phi_{\text{ES}} \Phi_{\text{F}}$$

where Φ_{R} is the reaction yield, Φ_{ES} reflects the ratio of the product accessing the excited state, and Φ_{F} is the fluorescent quantum yield of the reaction product.

In nature, several chemiluminescent substances have been reported, and synthetic analogs have been developed to facilitate their use as indicator molecules. The first analytical applications of CL date back to the late 1970s, just with the advent of synthetic CL molecules such as luminol and its derivatives, 1,2-dioxetanes, and acridinium esters [49]. The oxidation of luminol (5-amino-2,3-dihydro-phthalazine-1,4-dione), a diprotic acid, is one of the most studied CL reactions. During the CL reaction under basic conditions, in the presence of H_2O_2 , luminol is oxidized to radical anion in its excited state and releases a photon while returning to its ground state (**Fig. 1.8**).

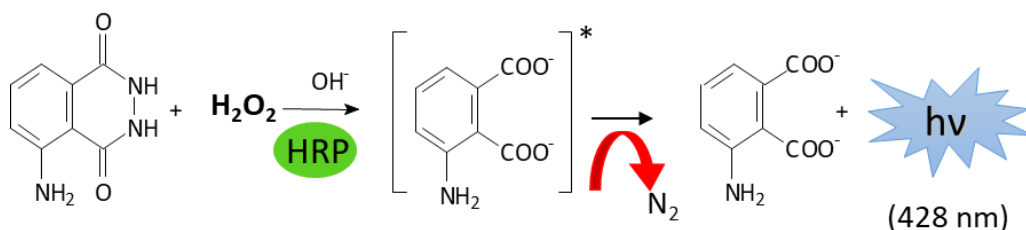


Figure 1.8: Reaction of luminol/ H_2O_2 in presence of horseradish peroxidase (HRP) with light emission at 428 nm.

The light is emitted at 428 nm (blue light emission) with a relatively low quantum yield of 1% [75]. The reaction may occur in the presence of horseradish

peroxidase (HRP) as a catalyst.

The CL system HRP-luminol-H₂O₂ is often used for the study of antioxidants, in their presence luminescence is inhibited until the antioxidants are exhausted, and the time of inhibition is proportional to the total concentration of antioxidants themselves [76].

Luminol and its analogs or derivatives have been widely used in bioanalytical applications such as sensing, bioimaging, and diagnostics due to their advantages including good water solubility, stable properties, low background signal, high chemiluminescence efficiency, simple synthesis, and eco-friendliness [77].

Due to the slow reaction rate between luminol and H₂O₂, catalysts or enhancer are often added to the luminescent system to accelerate the reaction and improve the chemiluminescence intensity. Specific chemicals and/or buffers and suitable pH conditions could enhance the light emitted up to 1000-fold, thus the light is detected easily, and the sensitivity of the reaction is increased. To improve the analytical performance of the HRP-catalyzed CL oxidation of luminol, it is possible to add to the CL cocktail some enhancers like p-iodophenol (PIP), 4- (1-imidazolyl)phenol [78], and other p-phenol derivatives, para-phenyl phenol and sodium tetraphenylborate as a synergistic enhancer, [79] or K₃Fe(CN)₆ as electron mediator [80]. These compounds allow to amplify and stabilize the CL signal making it easier to measure the analytical signal.

L-012 (8-amino-5-chloro-7-phenylpyrido[3,4-d] pyridazine-1,4(2H,3H) dione) is a luminol-based molecule that has been reported to produce much stronger CL emission and to better cross the plasmatic cell membranes than other CL probes such as lucigenin and luminol (**Fig. 1.9**) [81]. The luminol derivative L-012 has been used to evaluate the superoxide anion (O₂^{•-}) and other reactive oxygen species (ROS), derived in particular from NADPH oxidase (Nox). It has recently been used for non-invasive imaging for the identification of ROS and reactive nitrogen species (RNS) in mice subjected to pro-inflammatory conditions [81], [82].

Chemical luminescence detection showed wide dynamic ranges, thus facilitating the analysis of samples with very different analyte concentrations. This phenomenon has been exploited in a variety of bioanalytical formats including microtiter plates (96 and 384-well), microarrays, microfluidics, paper-based devices, and *in vitro* microscopy imaging.

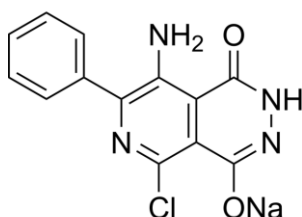


Figure 1.9: *L-012 chemical structure.*

1.3.3 Chemiluminescent systems for the evaluation of living cells intracellular biomarkers

Chemiluminescent probes are one of the most sensitive imaging modalities and bioassays for detecting reactive species, enzymes, and other related disease biomarkers, thus obtaining more accurate biological information in living cells and *in vivo* organisms.

During the past years, chemiluminescent substrates such as luminol and its derivatives, cyclic fluorescein analogs, and peroxyoxalate have shown low CL efficiency, and limited applications due to their chemical nature [77]. This limitation has been overcome thanks to the synthesis of 3,3,4-trimethyl-1,2-dioxetane in 1969 by Kopecky and Mumford [83]. Subsequently, several CL probes were designed using 1,2-dioxetanes as scaffolds to realize new CL bioassays with higher brightness and CL efficiency [84]. However, these molecules are particularly unstable and able to decompose spontaneously thus requiring the presence of special protective groups (PG) which are removed through hydrolysis or enzymatic reaction in the presence of the analyte of interest. The decomposition of the released dioxetane generates a high-energy intermediate with blue light emission at 470 nm. Different recognition sites and fluorophores can be flexibly added in the 1,2-dioxetane structure, making it suitable for imaging of various biomarkers in different types of cells or organisms,

and even dual-channel imaging *in vivo* [85]. Schaap et al, in 1987, described the first example of a 1,2-dioxetane-type enzyme-activated chemiluminescent probe, using alkaline phosphatase as a target, and thus realizing CL imaging of living cells [86]. The dioxetane designed by Schaap is the only known CL probe that presents a stable dioxetane moiety [87]. This kind of probe does not need an oxidation step to generate CL emission and for this reason, can detect a wide range of chemical and biological activities. As shown in **figure 1.10** Schaap's adamantylidene-dioxetane presents an analyte-responsive protecting group (PG), which covers the phenol moiety.

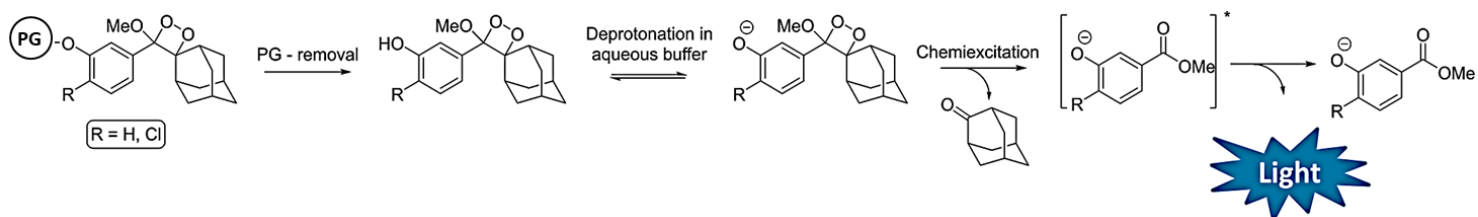


Figure 1.10: Mechanism of action of Schaap's dioxetane (PG: protecting group).

After the removal of the PG by the analyte of interest, an unstable phenolate-dioxetane species is generated, which decomposes through a chemiexcitation process to produce the excited intermediate benzoate ester and adamantanone. The excited intermediate decays to its ground state through the emission of a blue photon ($h\nu = 470 \text{ nm}$). The whole CL process is triggered upon reaction with the corresponding biomarker of interest according to the chemically induced electron exchange luminescence (CIEEL) theory suggested in 1977 by Koo et al. [88]. The CIEEL theory can be simply described as the fluorescence transfer of electrons from an effective electron donor to a high-energy electron acceptor, and then the effective fluorescent structure is excited to emit light. Due to the special structure of 1,2-dioxetane derivatives, the chance of generating the CIEEL mechanism is reached. The electron-rich group can be released by deprotecting the phenolate unit, thereby transferring intramolecular electrons to the cyclic peroxide bond, and the formation of the phenolate can occur by deprotonation of the phenolic unit. This is the complete process of the CIEEL mechanism in 1,2-dioxetane-based chemiluminescent probes, which can

efficiently generate excited states thus improving the CL quantum yield [89]. Notably, Schaap's adamantylidene–dioxetane has been applied to design probes for various biomarkers detection in cells such as hydrogen peroxide (H₂O₂), L-glutathione (GSH), alkaline phosphatase, cysteine, peroxyxynitrite, formaldehyde and hydrazine [90]. In bioassays, under aqueous conditions Schaap's dioxetanes suffer from an intrinsic limitation: their CL efficiency decreases drastically through non-radiative energy transfer processes (quenching) upon interaction with water molecules [69]. This issue can be partially solved by the addition of enhancers such as surfactants. Nevertheless, in terms of toxicity, these compounds are often not compatible with living systems thus limiting their applications in living cells or organisms [91]. In this context, to overcome these limitations, Shabat et al. have developed several strategies to increase the signal under physiological conditions, including the preparation of fluorophore conjugates with phenoxy-dioxetane turn-ON chemiluminescent probes, also allowing color modulation and red-shifting of the emitted light [92]. In addition, in order to find a way that would allow the use of the probes alone, they introduced an electron-withdrawing acrylic substituent (electron-withdrawing group: EWG) at the ortho position of the phenoxy-dioxetane resulting in an about 3000-fold increase of the CL quantum yield in aqueous media (**Fig. 1.11**) [93]. This innovation led to the development of all-in-one bioassays based on the use of CL probes that are extremely bright in an aqueous environment without additives.

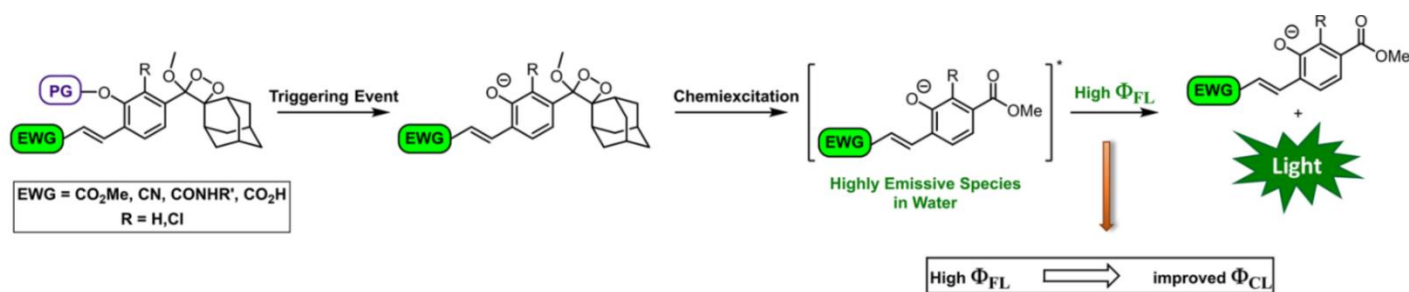
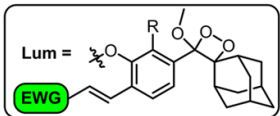
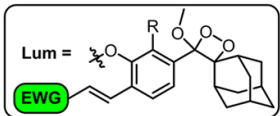
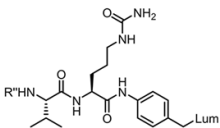
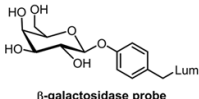
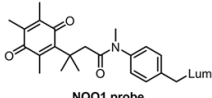
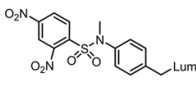
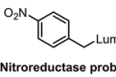
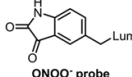
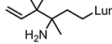


Figure 1.11: Mechanism of action of the 1,2 dioxetane after the improvement of luminophore's intrinsic properties (EWG: electron-withdrawing group)[69].

Although these innovative luminophores were reported only a few years ago, they have already been used for the construction of numerous efficient CL

probes for the detection of several biomarkers in living cells, summarized in **Table 1.1**. The first chemiluminescence microscopy images of living cells using 1,2-dioxetane probes were reported by Shabat et al. [94] who developed a CL probe for the imaging of the endogenous β -galactosidase activity in LacZ transfected cells. Recently through the use of these innovative CL probes, cysteine-protease cathepsin B [95], overexpressed in malignant tumors, peroxynitrite (ONOO-) [96], azanone (HNO) [97], NAD(P)H quinone oxidoreductase-1 (NQO1) [98], nitroreductase [99], superoxide anions [100], and cysteine [101] which play crucial roles in physiological and pathological processes in biological systems were investigated in living cells and animals. The imaging studies reported with these dioxetane-based probes show the advantages of chemiluminescence over fluorescence for *in vivo* applications, since issues such as autofluorescence and scattering of irradiated light are avoided. This group of compounds is useful in CL bioassays when the appropriate additives are added to the aqueous media. Thanks to the advantages of 1,2-dioxetane platform design and technology development, it is expected that 1,2-dioxetane-based CL probes will provide further development for *in vivo* imaging, which will certainly also make a great contribution to the diagnosis and treatment of major diseases.

Table 1: Examples of structures of various 1,2 dioxetane CL probes suitable for bioimaging (Lum: luminophore) [69].

Backbone CL probe	Biospecific targets		
 <p>Lum = </p> <p>R = H, Cl</p> <p>EWG = - CO₂Me, - CN, - COHNR', - CO₂H</p>	 <p>Cathepsin B probe</p>  <p>β-galactosidase probe</p>  <p>NQO1 probe</p>	 <p>RSH probe</p>  <p>H₂O₂ probe</p>  <p>Nitroreductase probe</p>  <p>ONOO⁻ probe</p>	 <p>Alkaline phosphatase probe</p>  <p>Cysteine probe</p>  <p>HNO probe</p>  <p>Formaldehyde probe</p>

1.4 References

- [1] S. Daunert, G. Barrett, J. S. Feliciano, R. S. Shetty, S. Shrestha, and W. Smith-Spencer, "Genetically Engineered Whole-Cell Sensing Systems: Coupling Biological Recognition with Reporter Genes," *Chem Rev*, vol. 100, no. 7, pp. 2705–2738, Jul. 2000, doi: 10.1021/cr990115p.
- [2] W. Zhang *et al.*, "Optical Biosensors Based on Nitrogen-Doped Graphene Functionalized with Magnetic Nanoparticles," *Adv Mater Interfaces*, vol. 3, no. 20, p. 1600590, Oct. 2016, doi: 10.1002/admi.201600590.
- [3] W. Wen *et al.*, "A highly sensitive nitric oxide biosensor based on hemoglobin–chitosan/graphene–hexadecyltrimethylammonium bromide nanomatrix," *Sens Actuators B Chem*, vol. 166–167, pp. 444–450, May 2012, doi: 10.1016/j.snb.2012.02.086.
- [4] N. Raut, G. O'Connor, P. Pasini, and S. Daunert, "Engineered cells as biosensing systems in biomedical analysis," *Anal Bioanal Chem*, vol. 402, no. 10, pp. 3147–3159, Apr. 2012, doi: 10.1007/s00216-012-5756-6.
- [5] Q. Liu, C. Wu, H. Cai, N. Hu, J. Zhou, and P. Wang, "Cell-Based Biosensors and Their Application in Biomedicine," *Chem Rev*, vol. 114, no. 12, pp. 6423–6461, Jun. 2014, doi: 10.1021/cr2003129.
- [6] Q. Gui, T. Lawson, S. Shan, L. Yan, and Y. Liu, "The Application of Whole Cell-Based Biosensors for Use in Environmental Analysis and in Medical Diagnostics," *Sensors*, vol. 17, no. 7, p. 1623, Jul. 2017, doi: 10.3390/s17071623.
- [7] D. R. Thévenot, K. Toth, R. A. Durst, and G. S. Wilson, "Electrochemical biosensors: recommended definitions and classification1International Union of Pure and Applied Chemistry: Physical Chemistry Division, Commission I.7 (Biophysical Chemistry); Analytical Chemistry Division, Commission V.5 (Electroanalytical Chemistry).1," *Biosens Bioelectron*, vol. 16, no. 1–2, pp. 121–131, Jan. 2001, doi: 10.1016/S0956-5663(01)00115-4.
- [8] I. Alkorta, L. Epelde, I. Mijangos, I. Amezaga, and C. Garbisu, "Bioluminescent Bacterial Biosensors for the Assessment of Metal Toxicity and Bioavailability in Soils," *Rev Environ Health*, vol. 21, no. 2, Jan. 2006, doi: 10.1515/REVEH.2006.21.2.139.

- [9] E. Zyracka, R. Zadrag, S. Koziół, A. Krzepiłko, G. Bartosz, and T. Biliński, "Yeast as a biosensor for antioxidants: simple growth tests employing a *Saccharomyces cerevisiae* mutant defective in superoxide dismutase.," *Acta Biochim Pol*, vol. 52, no. 3, pp. 679–84, 2005.
- [10] P. Banerjee and A. K. Bhunia, "Mammalian cell-based biosensors for pathogens and toxins," *Trends Biotechnol*, vol. 27, no. 3, pp. 179–188, Mar. 2009, doi: 10.1016/j.tibtech.2008.11.006.
- [11] E. Michelini and A. Roda, "Staying alive: new perspectives on cell immobilization for biosensing purposes," *Anal Bioanal Chem*, vol. 402, no. 5, pp. 1785–1797, Feb. 2012, doi: 10.1007/s00216-011-5364-x.
- [12] N. Raut, G. O'Connor, P. Pasini, and S. Daunert, "Engineered cells as biosensing systems in biomedical analysis," *Anal Bioanal Chem*, vol. 402, no. 10, pp. 3147–3159, Apr. 2012, doi: 10.1007/s00216-012-5756-6.
- [13] Y. Tian, Y. Lu, X. Xu, C. Wang, T. Zhou, and X. Li, "Construction and comparison of yeast whole-cell biosensors regulated by two RAD54 promoters capable of detecting genotoxic compounds," *Toxicol Mech Methods*, vol. 27, no. 2, pp. 115–120, Feb. 2017, doi: 10.1080/15376516.2016.1266540.
- [14] C. Lino, S. Barrias, R. Chaves, F. Adegá, P. Martins-Lopes, and J. R. Fernandes, "Biosensors as diagnostic tools in clinical applications," *Biochimica et Biophysica Acta (BBA) - Reviews on Cancer*, vol. 1877, no. 3, p. 188726, May 2022, doi: 10.1016/j.bbcan.2022.188726.
- [15] R. Edmondson, J. J. Broglie, A. F. Adcock, and L. Yang, "Three-Dimensional Cell Culture Systems and Their Applications in Drug Discovery and Cell-Based Biosensors," *Assay Drug Dev Technol*, vol. 12, no. 4, pp. 207–218, May 2014, doi: 10.1089/adt.2014.573.
- [16] H. Ben-Yoav, S. Melamed, A. Freeman, Y. Shacham-Diamand, and S. Belkin, "Whole-cell biochips for bio-sensing: integration of live cells and inanimate surfaces," *Crit Rev Biotechnol*, vol. 31, no. 4, pp. 337–353, Dec. 2011, doi: 10.3109/07388551.2010.532767.
- [17] M. Ngoepe *et al.*, "Integration of Biosensors and Drug Delivery Technologies for Early Detection and Chronic Management of Illness,"

- Sensors*, vol. 13, no. 6, pp. 7680–7713, Jun. 2013, doi: 10.3390/s130607680.
- [18] Y. Torisawa, H. Shiku, T. Yasukawa, M. Nishizawa, and T. Matsue, “Multi-channel 3-D cell culture device integrated on a silicon chip for anticancer drug sensitivity test,” *Biomaterials*, vol. 26, no. 14, pp. 2165–2172, May 2005, doi: 10.1016/j.biomaterials.2004.05.028.
- [19] P. Hameed and G. Manivasagam, “An overview of bio-actuation in collagen hydrogels: a mechanobiological phenomenon,” *Biophys Rev*, vol. 13, no. 3, pp. 387–403, Jun. 2021, doi: 10.1007/s12551-021-00804-x.
- [20] K. Duval *et al.*, “Modeling Physiological Events in 2D vs. 3D Cell Culture,” *Physiology*, vol. 32, no. 4, pp. 266–277, Jul. 2017, doi: 10.1152/physiol.00036.2016.
- [21] D. K. Mishra *et al.*, “Human lung cancer cells grown in an ex vivo 3D lung model produce matrix metalloproteinases not produced in 2D culture.,” *PLoS One*, vol. 7, no. 9, p. e45308, 2012, doi: 10.1371/journal.pone.0045308.
- [22] G. M. Whitesides and B. Grzybowski, “Self-Assembly at All Scales,” *Science (1979)*, vol. 295, no. 5564, pp. 2418–2421, Mar. 2002, doi: 10.1126/science.1070821.
- [23] O. Habanjar, M. Diab-Assaf, F. Caldefie-Chezet, and L. Delort, “3D Cell Culture Systems: Tumor Application, Advantages, and Disadvantages,” *Int J Mol Sci*, vol. 22, no. 22, p. 12200, Nov. 2021, doi: 10.3390/ijms222212200.
- [24] M. W. Tibbitt and K. S. Anseth, “Hydrogels as extracellular matrix mimics for 3D cell culture,” *Biotechnol Bioeng*, vol. 103, no. 4, pp. 655–663, Jul. 2009, doi: 10.1002/bit.22361.
- [25] H. O. Smith and K. W. Welcox, “A Restriction enzyme from *Hemophilus influenzae*,” *J Mol Biol*, vol. 51, no. 2, pp. 379–391, Jul. 1970, doi: 10.1016/0022-2836(70)90149-X.
- [26] R. Yoshimori, D. Roulland-Dussoix, and H. W. Boyer, “R Factor-Controlled Restriction and Modification of Deoxyribonucleic Acid: Restriction Mutants,” *J Bacteriol*, vol. 112, no. 3, pp. 1275–1279, Dec. 1972, doi: 10.1128/jb.112.3.1275-1279.1972.

- [27] P. H. Celie, A. H. Parret, and A. Perrakis, "Recombinant cloning strategies for protein expression," *Curr Opin Struct Biol*, vol. 38, pp. 145–154, Jun. 2016, doi: 10.1016/j.sbi.2016.06.010.
- [28] G. L. Rosano, E. S. Morales, and E. A. Ceccarelli, "New tools for recombinant protein production in *Escherichia coli*: A 5-year update," *Protein Science*, vol. 28, no. 8, pp. 1412–1422, Aug. 2019, doi: 10.1002/pro.3668.
- [29] P. v. Pham, "Medical Biotechnology," in *Omics Technologies and Bio-Engineering*, Elsevier, 2018, pp. 449–469. doi: 10.1016/B978-0-12-804659-3.00019-1.
- [30] T. M. Lanigan, H. C. Kopera, and T. L. Saunders, "Principles of Genetic Engineering," *Genes (Basel)*, vol. 11, no. 3, p. 291, Mar. 2020, doi: 10.3390/genes11030291.
- [31] D. A. Mead and B. Kemper, "Chimeric Single-Stranded DNA Phage-Plasmid Cloning Vectors," in *Vectors*, Elsevier, 1988, pp. 85–102. doi: 10.1016/B978-0-409-90042-2.50010-6.
- [32] J. Yin, G. Li, X. Ren, and G. Herrler, "Select what you need: A comparative evaluation of the advantages and limitations of frequently used expression systems for foreign genes," *J Biotechnol*, vol. 127, no. 3, pp. 335–347, Jan. 2007, doi: 10.1016/j.jbiotec.2006.07.012.
- [33] N. K. Tripathi and A. Shrivastava, "Recent Developments in Recombinant Protein-Based Dengue Vaccines," *Front Immunol*, vol. 9, Aug. 2018, doi: 10.3389/fimmu.2018.01919.
- [34] M.-E. Lalonde and Y. Durocher, "Therapeutic glycoprotein production in mammalian cells," *J Biotechnol*, vol. 251, pp. 128–140, Jun. 2017, doi: 10.1016/j.jbiotec.2017.04.028.
- [35] M. R. Ladisch and K. L. Kohlmann, "Recombinant human insulin," *Biotechnol Prog*, vol. 8, no. 6, pp. 469–478, Nov. 1992, doi: 10.1021/bp00018a001.
- [36] A. G. Goncalves, E. J. Hartzell, M. O. Sullivan, and W. Chen, "Recombinant protein polymer-antibody conjugates for applications in nanotechnology and biomedicine," *Adv Drug Deliv Rev*, vol. 191, p. 114570, Dec. 2022, doi:

10.1016/j.addr.2022.114570.

- [37] B. A. Baldo, "Chimeric Fusion Proteins Used for Therapy: Indications, Mechanisms, and Safety," *Drug Saf*, vol. 38, no. 5, pp. 455–479, May 2015, doi: 10.1007/s40264-015-0285-9.
- [38] X. Chen, J. L. Zaro, and W.-C. Shen, "Fusion protein linkers: Property, design and functionality," *Adv Drug Deliv Rev*, vol. 65, no. 10, pp. 1357–1369, Oct. 2013, doi: 10.1016/j.addr.2012.09.039.
- [39] K. Terpe, "Overview of tag protein fusions: from molecular and biochemical fundamentals to commercial systems," *Appl Microbiol Biotechnol*, vol. 60, no. 5, pp. 523–533, Jan. 2003, doi: 10.1007/s00253-002-1158-6.
- [40] M. Nagaoka, H.-L. Jiang, T. Hoshiba, T. Akaike, and C.-S. Cho, "Application of Recombinant Fusion Proteins for Tissue Engineering," *Ann Biomed Eng*, vol. 38, no. 3, pp. 683–693, Mar. 2010, doi: 10.1007/s10439-010-9935-3.
- [41] T. Head *et al.*, "An enhanced bioluminescence-based Annexin V probe for apoptosis detection in vitro and in vivo," *Cell Death Dis*, vol. 8, no. 5, pp. e2826–e2826, May 2017, doi: 10.1038/cddis.2017.141.
- [42] M. Carter and J. Shieh, "Visualizing Neural Function," in *Guide to Research Techniques in Neuroscience*, Elsevier, 2015, pp. 167–183. doi: 10.1016/B978-0-12-800511-8.00007-1.
- [43] S. L. Irons, A. C. Chambers, O. Lissina, L. A. King, and R. D. Possee, "Protein Production using the Baculovirus Expression System," *Curr Protoc Protein Sci*, vol. 91, no. 1, Jan. 2018, doi: 10.1002/cpps.45.
- [44] A. Contreras-Gómez, A. Sánchez-Mirón, F. García-Camacho, E. Molina-Grima, and Y. Chisti, "Protein production using the baculovirus-insect cell expression system," *Biotechnol Prog*, vol. 30, no. 1, pp. 1–18, Jan. 2014, doi: 10.1002/btpr.1842.
- [45] T. A. Kost and C. W. Kemp, "Fundamentals of Baculovirus Expression and Applications," 2016, pp. 187–197. doi: 10.1007/978-3-319-27216-0_12.
- [46] M. Hong *et al.*, "Genetic engineering of baculovirus-insect cell system to improve protein production," *Front Bioeng Biotechnol*, vol. 10, Sep. 2022, doi: 10.3389/fbioe.2022.994743.
- [47] R. D. Possee, A. C. Chambers, L. P. Graves, M. Aksular, and L. A. King,

- "Recent Developments in the Use of Baculovirus Expression Vectors," *Curr Issues Mol Biol*, pp. 215–230, 2020, doi: 10.21775/cimb.034.215.
- [48] A. Roda *et al.*, "Progress in chemical luminescence-based biosensors: A critical review," *Biosens Bioelectron*, vol. 76, pp. 164–179, Feb. 2016, doi: 10.1016/j.bios.2015.06.017.
- [49] A. Roda and M. Guardigli, "Analytical chemiluminescence and bioluminescence: latest achievements and new horizons," *Anal Bioanal Chem*, vol. 402, no. 1, pp. 69–76, Jan. 2012, doi: 10.1007/s00216-011-5455-8.
- [50] L. Hu and G. Xu, "Applications and trends in electrochemiluminescence," *Chem Soc Rev*, vol. 39, no. 8, p. 3275, 2010, doi: 10.1039/b923679c.
- [51] G. Moroni *et al.*, "Thermochemiluminescence-Based Sensitive Probes: Synthesis and Photophysical Characterization of Acridine-Containing 1,2-Dioxetanes Focusing on Fluorophore Push-Pull Effects," *ChemPhotoChem*, vol. 6, no. 1, Jan. 2022, doi: 10.1002/cptc.202100152.
- [52] Roda Aldo, *Chemiluminescence and Bioluminescence*. Cambridge: Royal Society of Chemistry, 2010. doi: 10.1039/9781849732024.
- [53] C. A. Marquette and L. J. Blum, "Chapter 14. Chemiluminescent and Bioluminescent Biosensors," in *Chemiluminescence and Bioluminescence*, Cambridge: Royal Society of Chemistry, 2010, pp. 488–510. doi: 10.1039/9781849732024-00488.
- [54] A. J. Syed and J. C. Anderson, "Applications of bioluminescence in biotechnology and beyond," *Chem Soc Rev*, vol. 50, no. 9, pp. 5668–5705, 2021, doi: 10.1039/D0CS01492C.
- [55] S. Inouye and O. Shimomura, "The Use of Renilla Luciferase, Oplophorus Luciferase, and Apoaequorin as Bioluminescent Reporter Protein in the Presence of Coelenterazine Analogues as Substrate," *Biochem Biophys Res Commun*, vol. 233, no. 2, pp. 349–353, Apr. 1997, doi: 10.1006/bbrc.1997.6452.
- [56] S. M. Marques and J. C. G. Esteves da Silva, "Firefly bioluminescence: A mechanistic approach of luciferase catalyzed reactions," *IUBMB Life*, vol. 61, no. 1, pp. 6–17, Jan. 2009, doi: 10.1002/iub.134.

- [57] B. R. Branchini, T. L. Southworth, J. P. DeAngelis, A. Roda, and E. Michelini, "Luciferase from the Italian firefly *Luciola italica*: molecular cloning and expression.," *Comp Biochem Physiol B Biochem Mol Biol*, vol. 145, no. 2, pp. 159–67, Oct. 2006, doi: 10.1016/j.cbpb.2006.06.001.
- [58] S. M. Marques and J. C. G. Esteves da Silva, "Firefly bioluminescence: A mechanistic approach of luciferase catalyzed reactions," *IUBMB Life*, vol. 61, no. 1, pp. 6–17, Jan. 2009, doi: 10.1002/iub.134.
- [59] S.-Y. Teow *et al.*, "Development of a luciferase/luciferin cell proliferation (XenoLuc) assay for real-time measurements of Gfp-Luc2-modified cells in a co-culture system," *BMC Biotechnol*, vol. 19, no. 1, p. 34, Dec. 2019, doi: 10.1186/s12896-019-0528-4.
- [60] S. Hosseinkhani, "Molecular enigma of multicolor bioluminescence of firefly luciferase," *Cellular and Molecular Life Sciences*, vol. 68, no. 7, pp. 1167–1182, Apr. 2011, doi: 10.1007/s00018-010-0607-0.
- [61] B. R. Branchini, T. L. Southworth, N. F. Khattak, E. Michelini, and A. Roda, "Red- and green-emitting firefly luciferase mutants for bioluminescent reporter applications," *Anal Biochem*, vol. 345, no. 1, pp. 140–148, Oct. 2005, doi: 10.1016/j.ab.2005.07.015.
- [62] H. H. Seliger, J. B. Buck, W. G. Fastie, and W. D. McElroy, "The Spectral Distribution of Firefly Light," *Journal of General Physiology*, vol. 48, no. 1, pp. 95–104, Sep. 1964, doi: 10.1085/jgp.48.1.95.
- [63] M. I. Koksharov and N. N. Ugarova, "Thermostabilization of firefly luciferase by in vivo directed evolution," *Protein Engineering, Design and Selection*, vol. 24, no. 11, pp. 835–844, Nov. 2011, doi: 10.1093/protein/gzr044.
- [64] T. Kuchimaru *et al.*, "A luciferin analogue generating near-infrared bioluminescence achieves highly sensitive deep-tissue imaging," *Nat Commun*, vol. 7, no. 1, p. 11856, Jun. 2016, doi: 10.1038/ncomms11856.
- [65] M. Kiyama, R. Saito, S. Iwano, R. Obata, H. Niwa, and S. A. Maki, "Multicolor Bioluminescence Obtained Using Firefly Luciferin," *Curr Top Med Chem*, vol. 16, no. 24, pp. 2648–2655, Aug. 2016, doi: 10.2174/1568026616666160413135055.
- [66] B. F. Eames, D. A. Benaron, D. K. Stevenson, and C. H. Contag,

- "<title>Construction and characterization of a red-emitting luciferase</title>," Jul. 1999, pp. 36–39. doi: 10.1117/12.351042.
- [67] S. Dorsaz, A. T. Coste, and D. Sanglard, "Red-Shifted Firefly Luciferase Optimized for *Candida albicans* In vivo Bioluminescence Imaging," *Front Microbiol*, vol. 8, Aug. 2017, doi: 10.3389/fmicb.2017.01478.
- [68] G. Zambito *et al.*, "Red-shifted click beetle luciferase mutant expands the multicolor bioluminescent palette for deep tissue imaging," *iScience*, vol. 24, no. 1, p. 101986, Jan. 2021, doi: 10.1016/j.isci.2020.101986.
- [69] N. Hananya and D. Shabat, "Recent Advances and Challenges in Luminescent Imaging: Bright Outlook for Chemiluminescence of Dioxetanes in Water," *ACS Cent Sci*, vol. 5, no. 6, pp. 949–959, Jun. 2019, doi: 10.1021/acscentsci.9b00372.
- [70] W. Wu *et al.*, "cybLuc: An Effective Aminoluciferin Derivative for Deep Bioluminescence Imaging," *Anal Chem*, vol. 89, no. 9, pp. 4808–4816, May 2017, doi: 10.1021/acs.analchem.6b03510.
- [71] G. R. Reddy, W. C. Thompson, and S. C. Miller, "Robust Light Emission from Cyclic Alkylaminoluciferin Substrates for Firefly Luciferase," *J Am Chem Soc*, vol. 132, no. 39, pp. 13586–13587, Oct. 2010, doi: 10.1021/ja104525m.
- [72] B. R. Branchini *et al.*, "Red-emitting chimeric firefly luciferase for in vivo imaging in low ATP cellular environments," *Anal Biochem*, vol. 534, pp. 36–39, Oct. 2017, doi: 10.1016/j.ab.2017.07.001.
- [73] M. Yasunaga, Y. Nakajima, and Y. Ohmiya, "Dual-color bioluminescence imaging assay using green- and red-emitting beetle luciferases at subcellular resolution," *Anal Bioanal Chem*, vol. 406, no. 23, pp. 5735–5742, Sep. 2014, doi: 10.1007/s00216-014-7981-7.
- [74] M. Vacher *et al.*, "Chemi- and Bioluminescence of Cyclic Peroxides," *Chem Rev*, vol. 118, no. 15, pp. 6927–6974, Aug. 2018, doi: 10.1021/acs.chemrev.7b00649.
- [75] R. Créton and L. F. Jaffe, "Chemiluminescence Microscopy as a Tool in Biomedical Research," *Biotechniques*, vol. 31, no. 5, pp. 1098–1105, Nov. 2001, doi: 10.2144/01315rv01.

- [76] R. Amorati and L. Valgimigli, "Advantages and limitations of common testing methods for antioxidants," *Free Radic Res*, vol. 49, no. 5, pp. 633–649, May 2015, doi: 10.3109/10715762.2014.996146.
- [77] M. Yang, J. Huang, J. Fan, J. Du, K. Pu, and X. Peng, "Chemiluminescence for bioimaging and therapeutics: recent advances and challenges," *Chem Soc Rev*, vol. 49, no. 19, pp. 6800–6815, 2020, doi: 10.1039/D0CS00348D.
- [78] Y. Dotsikas and Y. L. Loukas, "Employment of 4-(1-imidazolyl)phenol as a luminol signal enhancer in a competitive-type chemiluminescence immunoassay and its comparison with the conventional antigen–horseradish peroxidase conjugate-based assay," *Anal Chim Acta*, vol. 509, no. 1, pp. 103–109, Apr. 2004, doi: 10.1016/j.aca.2003.12.007.
- [79] R. S. Chouhan *et al.*, "Detection of methyl parathion using immuno-chemiluminescence based image analysis using charge coupled device," *Biosens Bioelectron*, vol. 21, no. 7, pp. 1264–1271, Jan. 2006, doi: 10.1016/j.bios.2005.05.018.
- [80] E. Marzocchi, S. Grilli, L. della Ciana, L. Prodi, M. Mirasoli, and A. Roda, "Chemiluminescent detection systems of horseradish peroxidase employing nucleophilic acylation catalysts," *Anal Biochem*, vol. 377, no. 2, pp. 189–194, Jun. 2008, doi: 10.1016/j.ab.2008.03.020.
- [81] J. Zielonka, J. D. Lambeth, and B. Kalyanaraman, "On the use of L-012, a luminol-based chemiluminescent probe, for detecting superoxide and identifying inhibitors of NADPH oxidase: a reevaluation," *Free Radic Biol Med*, vol. 65, pp. 1310–1314, Dec. 2013, doi: 10.1016/j.freeradbiomed.2013.09.017.
- [82] F. Rezende *et al.*, "Unchanged NADPH Oxidase Activity in Nox1-Nox2-Nox4 Triple Knockout Mice: What Do NADPH-Stimulated Chemiluminescence Assays Really Detect?," *Antioxid Redox Signal*, vol. 24, no. 7, pp. 392–399, Mar. 2016, doi: 10.1089/ars.2015.6314.
- [83] K. R. Kopecky and C. Mumford, "Luminescence in the thermal decomposition of 3,3,4-trimethyl-1,2-dioxetane," *Can J Chem*, vol. 47, no. 4, pp. 709–711, Feb. 1969, doi: 10.1139/v69-114.
- [84] Y. Wang, Y. Bian, X. Chen, and D. Su, "Chemiluminescent Probes Based

- on 1,2-Dioxetane Structures For Bioimaging,” *Chem Asian J*, vol. 17, no. 6, Mar. 2022, doi: 10.1002/asia.202200018.
- [85] H. Takakura, “Molecular Design of d-Luciferin-Based Bioluminescence and 1,2-Dioxetane-Based Chemiluminescence Substrates for Altered Output Wavelength and Detecting Various Molecules,” *Molecules*, vol. 26, no. 6, p. 1618, Mar. 2021, doi: 10.3390/molecules26061618.
- [86] A. P. Schaap, M. D. Sandison, and R. S. Handley, “Chemical and enzymatic triggering of 1,2-dioxetanes. 3: alkaline phosphatase-catalyzed chemiluminescence from an aryl phosphate-substituted dioxetane,” *Tetrahedron Lett*, vol. 28, no. 11, pp. 1159–1162, Jan. 1987, doi: 10.1016/S0040-4039(00)95314-0.
- [87] A. P. Schaap, T.-S. Chen, R. S. Handley, R. DeSilva, and B. P. Giri, “Chemical and enzymatic triggering of 1,2-dioxetanes. 2: fluoride-induced chemiluminescence from tert-butyldimethylsilyloxy-substituted dioxetanes,” *Tetrahedron Lett*, vol. 28, no. 11, pp. 1155–1158, Jan. 1987, doi: 10.1016/S0040-4039(00)95313-9.
- [88] J.-Y. Koo and G. B. Schuster, “Chemically initiated electron exchange luminescence. A new chemiluminescent reaction path for organic peroxides,” *J Am Chem Soc*, vol. 99, no. 18, pp. 6107–6109, Aug. 1977, doi: 10.1021/ja00460a050.
- [89] F. A. Augusto, G. A. de Souza, S. P. de Souza Júnior, M. Khalid, and W. J. Baader, “Efficiency of Electron Transfer Initiated Chemiluminescence,” *Photochem Photobiol*, vol. 89, no. 6, pp. 1299–1317, Nov. 2013, doi: 10.1111/php.12102.
- [90] J. Liu *et al.*, “A novel chemiluminescent probe for hydrazine detection in water and HeLa cells,” *Org Biomol Chem*, vol. 17, no. 29, pp. 6975–6979, 2019, doi: 10.1039/C9OB01407A.
- [91] M. A. Partearroyo, H. Ostolaza, F. M. Goñi, and E. Barberá-Guillem, “Surfactant-induced cell toxicity and cell lysis,” *Biochem Pharmacol*, vol. 40, no. 6, pp. 1323–1328, Sep. 1990, doi: 10.1016/0006-2952(90)90399-6.
- [92] N. Hananya, A. Eldar Boock, C. R. Bauer, R. Satchi-Fainaro, and D. Shabat, “Remarkable Enhancement of Chemiluminescent Signal by

- Dioxetane–Fluorophore Conjugates: Turn-ON Chemiluminescence Probes with Color Modulation for Sensing and Imaging,” *J Am Chem Soc*, vol. 138, no. 40, pp. 13438–13446, Oct. 2016, doi: 10.1021/jacs.6b09173.
- [93] O. Green, T. Eilon, N. Hananya, S. Gutkin, C. R. Bauer, and D. Shabat, “Opening a Gateway for Chemiluminescence Cell Imaging: Distinctive Methodology for Design of Bright Chemiluminescent Dioxetane Probes,” *ACS Cent Sci*, vol. 3, no. 4, pp. 349–358, Apr. 2017, doi: 10.1021/acscentsci.7b00058.
- [94] T. Eilon-Shaffer, M. Roth-Konforti, A. Eldar-Boock, R. Satchi-Fainaro, and D. Shabat, “ortho -Chlorination of phenoxy 1,2-dioxetane yields superior chemiluminescent probes for *in vitro* and *in vivo* imaging,” *Org Biomol Chem*, vol. 16, no. 10, pp. 1708–1712, 2018, doi: 10.1039/C8OB00087E.
- [95] M. E. Roth-Konforti, C. R. Bauer, and D. Shabat, “Unprecedented Sensitivity in a Probe for Monitoring Cathepsin B: Chemiluminescence Microscopy Cell-Imaging of a Natively Expressed Enzyme,” *Angewandte Chemie International Edition*, vol. 56, no. 49, pp. 15633–15638, Dec. 2017, doi: 10.1002/anie.201709347.
- [96] J. Cao, W. An, A. G. Reeves, and A. R. Lippert, “A chemiluminescent probe for cellular peroxynitrite using a self-immolative oxidative decarbonylation reaction,” *Chem Sci*, vol. 9, no. 9, pp. 2552–2558, 2018, doi: 10.1039/C7SC05087A.
- [97] W. An *et al.*, “A Chemiluminescent Probe for HNO Quantification and Real-Time Monitoring in Living Cells,” *Angewandte Chemie International Edition*, vol. 58, no. 5, pp. 1361–1365, Jan. 2019, doi: 10.1002/anie.201811257.
- [98] S. Son *et al.*, “Chemiluminescent Probe for the In Vitro and In Vivo Imaging of Cancers Over-Expressing NQO1,” *Angewandte Chemie International Edition*, vol. 58, no. 6, pp. 1739–1743, Feb. 2019, doi: 10.1002/anie.201813032.
- [99] J. Sun, Z. Hu, R. Wang, S. Zhang, and X. Zhang, “A Highly Sensitive Chemiluminescent Probe for Detecting Nitroreductase and Imaging in Living Animals,” *Anal Chem*, vol. 91, no. 2, pp. 1384–1390, Jan. 2019, doi:

10.1021/acs.analchem.8b03955.

- [100] Y. Gong, M. Yang, J. Lv, H. Li, J. Gao, and Z. Yuan, "A 1,2-Dioxetane-Based Chemiluminescent Probe for Highly Selective and Sensitive Detection of Superoxide Anions in Vitro and in Vivo," *Chempluschem*, vol. 87, no. 4, Apr. 2022, doi: 10.1002/cplu.202200054.
- [101] A. Fu, Y. Mao, H. Wang, and Z. Cao, "An activatable chemiluminescence probe based on phenoxy-dioxetane scaffold for biothiol imaging in living systems," *J Pharm Biomed Anal*, vol. 204, p. 114266, Sep. 2021, doi: 10.1016/j.jpba.2021.114266.

2

Aim of the thesis

The research activity carried out during my Ph.D. period was mainly focused on the development and optimization of effect-based bio-chemiluminescent cell bioassays for biomedical and nutraceutical applications. In particular, my project can be divided into two principal parts. The first one concerns the development of a CL assay for intracellular H₂O₂ detection in human living cells, based on the use of a selective probe with a dioxetanic structure. Its possible applications have been studied for the evaluation of the antioxidant activity of nutraceutical compounds, and for monitoring the cellular production of H₂O₂ in freshly isolated peripheral blood mononuclear cells (PBMCs) obtained from patients with high or very high CV risk who experienced 2-month treatment with the monoclonal antibody Evolocumab. The second part instead described the development of a bioluminescent recombinant protein, the Jagged1-FLuc, as a potential diagnostic tool for the high-throughput screening of colorectal cancer (CRC). CRC has a substantially favorable prognosis if diagnosed in the early stages, but available tests for CRC screening like fecal occult blood (FOBT) or colonoscopy are not very sensitive or badly tolerated by patients, therefore the discovery of new predictive biomarkers is highly demanded. Recent studies suggest a pivotal role of the “aberrant” Notch signaling activation in CRC, partially due to cross-talks with other pathways. In this context, we developed a recombinant protein using the Baculovirus expression system in insect cells. Specifically, the protein combines the extracellular domain (ECD) of the Notch high affinity mutated form of one of the selective Notch ligands defined as Jagged 1 (Jag1) with a Red emitting firefly luciferase, in order to understand if Jagged1-FLuc binding correlates with a Notch signaling overexpression and activation in CRC progression.

In chapter 3 the development and validation of the selective chemiluminescent TURN-ON quantitative bioassay for the evaluation of intracellular H₂O₂ is proposed. This selective CL probe for H₂O₂ consists of an adamantylidene - 1,2 - dioxetane containing an arylboronate moiety, which in the presence of H₂O₂ is converted to the correspondent phenol and

emits green light at 540 nm with high efficiency. Firstly, the correlation between the CL emission and the concentration of H₂O₂ was investigated in a cell-free system, and once the method was optimized, we moved on to human cell models. We used a primary culture of human umbilical vein endothelial cells (HUVEC) and two immortalized cell lines: human colorectal adenocarcinoma cells (Caco-2) and human keratinocytes (HaCaT). Menadione, phorbol myristate acetate (PMA), and lipopolysaccharide (LPS) were used as oxidative agents at different concentrations. To confirm the intracellular localization of the probe, we performed CL imaging experiments on the cell models. Finally, we used the dioxetane CL probe to develop a cellular CL assay for measuring the antioxidant activity of a *Brassica juncea* “broad-leaf” solutions as proof of concept.

In chapter 4 three red pomace extracts were evaluated on 3D human keratinocytes, to test their anti-inflammatory and antioxidant activities hypothesizing their possible application in the cosmeceutical field.

Phenolic compounds contained in red pomace were extracted using three different natural deep eutectic solvents (NaDES): betaine-citric acid (BET-CA), betaine-urea (BET-U), and betaine-ethylene glycol (BET-EG). The polyphenol content was determined by HPLC-MS/MS analysis. A permeation study using Franz cells model was performed to assess the bioavailability of these compounds. Cell viability and cytotoxicity were measured using spectrophotometric techniques. Antioxidant and anti-inflammatory activities were evaluated through the CL bioassay for the intracellular H₂O₂ detection mentioned above, and the ELISA assay for interleukin (IL)-8 release, respectively.

Chapter 5 reports the effects of *Lactiplantibacillus Plantarum* fermentation on the antioxidant and immunomodulatory properties of *Vaccinium floribundum* (VF) berries in HUVECs and macrophages (RAW264.7). The polyphenol profile was determined by HPLC-ESI MS/MS analysis. Spectrophotometric (SP) assays ensured the safety of berries solutions on HUVECs and

RAW264.7 viability. The antioxidant and immunomodulatory properties of fermented berries were measured through the CL bioassay, real-time polymerase chain reaction (RT-qPCR), and SP techniques.

High levels of low-density lipoprotein cholesterol (LDL-C) and the overproduction of reactive oxygen species (ROS) underlie vascular inflammation and the development of CVDs. Therefore, to reduce LDL-C levels, the novel drug Evolocumab which inhibits proprotein convertase subtilisin/kexin type 9 (PCSK9) has been recently introduced into clinical practice. Thus, in chapter 6 we present data from 18 male subjects with high or very high CV risk who experienced 2-month treatment of Evolocumab in association with Ezetimibe and/or a statin. Treatments showed an improvement in BP-adjusted carotid-femoral pulse wave velocity (cfPWV) (P-value= 0.0005), which was significantly associated with a decrease of H₂O₂ production in PBMCs (P-value= 0.02). Evaluation of H₂O₂ production in PBMCs was assessed through the CL bioassay based on the dioxetane probe.

In chapter 7 the development of the recombinant bioluminescent protein Jagged1-Fluc is reported. The protein was obtained using the baculovirus expression system to maintain the post-translational modifications typical of human proteins. Once the protein has been developed, we set up the optimized conditions for Jagged1-Fluc in a cell-free system and then we move on to a cell model of Caco-2 cells, which express high levels of the Notch3 isoform. In Caco-2 we observed that the BL signal increase was proportional to the Notch3 expression, with a linear range from 0.1 to 50 µg/mL of Jag1-FLuc obtaining a LOD and LOQ of 0.8 ± 0.2 and 6.0 ± 0.2 µg/mL, respectively. In parallel, imaging experiments were performed to examine the light output of the Jagged1-FLuc construct on Caco-2.

3

Selective chemiluminescent TURN-ON quantitative bioassay and imaging of intracellular hydrogen peroxide in human living cells

Reproduced from: “Selective chemiluminescent TURN-ON quantitative bioassay and imaging of intracellular hydrogen peroxide in human living cells”

*Donato Calabria, Massimo Guardigli, Mara Mirasoli, **Angela Punzo**, Emanuele Porru, Martina Zangheri, Patrizia Simoni, Eleonora Pagnotta, Luisa Ugolini, Luca Lazzeri, Cristiana Caliceti and Aldo Roda.*

Analytical biochemistry, 2020; 600, 113760.

Reproduced by permission of Elsevier

<https://www.elsevier.com/about/our-business/policies/copyright#Author-rights>

3.1 Introduction

In recent years, free radicals have gained increasing importance in biomedicine, owing to their dual role in the human body. Emerging data indicate that generation and reactivity of free radicals and other oxidants are harnessed to regulate numerous redox-dependent physiological processes. In turn, uncontrolled production and deregulation of redox signaling are implicated in the initiation and propagation of several pathological conditions, such as cardiometabolic, neurodegenerative, and cancer diseases [1]. Since reactive oxygen and nitrogen species include a broad range of chemically distinct species with diverse biological reactivities, it is essential to detect, localize and characterize these species accurately in biological systems to clearly attribute a particular cell event to a specific chemical entity. Hydrogen peroxide (H_2O_2) is one of the major members of reactive oxygen species (ROS) in living organisms and plays an important role in the regulation of a variety of biological processes [2]. However, when it is not properly managed by the body or is produced in excess (as under certain kinds of stress) it can lead to chronic pathologies [3]. In addition, various ROS are converted to H_2O_2 within cells [4], therefore a change in H_2O_2 level can reasonably reflect a general change in the intracellular ROS production. Several bioanalytical approaches have been proposed to detect intracellular H_2O_2 [5]. The most common technique consists in the use of fluorescent probes such as 2',7'-dichlorodihydrofluorescein diacetate (DCFH₂-DA), Amplex Red, dihydrorhodamine, phosphine-based fluorophores, lanthanide coordination complexes, and redox-responsive fluorescent substances [6, 7]. However, current fluorescent probes have several limitations, the main one being their insufficient selectivity to H_2O_2 over other ROS, which is critical for the accurate measurement of intracellular H_2O_2 levels [8, 9]. For example, the fluorescent probe DCFH₂-DA, widely used to detect intracellular oxidant species, does not directly react with H_2O_2 , and its fluorescence results from the interaction with strong oxidants, such as those produced from metal ion and peroxidase-catalyzed reactions of H_2O_2 and from the decomposition of ONOO^- [8, 10]. Indeed, we found that the fluorescence signal of DCFH₂ was enhanced by the concentration of Fe^{2+} , while for a fixed

amount of Fe^{2+} no correlation was observed between the fluorescence emission and the concentration of H_2O_2 up to $100 \mu\text{M}$ [11]. In addition, tissues, individual cells, and subcellular structures scatter visible light extensively [12], thus scattering of fluorescence emission occurs at the surface and inside live cells. Consequently, the use of fluorescent probes in imaging of biological samples may suffer from low signal-to-noise due to scattering of emitted fluorescence and sample autofluorescence. Poor photostability due to photobleaching could also represent an issue for some fluorophores [8]. Therefore, novel selective probes with reduced background interferences are required to perform quantitative studies on intracellular H_2O_2 . Chemiluminescence (CL)-based methods are gaining increased interest for studying biological systems, as they maintain the simplicity of optical techniques and provide easy signal quantification and high signal-to-noise ratios [13]. The absence of any external excitation light source is particularly attractive because it avoids the drawbacks of fluorescent probes, also facilitating imaging of relatively thick specimens as inferred from recent animal studies [14, 15]. On the other hand, the main limitation of CL is the weakness of the light signal and possible interference in the chemistry of the CL reaction (pH, ionic strength, etc). Chemiluminescence also offers some advantages over bioluminescence (BL) which could be used alternatively, as light generation can be initiated by a specific chemical reaction without further enzymatic dependency and no genetic cell engineering is required to express BL enzymes such as luciferases [16]. Spontaneous ultraweak photon emission, which is related to by-products of the chemical reactions of cell metabolisms, has been used to monitor ROS in cells, However, its applicability in biomedical studies is limited by the very low signal intensity that requires the use of ultra-high sensitive photon counting systems [17]. Chemiluminescent probes such as luminol, lucigenin and their derivatives, whose oxidation gives reasonably high yields of electronically excited, light-emitting products (the CL quantum yields of luminol and lucigenin are 0.012 [18] and 0.01-0.02 [19], respectively) solved this issue by increasing the photon output by several orders of magnitude. These probes have been applied in cell-based assays to investigate respiratory burst in polymorphonuclear neutrophils

and phagocytes and to non-invasively image ROS and reactive nitrogen species (RNS) in living mice under pro-inflammatory conditions [20, 21]. However, these compounds have low bioavailability and cannot discriminate between different ROS species. So far, only a few CL systems specific for the selective detection of H₂O₂ and suitable for quantitative assays or *in vitro* and *in vivo* imaging have been described. For example, nanoparticles containing a peroxalate derivative and a fluorescent acceptor have been employed for H₂O₂ measurements, although reports regard *in vivo* imaging in mice models [22 - 24] or *in vitro* measurements in cells challenged with the exogenous addition of H₂O₂ [25] rather than evaluation of increase of intracellular H₂O₂ as a result of physiological pro-oxidant stimuli (such as inflammatory cytokines). Recently, a new family of CL dioxetane-based luminophores that emit light under physiological conditions (i.e. pH 7.4) with high efficiency has been developed [26]. Since spontaneous decomposition and chemiexcitation followed by light emission of such molecules can be triggered by the presence of a phenolic group, specific turn-on CL probes have been obtained by introducing in the luminophore a phenolic function masked by target-responsive groups. Chemiluminescent probes based on these luminophores have been successfully developed for the selective detection of various species, from enzymes (e.g., alkaline phosphatase, β -galactosidase and nitroreductase) to molecules such as formaldehyde, peroxyxynitrite and H₂O₂ [26]. In particular, the H₂O₂ CL probe employed an aromatic boronate as the target-responsive group. Indeed, aromatic boronates, which have already been exploited to increase the selectivity of fluorescent H₂O₂ probes, are particularly suited as responsive groups for CL dioxetane-based luminophores because they react with H₂O₂ to form the corresponding phenol with reaction yields close to 100% [27, 28]. In this work, we exploited for the first time the possibility of using a dioxetane-based CL probe containing a boronate moiety selective for H₂O₂ [29, 30] for quantitative monitoring of the intracellular production of H₂O₂ in different types of human living cells, i.e., endothelial, intestinal and keratinocyte cells, and evaluation of its inhibition by antioxidants (**Fig. 3.1**). As a proof of concept, the bioassay has been used to measure the antioxidant activity of extracts from

different tissues of a *Brassica juncea* “broad-leaf” selection which has a high biomass production and contains glucosinolates (GSLs), isothiocyanates (ITCs) and other antioxidant molecules characteristic of *Brassicaceae* family [31]. Our aim was to set up and validate an *in vitro* highly predictive cell-based assay capable to mimic the physiological oxidative stress and its response to external stimuli without employing any genetic manipulation.

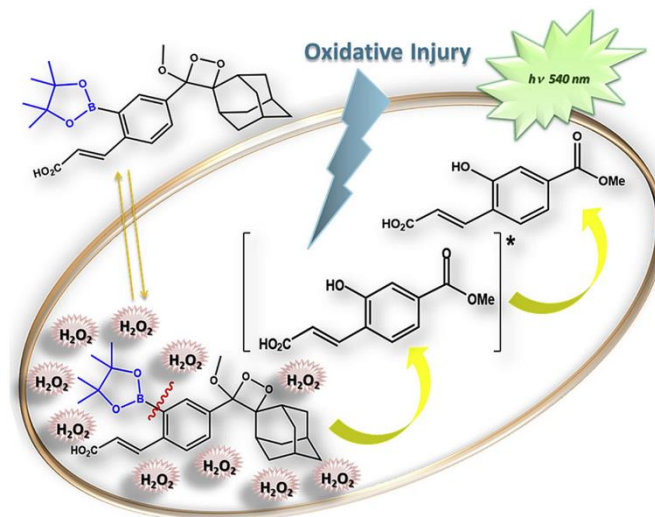


Figure 3.1: Schematic representation of chemiluminescent probe mechanism inside the cell.

3.2 Material and Methods

3.2.1 Chemicals

The dioxetane CL probe (AquaSpark™ Peroxide Probe) was kindly provided by Biosynth (Staad, Switzerland). A 10 mM stock solution was prepared by dissolving the probe in DMSO (the CL probe solution is stable for months when stored at 4 °C and protected from light). Phosphate-buffered saline (PBS) tabs (giving a 137 mM NaCl, 2.7 mM KCl and 10 mM phosphate buffer solution, pH 7.4), H₂O₂ solution, gelatine from bovine skin, trypsin-EDTA, oxidative stress inducers (menadione, phorbol myristate acetate - PMA and lipopolysaccharide - LPS), antioxidants (Trolox, lipoic acid and gallic acid), phenethylisothiocyanate, allyl isothiocyanate and N(G)- monomethyl-L-arginine monoacetate (L-NMMA) were purchased from Sigma-Aldrich (St Louis, MO, USA). All other chemicals and

solvents were of the highest analytical grade. Stock solutions of the pro-oxidants menadione (100 mM), phorbol myristate acetate (PMA, 10 mM) and lipopolysaccharide (LPS, 5 mg mL⁻¹) were prepared by dissolving the compounds in DMSO (menadione and PMA) or PBS (LPS). Stock solutions of antioxidants (Trolox, lipoic acid and gallic acid) were obtained by dissolving the antioxidants in DMSO to a final concentration of 10 mM. Dulbecco's Modified Eagle Medium (DMEM) high glucose and MEM Non-Essential Amino Acids solution 100X were purchased from Microgem (Naples, Italy). M200 medium, Low Serum Growth Supplements 50X (LSGS) and Fetal Bovine Serum (FBS) were from Thermo Fischer Scientific (Waltham, MA, USA). Antibiotic solution 100X (10,000 U/mL penicillin and 10 mg/mL streptomycin) was purchased from Sigma-Aldrich. The ROS-Glo™ H₂O₂ Assay and the Cytotoxicity LDH Assay kits were purchased from Promega (Madison, Wisconsin, USA) and Dojindo Molecular Technologies (Rockville, MD, USA), respectively.

3.2.2 Plant material

Brassica juncea "broad-leaf" selection was provided from the *Brassicaceae* seed collection of CREA-CI [31]. This *B. juncea* has some interesting peculiarities with respect to the other varieties, such as a high biomass production both in pot and open field. Two plants for container were grown in square pots (22 cm side and 8 L volume). Tissue samples were collected at completely developed inflorescences. Four plants randomly chosen from 6 pots were harvested, and roots, stem, and leaves tissues were separately collected and immediately frozen. Samples were finally freeze-dried and finely powdered to 0.5 mm size. Extraction and characterization of bioactive molecules are described in supplementary materials.

3.2.3 Cell cultures

Human umbilical vein endothelial cells (HUVEC), purchased from Life Technologies, were plated on gelatin-coated tissue culture dishes and maintained in phenol red-free basal medium M200 containing 10% FBS and LSGS at 37 °C with 5% CO₂. Actively proliferating cells (passages 3 to 7, 70 – 90% confluency)

were harvested for experiments. Caco-2 cells, obtained from the American Type Culture Collection (ATCC), were maintained in DMEM high glucose containing 10% FBS, 2.5 mM L-glutamine, Antibiotic-Antimycotic solution and MEM Non-Essential Amino Acids solution. HaCaT cells, kindly gifted by Prof. F. Martini (University of Ferrara), were maintained in DMEM high glucose containing 10% FBS, 2.5 mM L-glutamine and Antibiotic-Antimycotic solution.

3.2.4 Cytotoxicity assay

Lactate dehydrogenase (LDH) release from cells was monitored in the culture medium using a spectrophotometric LDH assay (Cytotoxicity LDH Assay Kit). The assay was performed in the standard 96-well microtiter plate format according to manufacturer's instructions and the absorbance increase after 24 h of incubation at 37 °C was monitored using a Varioskan™ Flash Multimode Reader (Thermo Scientific) [32].

3.3 Bioassay procedure

3.3.1 Principle of the bioassay

The selective CL probe for H₂O₂ designed by Shabat's research group [27] was based on the previous Schaap's adamantylidene-dioxetane probes [33]. Adamantylidene-dioxetane probes are single-component CL systems characterized by reasonable aqueous solubility, and therefore they do not require to be included in nanoparticles. For these features, such probes are ideally suited for intracellular imaging of H₂O₂ with negligible cytotoxicity and/or cellular perturbation effects. Differently from the Schaap's probes, the presence of an electron-withdrawing acrylic group in the aromatic ring results in the production of excited species that emits light with greater efficiency in aqueous solution, thus increasing CL emission intensity. Detection of H₂O₂ relies on a deprotection mechanism (**Fig. 3.2**). Nucleophilic addition of H₂O₂ to the boronate ester (**1**) generates the charged tetrahedral boronate complex (**2**), which undergoes a "1,2-insertion" by the C—B bond migration to one of the electrophilic peroxide oxygens. The borate ester (**3**) is then hydrolyzed to the

phenol generating an unstable phenolate–dioxetane species (**4**), which produces the excited- state benzoate ester (**5**) *via* a chemically-initiated electron-exchange luminescence (CIEEL) mechanism. The excited benzoate ester then decays to its ground state (**6**) with emission of photons at 540 nm.

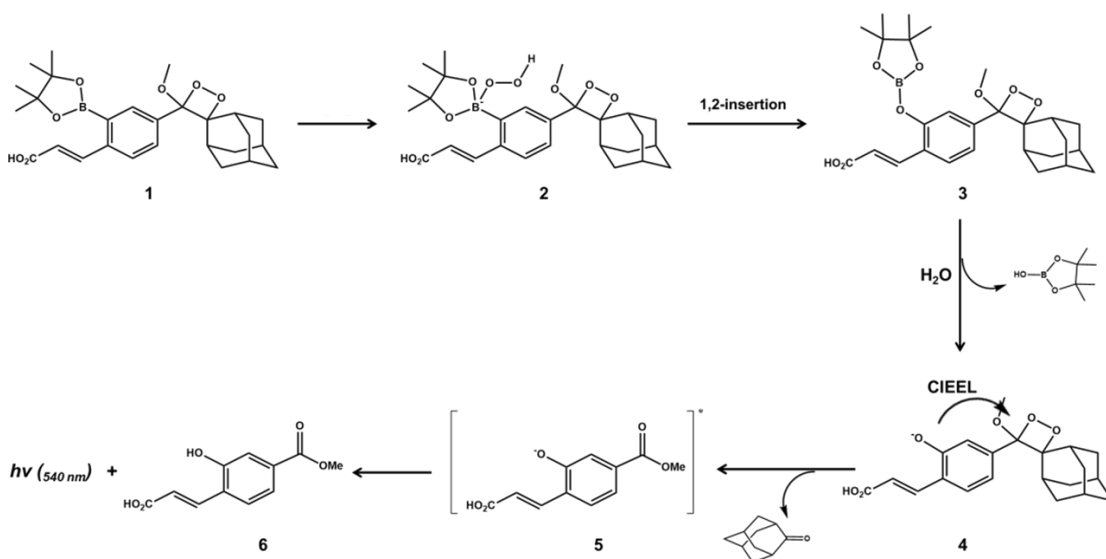


Figure 3.2: Activation pathway of H₂O₂ CL probe, adapted with permission from Ref. [30]. Copyright (2017) American Chemical Society.

3.3.2 Calibration curve for quantification of H₂O₂

The dioxetane CL probe working solution (10 μM) was prepared by diluting the 10 mM stock solution with PBS. The H₂O₂ standard solutions for generating the calibration curve (concentration range 0.5 – 40 μM) were prepared in PBS. For the cell-free CL measurement, 100 μL of the H₂O₂ standard solutions (PBS for the blank) were dispensed in the wells of a 96-well black microtiter plate, then the reaction was started by adding 100 μL of the dioxetane CL probe working solution and the resulting CL emission was monitored for 60 min using a luminometric plate reader (ThermoFisher Scientific). The calibration curve was obtained by plotting the CL signal (evaluated as the CL emission integrated between 40 and 60 min after addition of the CL probe) versus the actual concentration of H₂O₂ and fitting the experimental data to a straight line using

the method of least squares. The limits of detection (LOD) and quantification (LOQ) of the assay were evaluated as the concentrations of H₂O₂ giving CL signals corresponding to those of the blank plus three and ten times its standard deviation, respectively.

3.3.3 Quantification of intracellular H₂O₂ in human living cells

Standard solutions of the pro-oxidants menadione (3.2 to 50 μM), PMA (12.5 to 100 μM) and LPS (3.25 to 75 μg mL⁻¹) were prepared in PBS. HUVEC (10 × 10³ cells well⁻¹), Caco-2 (25 × 10³ cells well⁻¹) or HaCat (100 × 10³ cells well⁻¹) cells were plated in the wells of a 96-well black microtiter plate for 24 hours and then incubated for 20 min with 100 μL of the dioxetane CL probe working solution. Then, 100 μL of standard solutions of the pro-oxidant (PBS as the negative control) were added to induce intracellular H₂O₂ production and the CL emission was monitored for 40 min using a luminometric plate reader. The whole assay was conducted at 37 °C and the dose-response curve was obtained by plotting the CL signal versus the actual concentration of the pro-oxidant and fitting the experimental data to a straight line using the method of least squares.

3.3.4 Method validation

Method validation was performed by comparison with the commercial bioluminescent (BL) enzymatic assay (ROS-Glo™ H₂O₂ Assay from Promega, Madison, Wisconsin, USA) for the measurement of intracellular H₂O₂ after cell lysis. The BL emission was measured in black 96-well microtiter plates according to manufacturer's instructions using a luminometric plate reader.

3.3.5 Assay for antioxidant activity in human living cells

All the assays were conducted at 37°C in 96-well black microtiter plates; CL signals were measured employing a luminometric plate reader.

Caco-2 cells were plated in the wells for 24 hours at a seeding density of 25 × 10³ cells well⁻¹ and then incubated for 20 min with 100 μL of PBS containing one antioxidant (Trolox, lipoic acid or gallic acid, concentration range 0.02 – 20 μM) and the dioxetane CL probe (10 μM). Then, 100 μL of PBS solutions of

menadione (50 μM), PMA (100 μM) or LPS (75 $\mu\text{g mL}^{-1}$) were added and the CL emission was monitored for 40 min. The dioxetane CL probe working solution was used as the control.

B. juncea extracts were diluted with PBS to obtain concentrations ranging from 1.0 to 0.015 $\mu\text{g mL}^{-1}$ (referred to the starting lyophilized material). Caco-2 cells were plated in the wells for 24 hours at a seeding density of 25×10^3 cells well⁻¹ and treated for 24 h with 100 μL of the extracts. Upon removing the solution, cells were incubated for 20 min with 100 μL of the dioxetane CL probe working solution. Finally, 100 μL of PBS solution of menadione (50 μM) were added and the CL emission was monitored as described above.

3.3.6 Chemiluminescence imaging experiments

Imaging experiments were performed using an Olympus IX73 inverted microscope (Olympus Corporation, Tokyo, Japan) equipped with an ultrasensitive EM-CCD camera (ImagEM X2, Hamamatsu Photonics KK, Shizuoka, Japan) controlled by the proprietary software HCLImage v.

4.2.6.1 and enclosed in a dark box to prevent interference from ambient light. Caco-2 cells (100×10^3 cells well⁻¹) were grown in a 24-well transparent microtiter plate for 24 h at 37 °C with 5%CO₂, then the medium was removed and the cells were incubated for 20 min at 37 °C with 500 μL of a 10 μM dioxetane CL probe working solution. Afterwards, 500 μL of a 50 μM solution of menadione was added and the CL emission was imaged for 30 min using a 5-min exposure time. Image processing was performed using the freely available Java-based software ImageJ v. 1.52d [34].

3.3.7 Data analysis

GraphPad Prism v. 6.05 (GraphPad Software, Inc., La Jolla, CA, USA) was used to plot the experimental data and for the least-squares fitting of calibration, dose-response curves (for evaluation of antioxidants and extracts IC₅₀ values) and assay comparison graphs.

3.4 Results and discussion

3.4.1 Quantitative detection of H₂O₂ in cell-free system

First, the correlation between the CL emission and the concentration of H₂O₂ was investigated in a cell-free system. We were particularly interested in the possibility to detect small H₂O₂ amounts because we expected low intracellular H₂O₂ levels, which to our knowledge have never been quantitatively evaluated by CL. As shown in **figure 3.3A**, CL measurements were carried out between 40 and 60 min after addition of the CL probe and the integrated CL emission in this time interval was used as the analytical signal. This signal integration period was chosen to avoid any contribution due to the nonspecific CL emission observed at short times, which is presumably owing to the presence of small amounts of free dioxetane in the probe (the CL probe itself is stable in the assay conditions: as shown in [30], RP-HPLC analysis indicated no decomposition even after 3 hours at room temperature). The same signal integration period has been used in cell-based experiments, thus making the calibration curve suitable for evaluation of intracellular H₂O₂. The calibration curve showed a good linear correlation between the CL signal and the concentration of H₂O₂ up to 20 μM (**Fig. 3.3B**). The LOD and LOQ of the assay were 0.18 μM and 0.60 μM, respectively, which corresponded to 3.6×10^{-11} and 1.2×10^{-10} mol well⁻¹ of H₂O₂.

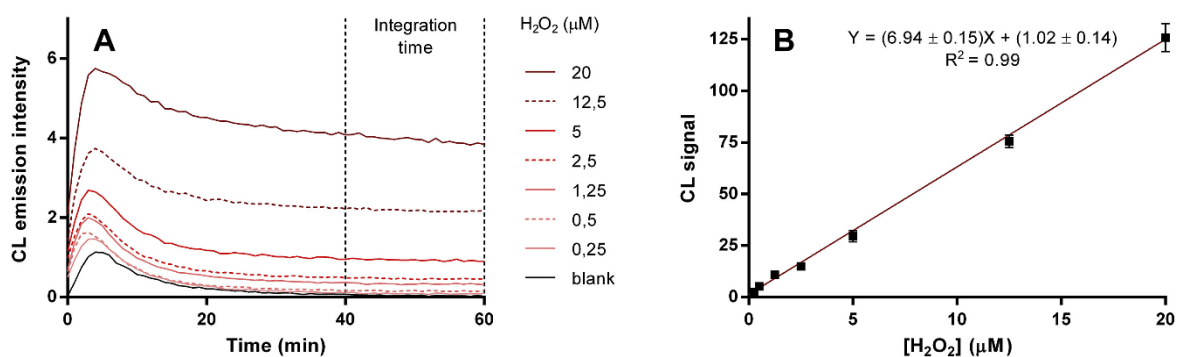


Figure 3.3: (A) Chemiluminescence kinetic profiles obtained in PBS containing the dioxetane CL probe (5 μM) and different concentrations of H₂O₂. (B) Calibration curve showing the correlation between the CL signal and the concentration of H₂O₂. Each point represents the mean ± SD of three independent measurements.

3.4.2 Quantification of intracellular H₂O₂ in human living cells

The dioxetane CL probe was employed to measure the intracellular concentration of H₂O₂ in different human cell models upon pro-oxidant stimuli. We used a primary culture of human umbilical vein endothelial cells (HUVEC) and two immortalized cell lines, human colorectal adenocarcinoma cells (Caco-2) and human keratinocytes (HaCaT). Menadione, PMA and LPS were used as pro-oxidants. Menadione is a polycyclic aromatic ketone that increases intracellular H₂O₂ production by affecting mitochondrial respiration and glutathione depletion [35, 36], PMA is known to stimulate intracellular NADPH oxidase [37] and LPS is a glycolipid component of the cell wall of Gram-negative bacteria commonly considered as a molecular pattern triggering the production of proinflammatory mediators and oxidative stress into cells [38].

Figure 3.4A shows the kinetic profiles of the CL emission measured in Caco-2 cells upon treatment with different concentrations of menadione. As expected, the CL emission intensity increased with the concentration of the stimulant (**Fig. 3.4B**). By using the calibration curve obtained in the cell-free system, the amount of H₂O₂ in Caco-2 cells treated with 25 μM menadione was estimated to be 1.6×10^{-10} mol well⁻¹, while the H₂O₂ content of control cells was comparable to the LOD of the assay, *i.e.*, around 3×10^{-11} mol well⁻¹.

Moreover, we evaluated the precision of our bioanalytical procedure, obtaining intra-assay CV% lower than 10.0% (<25% Acceptance Criteria) and inter-assay CV% lower than 20.0% (<25% Acceptance Criteria). To confirm the intracellular localization of the emission of the probe, we also performed CL microscope imaging experiments on Caco-2 cells. The results (**Fig. 3.4C**) clearly showed that the CL emission is localized inside the cells, thus confirming the ability of the probe to penetrate in the cells and react with intracellular H₂O₂. This conclusion was also supported by the high value ($\log D_{ow} = 5.49$) of the octanol/water distribution coefficient of the probe evaluated *in silico* at pH = 7.4 using the AlogPs (v. 2.1) *on-line* tool [39]. To confirm the intracellular localization of the emission of the probe, we also performed CL microscope imaging experiments on the three cell models using all the pro-oxidant stimuli (menadione, LPS and PMA). Menadione-treated Caco-2 cells showed the

highest CL signals (**Fig. 3.4C**), and the localization of the CL signals inside cells clearly demonstrated the ability of the probe to penetrate in the cells and react with intracellular H_2O_2 . Moreover, we directly treated cells with H_2O_2 (10–100 μM) after medium replacement and we observed by microscope imaging experiments that the CL signal was mainly confined inside the cells, confirming the intracellular accumulation of the probe (data not shown). We have not routinely carried out the medium replacement to avoid cell detachment.

We also excluded the possibility that the CL probe is oxidized in medium and then the phenolate–dioxetane species diffuse into cells considering the higher cell membrane permeability of the boronate ester ($\text{LogP} = 5.49$ calculated by *in silico* analysis) compared to both phenol ($\text{LogP} = 3.80$) and phenolate ($\text{LogP} = 3.54$) intermediates. Moreover, the reaction of boronic ester with H_2O_2 is quite slow ($k \sim 1\text{--}2 \text{ M}^{-1}\text{s}^{-1}$) [40], as also shown by the CL kinetics obtained in the cell-free system, thus the concentration of the CL probe in solution should remain high enough to effectively enter in cells.

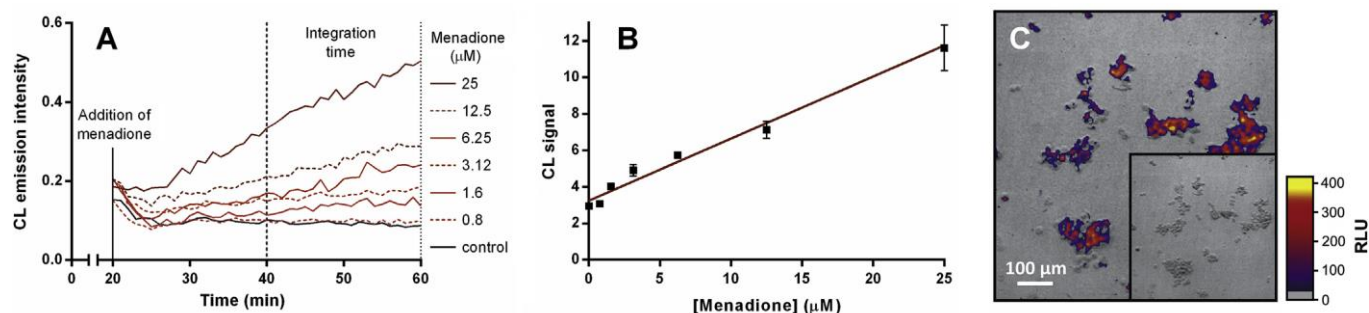


Figure 3.4: (A) Chemiluminescence kinetic profiles obtained for Caco-2 cells in the presence of the dioxetane CL probe and different concentrations of menadione. (B) Dose-response showing the correlation between the CL signal and the concentration of menadione. Each point represents the mean \pm SD of three independent measurements. (C) Overlay of CL image taken 20 min after addition of menadione (converted in pseudocolors according to the intensity of the emission) and of live image of Caco-2 cells (objective magnification 10X) obtained in the presence of the dioxetane CL probe and of 25 μM menadione (inset: live image of the cells). Bar represents 100 μm .

A good correlation between the CL signal and the concentration of the pro-oxidant stimulus was observed for all the investigated cell models (**Fig. 3.5 A-C** and **Table 3.1**), which was consistent with the physiological regulation mechanisms of intracellular H₂O₂ production.

The concentrations of pro-oxidants required to obtain a detectable increase in the CL signal were in the micromolar range for menadione and PMA (i.e., 1.5 - 3.0 μM for menadione and 2.0 - 10.0 μM for PMA, depending on the cell model) and ranged from 0.5 to 2.5 μg mL⁻¹ for LPS.

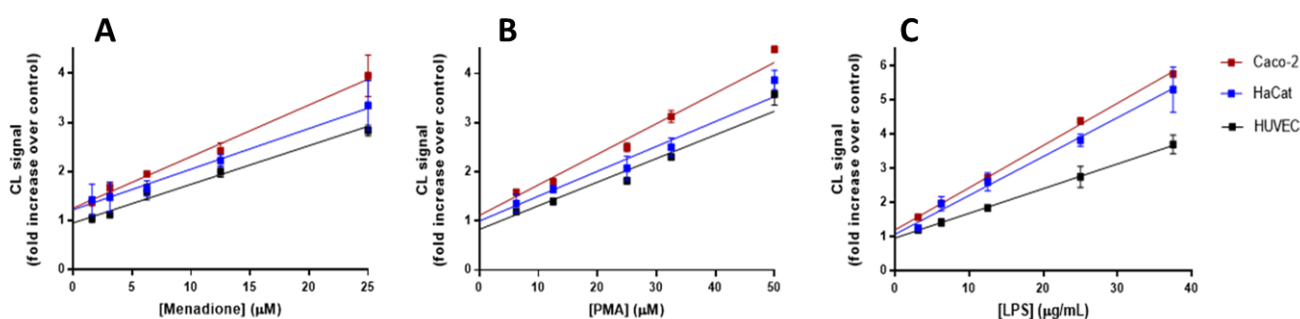


Figure 3.5: Chemiluminescence signals obtained in Caco-2, HaCat and HUVEC cells in the presence of the dioxetane CL probe and of different concentrations of (A) menadione, (B) PMA, and (C) LPS. To facilitate the comparison between different inductors or cell types, the CL signals were reported as the ratio between the signal obtained in the presence of the pro-oxidant and the signal of the control. Each point represents the mean \pm SD of three independent measurements.

Interestingly, for all the pro-oxidants the highest CL signal increment was obtained in Caco-2 cells, which is consistent with their nature (Caco-2 cells originated from a colorectal adenocarcinoma and cancer cells are generally characterized by an increased H₂O₂ production rate and an impaired redox balance [41]).

Since different cell models vary in both H₂O₂ production and, possibly, in permeability of cell membrane to the CL probe, we related the CL signal upon pro-oxidant stimuli treatment to the value of blank (i.e., untreated cells) in order to obtain just the increase of H₂O₂ level independently to the nature of cells.

Since a pro-oxidant stimulus causes cells to produce a variety of reactive species other than H_2O_2 , probe selectivity represents a critical issue for the accurate quantification of H_2O_2 .

Green et al. [33] already investigated the selectivity of the H_2O_2 CL probe towards various ROS by measuring its response to tert-butyl hydroperoxide, hypochlorite, singlet oxygen, hydroxyl radical and tert-butoxyradical in a cell-free system. Peroxynitrite (ONOO^-) represents another potentially interfering species due to its rapid reaction with aromatic boronates at physiological pH [42].

Peroxynitrite derives from the reaction of superoxide with nitric oxide, which is mainly produced by enzymes belonging to the family of nitric oxide synthases (NOS), thus inhibition of NOS activity should efficiently suppress the production of ONOO^- by cells. Therefore, to exclude any interference from ONOO^- in the detection of H_2O_2 we also performed experiments in the presence of the cell- permeable competitive NOS inhibitor N(G)-monomethyl-L-arginine monoacetate (L-NMMA).

As shown in **Supplementary Figure S1A**, we didn't observe any significant CL signal change in Caco-2 cells treated with 25 μM PMA upon exposition to 100 μM L-NMMA for 6 and 24 hours. We also investigated the CL signals in cells preincubated with 50 ng/ml of $\text{TNF}\alpha$ for 24 hours, able to induce the expression of the inducible NOS isoform (iNOS) [43]. **Supplementary Figure S1B** clearly showed that even in this case a contribution to the CL emission due to the reaction of the probe with ONOO^- can be excluded.

These results suggest that the bioassay could be used to selectively quantify H_2O_2 in real time in living cells. According to the literature, at physiological pH the reaction between ONOO^- and boronates is very fast [42].

Therefore, the absence of any significant contribution to the CL signal due to the reaction of the probe with ONOO^- can be explained assuming that intracellular peroxynitrite levels are lower than that of H_2O_2 . It should be also considered that the higher specificity of ONOO^- towards aryl-boronate esters was mainly tested using concentrations hundreds of folds higher than the physiological levels [44].

Table 3.1: Slopes and coefficients of correlation (R^2) of the linear relationships between the CL signal and the concentration of pro-oxidant stimulus obtained in Caco-2, HaCat and HUVEC cells. Each result is the mean \pm SD of the independent experiments.

Pro-oxidant stimulus	Caco-2 cells		HaCat cells		HUVEC cells	
	Slope \pm SD	R^2	Slope \pm SD	R^2	Slope \pm SD	R^2
Menadione	0.105 \pm 0.007	0.988	0.083 \pm 0.005	0.991	0.079 \pm 0.007	0.977
PMA	0.062 \pm 0.006	0.977	0.051 \pm 0.006	0.963	0.048 \pm 0.006	0.956
LPS	0.124 \pm 0.002	0.999	0.114 \pm 0.008	0.985	0.072 \pm 0.001	0.999

3.4.3 Method validation

Being a cellular standard reference material with known intracellular H_2O_2 content not available, the assay accuracy was evaluated by comparing our results with those obtained employing ROS-Glo™ H_2O_2 assay, a BL enzymatic assay that measures H_2O_2 on lysed cells. This assay employs a modified luciferin substrate that, upon cell lysis, reacts with H_2O_2 generating a luciferin precursor, which is then converted to luciferin upon the addition of a solution containing D-cysteine. Finally, luciferin is detected by BL upon addition of a recombinant luciferase. Even if this method used cell lysates and requires longer assay times, results are comparable. For all cell types, we found a good correlation between the luminescence signals obtained in the presence of increasing concentrations of menadione (**Fig. 3.6**), thus demonstrating the ability of the dioxetane CL probe to provide accurate results. Furthermore, in comparison to the ROS-Glo™ Assay, the CL probe allowed easier and real-time measurement of intracellular H_2O_2 even in a small number of cells, avoiding long reagent preparations (the CL probe is the only reactant) and time-consuming pre-treatment procedures (no cell lysis is required).

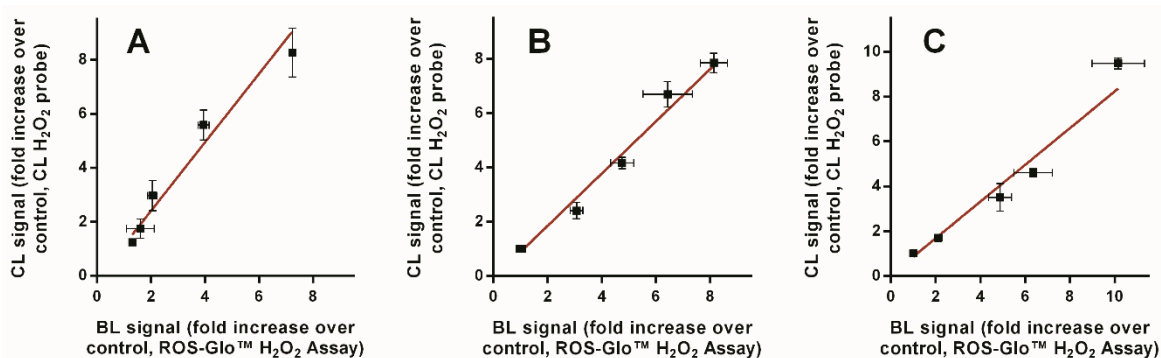


Figure 3.6: Comparison of the luminescence signal observed in (A) Caco-2, (B) HaCat, and (C) HUVEC cells in the presence of different concentrations of menadione (up to 50 μM) using the CL H_2O_2 probe and the ROS-Glo™ H_2O_2 Assay. To facilitate the comparison between the assays, the signals were reported as the ratio between the signal obtained in the presence of the pro-oxidant and the signal of the control. Each point represents the mean \pm SD of three independent measurements.

3.4.4 Cell-based assay for antioxidant activity

Finally, we used the dioxetane CL probe to develop a cellular CL assay for measuring antioxidant activity. As standard antioxidant compounds we used well-known molecules such as Trolox (a water-soluble analogue of vitamin E), lipoic and gallic acids. Trolox has advantages over α -tocopherol, which is lipid soluble, because it can be enter in both aqueous and lipidic compartments of cells [45]. Moreover, Satoh et al. have claimed that the antioxidant property of Trolox surpasses that of α -tocopherol [46]. α -Lipoic acid itself is not a strong antioxidant, but its reduction within cells produces the dithiol derivative (dihydrolipoic acid, DHLA), a more powerful antioxidant [47]. PEG-conjugated catalase was not assayed as an intracellular antioxidant because of its complex and quite long mechanism of access into the cell [48, 49].

Simultaneous treatment of cells with pro-oxidants and various concentrations of antioxidants in the presence of the dioxetane CL probe allowed to measure the decrease of intracellular H_2O_2 due to the presence of antioxidants, then to obtain the dose-response curves (data not shown) and the antioxidant IC₅₀ values.

Table 3.2 shows the IC₅₀ values of Trolox and lipoic acid obtained in Caco-2 cells using different pro-oxidant stimuli.

No results are shown for gallic acid because the CL signal increased with the concentration of the antioxidant (data not shown). We attributed this behavior to the generation of H₂O₂ in solution due to the reaction of gallic acid with atmospheric oxygen, a reaction already reported for various phenolic compounds [50, 51].

No cytotoxic effect (assessed by LDH release in the cell medium) was observed in treated cells, thus excluding the possibility that the decrease in H₂O₂ concentration was due to nonspecific effects on cell metabolism during the experiments (data not shown).

To confirm the ability of the bioassay to identify new physiological antioxidants, we measured the antioxidant activity of extracts derived from different tissues of *B. juncea* (oriental mustard), which contains the characteristic glucosinolate-myrosinase endogenous plant defense system of the Brassicaceae family. Its products (mainly isothiocyanates) have a recognized antioxidant activity, being powerful inducers of mammalian cytoprotective proteins through the Keap1–Nrf2–ARE pathway (the major regulator of cytoprotective responses to oxidative and electrophilic stress) [52].

According to the cell-based assay, the IC₅₀ values of the extracts were in the order of 0.1 – 0.2 µg mL⁻¹ (referred to the starting freeze-dried powders). To our knowledge, the high content of ITCs (supplementary materials), especially in *B. juncea* roots, can explain the reduced response to pro-oxidant stimuli observed in Caco-2 cells after a 24 hours incubation with the extracts. Leaves and stems extracts, despite their lower content of ITCs compared to roots, gave similar IC₅₀ values, probably because of other antioxidant molecules with a synergic effect with ITCs, as already described in literature for sulforaphane [53, 54].

As in previous experiments, monitoring of LDH release in cell medium excluded any cytotoxic effect of the extracts (data not shown).

Table 3.2: IC₅₀ values measured in Caco-2 cells for the reference antioxidants Trolox and lipoic acid using different pro-oxidant stimuli. Each value represents the mean ± SD of three replicate measurements.

Pro-oxidant	IC ₅₀ (μM)	
	Trolox	Lipoic acid
Menadione ^a	0.23 ± 0.07	2.05 ± 0.18
PMA ^b	0.68 ± 0.03	1.52 ± 0.02
LPS ^c	0.19 ± 0.05	0.51 ± 0.03

^aConcentration 25 μM, ^bConcentration 50 μM, ^cConcentration 37.5 μg mL⁻¹.

3.4 Conclusions

One of the challenges in studying ROS in complex matrix is robust detection since ROS are short-lived and their direct detection is seldom feasible. Intracellular H₂O₂ level can reasonably reflect a general change in the intracellular ROS production when various ROS are converted to H₂O₂ within cells [3], therefore the selective measurement of H₂O₂ over different ROS is critical for the accurate evaluation of oxidative stress. Here, we report the development and optimization of a selective intracellular antioxidant bioassay based on an adamantylidene - 1,2 - dioxetane probe containing an arylboronate moiety. The probe, in the presence of H₂O₂, is converted to the correspondent phenol, which emits green light with high efficiency. The assay low LOD enables the quantitative detection of H₂O₂ in complex biological samples, such as human living cells in physiological conditions. Notably, even small changes in intracellular H₂O₂ concentration in the presence of oxidants and antioxidants could be evaluated, which could provide a rapid first-level antioxidant screening in complex biological matrices for pharmaceutical and nutraceutical field.

The developed method is characterized by a good precision and is able to produce relative information that quantitatively scores an increased or decreased of intracellular H₂O₂ production with respect to basal level, as a

consequence of pro- or antioxidant treatment.

These results were achieved with, as far as we know, the shortest incubation time ever used for a luminescence-based bioassay. Moreover, our cell-based bioassay is one of the fastest assays among other intracellular H₂O₂ selective CL bioanalytical methods [55 - 63].

For the first time, scientists now have an effective, rapid, reproducible, robust single-entity CL tool that can be used to evaluate biological processes, i.e., intracellular H₂O₂ production. This rapid cell- based bioassay has the potential to provide both the researcher and the diagnostician with a powerful tool to look within the cells, in real-time, at the fundamental biochemistry and production of H₂O₂ and correspondingly the redox state of the metabolism.

3.5 Acknowledgments

We wish to thank Prof. Fernanda. Martini (University of Ferrara) for providing HaCat cells and Biosynth (Staad, Switzerland) for kindly providing the dioxetane CL probe AquaSpark™ Peroxide Probe.

3.6 References

- [1] C.C. Winterbourn, *Nat. Chem. Biol.* 4 (2008) 278–286, <https://doi.org/10.1038/nchembio.85>.
- [2] B. Halliwell, *Pathophysiol. Haemostasis Thrombosis* 23 (1) (1993) 118–126, <https://doi.org/10.1159/000216921>.
- [3] A. Alfadda, R. Sallam, *J. Biomed. Biotechnol.* (2012) 2012, <https://doi.org/10.1155/2012/936486>.
- [4] N. Di Marzo, E. Chisci, R. Giovannoni, *Cells* 7 (10) (2018) 156, <https://doi.org/10.3390/cells7100156>.
- [5] S.G. Rhee, T.S. Chang, W. Jeong, D. Kang, *Mol. Cell.* 29 (6) (2010) 539–549, <https://doi.org/10.1007/s10059-010-0082-3>
- [6] H. Wang, J.A. Joseph, *Free Radic. Biol. Med.* 27 (5–6) (1999) 612–616, [https://doi.org/10.1016/s0891-5849\(99\)00107-0](https://doi.org/10.1016/s0891-5849(99)00107-0).
- [7] A. Gomes, E. Fernandes, J.L. Lima, *J. Biochem. Biophys. Methods* 65 (2–3) (2005) 45–80, <https://doi.org/10.1016/j.jbbm.2005.10.003>.
- [8] B. Kalyanaraman, V. Darley-Usmar, K.J. Davies, P.A. Dennery, H.J. Forman, M.B. Grisham, G.E. Mann, K. Moore, L.J. Roberts 2nd, H. Ischiropoulos, *Free Radic. Biol. Med.* 52 (2012) 1–6, <https://doi.org/10.1016/j.freeradbiomed.2011.09.030>.
- [9] P. Wardman, *Free Radic. Biol. Med.* 43 (2007) 995–1022, <https://doi.org/10.1016/j.freeradbiomed.2007.06.026>.
- [10] M. Karlsson, T. Kurz, U.T. Brunk, S.E. Nilsson, C.I. Frennesson, *Biochem. J.* 428(2010) 183–190, <https://doi.org/10.1042/BJ20100208>.
- [11] C. Caliceti, A.L. Capriotti, D. Calabria, F. Bonvicini, R. Zenezini Chiozzi, C.M. Montone, S. Piovesana, M. Zangheri, M. Mirasoli, P. Simoni, A. Laganà, A. Roda, *Oxid. Med. Cell. Longev.* (2019) 1046504, <https://doi.org/10.1155/2019/1046504>.
- [12] A.G. Yodh, B. Chance, *Phys. Today* 48 (3) (1995) 34–40, <https://doi.org/10.1063/1.881445>.
- [13] A. Roda, M. Mirasoli, E. Michelini, M. Di Fusco, M. Zangheri, L. Cevenini, B. Roda, P. Simoni, *Biosens. Bioelectron.* 15 (76) (2016) 164–179, <https://doi.org/10.1016/j.bios.2015.06.017>.

- [14] A. Roda, M. Guardigli, *Anal. Bioanal. Chem.* 402 (1) (2012) 69–76, <https://doi.org/10.1007/s00216-011-5455-8>.
- [15] L. Kricka, *Anal. Chim. Acta* 500 (2003) 279, [https://doi.org/10.1016/S0003-2670\(03\)00809-2](https://doi.org/10.1016/S0003-2670(03)00809-2).
- [16] L. Kricka, *Clin. Chem.* 37 (9) (1991) 1472–1481.
- [17] J.A. Ives, E.P.A. van Wijk, N. Bat, C. Crawford, A. Walter, W.B. Jonas, R. van Wijk, J. van der Greef, *PloS One* 9 (2) (2014) e87401, , <https://doi.org/10.1371/journal.pone.0087401>.
- [18] D.J. O'Kane, J. Lee, *Methods Enzymol.* 305 (2000) 87–96, [https://doi.org/10.1016/s0076-6879\(00\)05479-3](https://doi.org/10.1016/s0076-6879(00)05479-3).
- [19] D. Betteridge, *Anal. Chem.* 50 (1978) 823A–833A, <https://doi.org/10.1021/ac50031a001>.
- [20] P. Khan, D. Idrees, M.A. Moxley, J.A. Corbett, F. Ahmad, G. von Figura, W.S. Sly, A. Waheed, M.I. Hassan, *Appl. Biochem. Biotechnol.* 173 (2) (2014) 333–355, <https://doi.org/10.1007/s12010-014-0850-1>.
- [21] A. Kielland, T. Blom, K.S. Nandakumar, R. Holmdahl, R. Blomhoff, H. Carlsen, *Free Radic. Biol. Med.* 47 (6) (2009) 760–766, <https://doi.org/10.1016/j.freeradbiomed.2009.06.013>.
- [22] D. Lee, S. Khaja, J.C. Velasquez-Castano, M. Dasari, C. Sun, J. Petros, W.R. Taylor, N. Murthy, *Nat. Mater.* 6 (10) (2007) 765–769, <https://doi.org/10.1038/nmat1983>.
- [23] Y.D. Lee, C.K. Lim, A. Singh, J. Koh, J. Kim, I.C. Kwon, S. Kim, *ACS Nano* 6 (8)(2012) 6759–6766, <https://doi.org/10.1021/nn3014905>.
- [24] X. Zhen, C. Zhang, C. Xie, Q. Miao, K.L. Lim, K. Pu, *ACS Nano* 10 (2016) 6400–6409, <https://doi.org/10.1021/acsnano.6b02908>.
- [25] J. Zhou, J. Gu, C. Tian, D. Jiang, Y. Chen, K. Xi, *RSC Adv.* 6 (45) (2016) 39480–39483, <https://doi.org/10.1039/C6RA04029B>.
- [26] O. Green, T. Eilon, N. Hananya, S. Gutkin, C.R. Bauer, D. Shabat, *ACS Cent. Sci.* 3 (4) (2017) 349–358, <https://doi.org/10.1021/acscentsci.7b00058>.
- [27] N. Hananya, D. Shabat, *ACS Cent. Sci.* 5 (6) (2019) 949–959, <https://doi.org/10.1021/acscentsci.9b00372>.

- [28] S. Gnaim, O. Green, D. Shabat, *Chem. Commun.* 54 (2018) 2073–2085, <https://doi.org/10.1039/C8CC00428E>.
- [29] E.W. Miller, A.E. Albers, A. Pralle, E.Y. Isacoff, C.J. Chang, *J. Am. Chem. Soc.* 127(47) (2005) 16652–16659, <https://doi.org/10.1021/ja054474f>.
- [30] A.R. Lippert, G.C. Van de Bittner, C.J. Chang, *Acc. Chem. Res.* 44 (9) (2011) 793–804, <https://doi.org/10.1021/ar200126t>.
- [31] L. Lazzeri, L. Malaguti, S. Cinti, L. Ugolini, G.R. De Nicola, M. Bagatta, N. Casadei, L. D'Avino, G. Patalano, *Acta Hortic.* 1005 (2013) 375–382, <https://doi.org/10.17660/ActaHortic.2013.1005.44>.
- [32] E. Porru, P. Franco, D. Calabria, S. Spinuzzi, M. Roberti, C. Caliceti, A. Roda, *Anal. Bioanal. Chem.* 410 (15) (2018) 3533–3545, <https://doi.org/10.1007/s00216-018-0884-2>.
- [33] O. Green, S. Gnaim, R. Blau, A. Eldar-Boock, R. Satchi-Fainaro, D. Shabat, *J. Am. Chem. Soc.* 139 (37) (2017) 13243–13248, <https://doi.org/10.1021/jacs.7b08446>.
- [34] W.S. Rasband, ImageJ, U.S. National institutes of health, Bethesda, Maryland, USA <https://imagej.nih.gov/ij/> 1997-2018.
- [35] J.P. Monteiro, A.F. Martins, C. Nunes, C.M. Morais, M. Lúcio, S. Reis, T.J.T. Pinheiro, C.F.G.C. Geraldes, P.J. Oliveira, A.S. Jurado, *B.B.A.-Biomembranes* 1828 (8) (2013) 1899–1908, <https://doi.org/10.1016/j.bbamem.2013.04.006>.
- [36] V. Klaus, T. Hartmann, J. Gambini, P. Graf, W. Stahl, A. Hartwig, L.O. Klotz, *Arch. Biochem. Biophys.* 496 (2) (2010) 93–100, <https://doi.org/10.1016/j.abb.2010.02.002>.
- [37] W.M. Nauseef, *Biochim. Biophys. Acta* 1840 (2) (2014) 757–767, <https://doi.org/10.1016/j.bbagen.2013.04.040>.
- [38] G. Gloire, S. Legrand-Poels, J. Piette, *Biochem. Pharmacol.* 72 (11) (2006) 1493–1505, <https://doi.org/10.1016/j.bcp.2006.04.011>.
- [39] I.V. Tetko, J. Gasteiger, R. Todeschini, A. Mauri, D. Livingstone, P. Ertl, V.A. Palyulin, E.V. Radchenko, N.S. Zefirov, A.S. Makarenko, V.Y. Tanchuk, V.V. Prokopenko, *J. Comput. Aided Mol. Des.* 19 (2005) 453–463 <http://www.vcclab.org>.

- [40] J. Zielonka, A. Sikora, M. Hardy, J. Joseph, B.P. Dranka, B. Kalyanaraman, *Chem. Res. Toxicol.* 25 (9) (2012) 1793–1799, <https://doi.org/10.1021/tx300164j>.
- [41] A. Glasauer, N.S. Chandel, *Biochem. Pharmacol.* 92 (2014) 90–101, <https://doi.org/10.1016/j.bcp.2014.07.017>.
- [42] C.C. Winterbourn, *BBA-Gen. Subjects* 1840 (2) (2014) 730–738, <https://doi.org/10.1016/j.bbagen.2013.05.004>.
- [43] G. Koliosa, N. Rooneyb, C.T. Murphya, D.A.F. Robertsonc, J. Westwicka. *Gut* 43(1998) 56–63, <https://doi.org/10.1136/gut.43.1.56>.
- [44] X. Jiang, L. Wang, S.L. Carroll, J. Chen, M.C. Wang, J. Wang, *Antioxidants Redox Signal.* 29 (6) (2018) 518–540, <https://doi.org/10.1089/ars.2017.7491>.
- [45] I. Hamad, N. Arda, M. Pekmez, S. Karaer, G. Temizkan, *J. Nat. Sci. Biol. Med.* 1 (1) (2010) 16–21, <https://doi.org/10.4103/0976-9668.71667>.
- [46] K. Satoh, T. Kadofuku, H. Sakagami, *Anticancer Res.* 17 (4A) (1997) 2459–2463 PMID: 9252663.
- [47] A. Constantinescu, U. Pick, G.J. Handelman, N. Haramaki, D. Han, M. Podda, H.J. Tritschler, L. Packer, *Biochem. Pharmacol.* 50 (1995) 253–261, [https://doi.org/10.1016/0006-2952\(95\)00084-d](https://doi.org/10.1016/0006-2952(95)00084-d).
- [48] L.T. Boni, J.S. Hah, S.W. Hui, P. Mukherjee, J.T. Ho, C.Y. Jung, *Biochem. Biophys. Acta.* 775 (1984) 409–418, [https://doi.org/10.1016/0005-2736\(84\)90198-6](https://doi.org/10.1016/0005-2736(84)90198-6).
- [49] J.S. Beckman, R.L. Minor Jr., C.W. White, J.E. Repine, G.M. Rosen, B.A. Freeman, *J. Biol. Chem.* 263 (14) (1988) 6884–6892.
- [50] M. Akagawa, T. Shigemitsu, K. Suyama, *Biosc. Biotech. Biochem.* 67 (12) (2003) 2632–2640, <https://doi.org/10.1271/bbb.67.2632>.
- [51] H.J. Forman, K.J. Davies, F. Ursini, *Free Radic. Biol. Med.* 66 (2014) 24–35, <https://doi.org/10.1016/j.freeradbiomed.2013.05.045>.
- [52] A. Sharma, P.K. Rai, S. Prasad, *Microchem. J.* 138 (2018) 488–493, <https://doi.org/10.1016/j.microc.2018.01.015>.
- [53] F. Elbarbry, N. Elrody, *J. Med. Plants Res.* 5 (4) (2011) 473–484.

- [54] A. Papi, F. Farabegoli, R. Iori, M. Orlandi, G.R. De Nicola, M. Bagatta, D. Angelino, L. Gennari, P. Ninfali, *Food Chem.* 138 (2–3) (2012) 1521–1530, <https://doi.org/10.1016/j.foodchem.2012.11.112>.
- [55] Y. Li, K.H. Stansbury, H. Zhu, M.A. Trush, *Biochem. Biophys. Res. Commun.* 262 (1)(1999) 80–87.
- [56] C. Shi, X. Chen, Z. Liu, R. Meng, X. Zhao, Z. Liu, N. Guo, *Biomed. Pharmacother.* 85 (2017) 740–748.
- [57] K. Zhou, F. Zhang, J. Xu, H. He, W. Wei, Z. Xia, *Part. Part. Syst. Char.* 35 (2) (2018) 1700329.
- [58] B.C. Dickinson, R.E. Haskew-Layton, R.R. Ratan, *Cell Biosci.* 4 (1) (2014) 64, <https://doi.org/10.1186/2045-3701-4-64> 27.
- [59] J. Meier, E.M. Hofferber, J.A. Stapleton, N.M. Iverson, *Chemosensors* 7 (4) (2019) 64, <https://doi.org/10.3390/chemosensors7040064>.
- [60] E.W. Miller, O. Tulyathan, E.Y. Isacoff, C.J. Chang, *Nat. Chem. Biol.* 3 (2007) 263–267, <https://doi.org/10.1038/nchembio871>.
- [61] D. Srikun, A.E. Albers, C.I. Nam, A.T. Iavarone, C.J. Chang, *Am. Chem. Soc.* 132 (12) (2010) 4455–4465, <https://doi.org/10.1021/ja100117u>.
- [62] D.1 Jacewicz, K.2 Siedlecka-Kroplewska, J.1 Drzeżdżon, A.1 Piotrowska, D. Wyrzykowski, A. Tesmar, K. Żamojć, L. Chmurzyński, *Sci. Rep.* 7 (2017) 45673, <https://doi.org/10.1038/srep45673> 30.
- [63] Y.G. Ermakova, N.M. Mishina, C. Schultz, V.V. Belousov, *Methods Mol. Biol.* 1982 (2019) 259–274, https://doi.org/10.1007/978-1-4939-9424-3_15.

3.7 Supplementary material

3.7.1 Extracts of Brassicaceae

Extraction of bioactive molecules from *B. juncea* wastes (roots, stems, leaves) was performed following a published procedure [1] with minor modifications. Briefly, 100 mg of lyophilized samples were extracted with 5 mL of methanol/water (60:40, v/v) using sonication for 30 min at room temperature. Then, the extracts were centrifuged (10 min, 10000 × g) and the supernatants were collected. Further analyses were performed directly on the hydroalcoholic extracts or on a DMSO solution obtained by removing the solvent under reduced pressure and dissolving the dried extracts in DMSO. In both cases, solutions were stored at 4 °C until analysis.

3.7.2 Glucosinolate and isothiocyanate analysis

Glucosinolate content and profile were determined by HPLC-UV analysis of desulfo-GSLs following the ISO 9167-1 method with some minor modifications [2], after myrosinase deactivation in boiling bath for ten minutes. The desulfo-GSLs were detected monitoring their absorbance at 229 nm and identified through their retention times [3, 4, 5]. Their amounts were estimated using (2R)-2-hydroxybut-3-enylglucosinolate as an internal standard and applying suitable response factors (0.92, 0.87, and 0.18 for allyl glucosinolate, phenylethyl glucosinolate and N-methoxyglucobrassicin, respectively). For isothiocyanate analysis, 700 µL of hydroalcoholic extracts, were partitioned in 250 µL dichloromethane and 1 µL of the organic fraction was injected in a Varian Saturn CP-3800 gas chromatograph (Agilent Technologies, Santa Clara, CA, USA) equipped with a flame ionization detector (FID) and using a J&W HP-5 GC column (Agilent Technologies, 30 m × 0.25 mm i.d, 0.25 µm film thickness). The analytical conditions were: injection temperature 250 °C; detector temperature 240 °C; carrier gas (nitrogen) flow 1 mL min⁻¹; column oven temperature initially maintained at 60 °C for 4 min, followed by a gradient (rate 10 °C min⁻¹) up to 220 °C and by 2 min at 220 °C. The split mode (1:20) was used for injection. Isothiocyanates were quantified on calibration curves generated by analysing allyl isothiocyanate and phenethyl isothiocyanate standards.

3.7.3 Bioassay procedure in Caco-2 cells in the presence of a NOS inhibitor

Caco-2 (25×10^3 cells well⁻¹) cells were plated in the wells of a 96-well black microtiter plate for 24 hours and then incubated for 6 and 24 hours with the cell-permeable competitive NOS inhibitor N(G)-monomethyl-L-arginine monoacetate (L-NMMA) (100 μ M) in the presence or absence of 50 ng/ml of TNF α to induce iNOS expression [9]. After these treatments, cells were starved and incubated for 20 min with 100 μ L of the dioxetane CL probe working solution and then 100 μ L of the pro-oxidant PMA (50 μ M) were added to induce intracellular H₂O₂ production and the CL emission was monitored for 40 min using a Luminoskan™ Ascent luminometric plate reader. PBS was used as the negative control. All the assay was conducted at 37 °C and. The dose-response curve was obtained by plotting the CL signal versus the actual concentration of the pro-oxidant and fitting the experimental data to a straight line using the method of least squares.

3.7.4 Results

3.7.4.1 Characterization of plant extracts

The chemical analyses showed that the plant extracts contained small quantities of GSLs (allyl glucosinolate and phenylethyl glucosinolate) and much higher amounts of ITCs (**Table S1**), which evidenced - in line with recent literature [6, 7, 8] - a high activity of the enzyme myrosinase, especially at root level. Glucosinolate profiles revealed the characteristic presence of phenylethyl glucosinolate, allyl glucosinolate and the indolic N-methoxyglucobrassicin in roots, while allyl glucosinolate was the main GSL in both stems and leaves. Traces of glucobrassicin in roots were also detected.

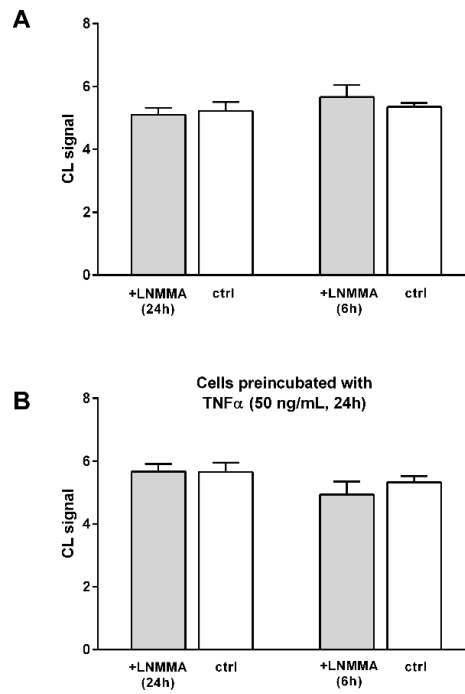
Table S1. *Glucosinolate and isothiocyanate content of the B. Juncea wastes (contents are referred to the starting freeze-dried powders).^a*

Compound	Roots ($\mu\text{g g}^{-1}$)	Stems ($\mu\text{g g}^{-1}$)	Leaves ($\mu\text{g g}^{-1}$)
Allyl glucosinolate	3.78 ± 0.04	7.9 ± 1.2	7.9 ± 2.0
Phenylethyl glucosinolate	3.46 ± 0.30	0.38 ± 0.04	n.d.
N-methoxyglucobrassicin	0.38 ± 0.09	n.d.	n.d.
Allyl isothiocyanate	115 ± 6	84 ± 5	36 ± 5
Phenethyl isothiocyanate	232 ± 63	n.d.	n.d.

^a Each value represents the mean \pm SD of three replicate measurements.

3.7.4.2 Quantification of intracellular H_2O_2 in Caco-2 human living cells in the presence of a NOS inhibitor

Since peroxynitrite (ONOO^-) represents another potentially interfering species due to its rapid reaction with aromatic boronates at physiological pH [10], we evaluated H_2O_2 detection in Caco-2 cells in the presence of the cell-permeable competitive nitric oxide synthases NOS inhibitor N(G)-monomethyl-L-arginine monoacetate (L-NMMA). Indeed, ONOO^- derives from the reaction of superoxide with nitric oxide, which is mainly produced by enzymes belonging to the family of NOS and inhibition of NOS activity should efficiently suppress the production of ONOO^- by cells. As shown in Supplementary Figure 1A we didn't observe any significant difference in CL signals, in Caco-2 cells treated with 25 μM PMA and previously exposed to 100 μM L-NMMA for 6 and 24 hours. To confirm these data, we also investigated the CL signals in cells preincubated with 50 ng/ml of $\text{TNF}\alpha$ for 24 hours, to induce the expression of the inducible NOS isoform (iNOS) [9] and Supplementary Figure S1B clearly showed that a significant contribution to the CL emission due to the reaction of the probe with ONOO^- can be excluded.



Supplementary Figure 1.1: (A) Chemiluminescence signal obtained for Caco-2 cells treated with 100 μ M L-NMMA for 6 and 24 hours and then incubated with the dioxetane CL probe and 25 μ M PMA. (B) Chemiluminescence signal obtained for Caco-2 cells treated with 100 μ M L-NMMA for 6 and 24 hours in the presence or absence of 50 ng/ml TNF α for 24 hours and then incubated with the dioxetane CL probe and 25 μ M PMA. Each bar represents the mean \pm SD of three independent measurements.

3.7.5 References

- [1] J. Sun, Z. Xiao, L.Z. Lin, G.E. Lester, Q. Wang, J.M. Harnly, P. Chen, *J. Agric. Food Chem.*, 2013, 61(46), 10960-10970.
- [2] E. Pagnotta, N. Agerbirk, C.E. Olsen, L. Ugolini, S. Cinti, L. Lazzeri, *J. Agric. Food Chem.*, 2017, 65(15), 3167-3178.
- [3] O. Leoni, R. Iori, T. Haddoum, M. Marlier, J.P. Wathelet, P. Rollin, S. Palmieri, *Ind. Crops Prod.*, 1998, 7(2-3), 335-343.
- [4] J. Barillari, D. Gueyrard, P. Rollin, R. Iori, *Fitoterapia*, 2001, 72(7), 760-764.
- [5] M. Haack, M Lowinger, D. Lippmann, A. Kipp, E. Pagnotta, R. Iori, B.H. Monien, H. Glatt, B.M. Brauer, L.A. Wessjohann, *Biol. Chem.*, 2010, 391(11), 1281-1293.
- [6] F. Elbarbry, N.J. Elrody, *Med. Plant. Res.*, 2011, 5(4), 473-484.
- [7] A. Papi, F. Farabegoli, R. Iori, M. Orlandi, G.R. De Nicola, M. Bagatta, D. Angelino, L. Gennari, P. Ninfali, *Food Chem.*, 2013, 138(2-3), 1521-1530.
- [8] F. Fuentes, Y. Gomez, X. Paredes-Gonzalez, A. Barve, S. Nair, S. Yu, C.L.L. Saw, A.N.T. Kong, *J. Chin. Pharm. Sci.*, 2016, 25(8), 559-569.
- [9] X.X. Wu, X.L. Huang, R.R. Chen, T. Li, H.J. Ye, W. Xie, Z.M. Huang, G.Z. Cao. *Inflammation*. 2019. doi: 10.1007/s10753-019-01085-z. [Epub ahead of print]
- [10] C. Winterbourn. *Biochimica et Biophysica Acta*. 2014, 1840: 730–738.

4

Grape Pomace for Topical Application: Green NaDES Sustainable Extraction, Skin Permeation Studies, Antioxidant and Anti-Inflammatory Activities Characterization in 3D Human Keratinocytes

Reproduced from: “Grape Pomace for Topical Application: Green NaDES Sustainable Extraction, Skin Permeation Studies, Antioxidant and Anti-Inflammatory Activities Characterization in 3D Human Keratinocytes”

***Angela Punzo** , Emanuele Porru, Alessia Silla, Patrizia Simoni, Paola Galletti, Aldo Roda, Emilio Tagliavini, Chiara Samori and Cristiana Caliceti.*

Biomolecules, 2021; 11(8), 1181

Reproduced by permission of MDPI

<https://www.mdpi.com/openaccess>

4.1 Introduction

Each year, an estimated one-third of all food produced—equivalent to 1.3 billion tonnes worth around USD 1 trillion—ends up rotting in the bins of consumers and retailers or spoiling due to poor transportation and harvesting practices. Food waste is also a serious problem for food processing industries, especially when it represents a loss of a valuable source of nutrients and phytochemicals [1]. Exploitation of new extraction processes and further valorization of these by-products can increase resource efficiency and promote sustainable lifestyles.

Italy is a traditional wine-producing country and one of the world's leading wine producers, ranked first for volume of exports and second after France for value [2]. During winemaking, only a minor part of the grape's phytochemicals are extracted into the wine, so grape pomace, representing about 20%wt of the processed grapes, is enriched in high-value compounds, such as polyphenols [3]. Regulation EC 479n2008 of the European Union introduced important new elements to the legal framework of the wine sector, offering member states the possibility of defining the end-use of pomace. Italy implemented the above regulation through a ministerial decree, which, as an alternative to distillation, allows it to be collected under control for the recovery of anthocyanins, the production of agricultural products (direct or indirect agronomical use), energy recovery (using by-products such as biomass for the production of biogas or for fueling energy-production plants) and the extraction of molecules with a high added value for pharmaceutical and cosmetic purposes. When the target compounds of grape pomace are soluble or weakly bound, such as polyphenols, the most common extraction technique is solid–liquid extraction, mainly based on toxic organic solvents [4]. Here, we exploited the profiles of the major classes of flavonoids present in red grape skin of traditional varieties of the Emilia Romagna region (“Sangiovese” red wines), typically cultivated in a niche area in northern Italy, along with their bioavailability and biological activities for innovative cosmeceutical applications. Specifically, we developed novel eco-friendly formulations based on polyphenols extracted with natural deep eutectic

solvents (NaDESs), aiming at demonstrating a novel approach for the valorization of winery by-products for human skin protection. NaDESs are playing an increasingly relevant role in the field of the extraction of polar molecules (like polyphenols) from natural matrices [5]; however, the use of NaDESs as polyphenols carriers, incorporating NaDESs into bioactive formulations, is a relatively new concept [6]. This is mainly because the exploitation of NaDESs as a part of bioactive formulations for peculiar biological applications, like cosmetic ones, requires a strict evaluation of their potential toxic effects (in the present case against skin cells).

The NaDESs used in the present study were based on betaine and three different hydrogen bond donors (urea, citric acid and ethylene glycol), chosen based on their proven biocompatibility.

The low harmfulness/toxicity and the compatibility of these single components are well-established and their use in the cosmetic field is legally allowed; moreover, the characterization of NaDES extracts used in this work in sugars and total polyphenols content has already been performed [4]. However, a deep study in anthocyanin and flavonol profiles has not been detailed so far and it is still not clear if there is a correlation between the composition of NaDES extracts and their biological effects in human skin. To this purpose, keratinocytes were used here as a cell model to directly verify the suitability of polyphenol–NaDES formulations in the cosmetic field. Keratinocytes play a major role in the structural and barrier functions of the epidermis [7], so they have been regarded as a prime choice for non-animal skin toxicity assessment to evaluate grape pomace bioactivity [8,9]. However, two-dimensional (2D) human keratinocytes have several limitations when they are used as a substitute for animal experiments. The main limitations include their failure to replicate the *in vivo* complexity and actual cellular architecture comprising the extracellular matrix (ECM) microenvironment and cell–cell interactions. Three-dimensional cell culture systems overcome many of the limitations of traditional 2D cell culture systems, more closely mimicking the complex phenotypic heterogeneity that chemical gradients produce during cell growth. In the current study, 3D keratinocytes were thus used to investigate the

potential beneficial skin activities of grape pomace extracts [10].

The innovative extraction with NaDESs combined with a validated bioanalytical approach based on the assessment of anthocyanin content in pomace extracts and their bioavailability in the skin in NaDES formulations, along with their relationship with *in vitro* beneficial activity in human 3D keratinocytes represents a smart and powerful tool for complete cosmeceutical profiling. Our final aim was to propose a correct and sustainable approach to better reutilizing pomace extracts in order to open new perspectives on their use for possible future applications in the cosmetic field (**fig. 4.1**).



Figure 4.1: Schematic representation of the study.

4.2 Material and Methods

4.2.1 Chemicals

The chemiluminescent probe (AquaSpark™ 510 Peroxide Probe) was provided by Biosynth Carbosynth (Staad, Switzerland). A 10 mM stock solution was prepared by solubilizing the probe in DMSO. This solution is stable for months when stored at 4 °C in the dark. Phosphate-buffered saline (PBS) tabs (giving a 137 mM NaCl, 2.7 mM KCl phosphate buffer solution, pH 7.4, final concentration 0.01M), H₂O₂ solution, trypsin-EDTA, oxidative stress inductor 2-methyl-1,4-naphthoquinone (menadione), malvidin, the antibiotic solution 100X (10,000 U mL⁻¹ penicillin and 10 mg mL⁻¹ streptomycin) and the internal standard hydroxy-tyrosol for HPLC-ESI-MS/MS analysis were purchased from Sigma-Aldrich (St Louis, MO, USA). Anthocyanins standards for HPLC-ESI-MS/MS analysis were bought from Biosynth Carbosynth (Staad

SG, SANKT GALLEN, Switzerland). A stock solution of menadione (100 mM) was prepared in DMSO. Dulbecco's Modified Eagle Medium (DMEM) high glucose was purchased from Microgem (Naples, Italy) and fetal bovine serum (FBS) was purchased from Thermo Fischer Scientific (Waltham, MA, USA). The lactate dehydrogenase (LDH) cytotoxicity assay kit was purchased from Dojindo Molecular Technologies (Rockville, MD, USA).

4.2.2 Red Pomace Materials and Extracts

Red grape pomace from red grape (*Vitis vinifera* L.) varieties was collected during September 2015 in the Emilia Romagna region (Italy) and obtained by processing "Sangiovese" red wines from Caviro Extra s.p.a. (Faenza, Italy); after the collection, the pomace was immediately freeze-dried, ground with a domestic miller and stored at 4 °C until the preparation of the NaDES formulations. NaDESs (betaine: citric acid, BET-CA; betaine: ethylene glycol, BET-EG; betaine: urea, BET-U) were prepared by mixing betaine (BET; hydrogen bond acceptor (HBA)) and three different hydrogen bond donors (HBDs) at the appropriate stoichiometric ratio: citric acid (CA, 1:1), ethylene glycol (EG, 1:2), urea (U, 1:2). The mixtures were heated at 70°C and magnetically stirred until uniform colourless liquids were obtained; then, distilled water (40 wt%) was added to get a homogeneous liquid phase. Each NaDES (10 g) was added to freeze-dried red grape pomace (250 mg) and the mixture was stirred at rt for 24 h. After 24 h, each mixture was centrifuged and separated from the residual biomass. Each extraction was performed in triplicate [4]. Since several reports have shown that the NaDES extraction method makes it possible to obtain an higher content of polyphenolics from food by-products than classical extraction with EtOH, H₂O or a mixture of both as a solvent [4,11], in this work, grape pomace polyphenols were only extracted through selected environmentally friendly NaDES formulations.

4.2.3 HPLC-ESI-MS/MS Method

Liquid chromatography analysis was performed using a 2690 Alliance system (Waters, Milford, MA, USA). Analytical separation was performed using

Phenyl-Hexyl (1.7 μm , 150 mm x 2.1 mm i.d; Waters, Milford, MA, USA). The mobile phase was constituted as follows: 15 mM ammonium acetate in water adjusted to pH 8.0 with ammonia (solvent A) and methanol 99.9% (solvent B). Chromatographic separation was achieved at a 0.15 mL min⁻¹ flow rate under gradient elution conditions: 95% A for 5 min, 95–40% A from 5 to 15 min, 40–20% from 15 to 20 min, 20% A from 20 to 25 min, 20–95% A from 25 to 27 min and 95% A from 27 to 35 min. All the changes in the mobile phase composition were linear. The injected sample volume was 5 μL . The analytical column was maintained at 30 °C. The column effluent was introduced into the ESI source, operating in positive ionization mode, connected to a triple quadrupole mass spectrometer (Quattro-LC, Micromass), operating in the multiple reaction monitoring (MRM) acquisition mode. Standard solutions of three anthocyanins were used to evaluate the polyphenol profiles of each extract: malvidin-3-oglucoside (MAL), quercetin-3-oglucoside (QUE) and malvidin aglycon. The most abundant signals for each compound in the MRM acquisition mode were monitored for the quantification (m/z 3309 \rightarrow 330.9 (malvidin, aglycon), m/z 302.9 \rightarrow 302.9 (quercetin-O-glucoside), m/z 330.9 \rightarrow 330.9 (malvidin-O-glucoside and m/z 153.6 \rightarrow 125.6 (hydroxytyrosol)). The analytical method was developed and validated according to ICH guidelines to satisfy high analytical parameters in terms of accuracy and reproducibility. The limit of detection (LOD) and limit of quantification (LOQ) were determined by the signal-to-noise ratio (LOD = 3, LOQ = 10). The recovery and the matrix effect were evaluated for each compound before the sample analysis. A seven-point calibration curve (0.5, 1, 2.5, 5, 10, 25 and 50 ng mL⁻¹) was used for the quantification of each compound using standard solutions in the mobile phase (phase A: phase B 95:5). An internal standard was used for calibration curves at a fixed concentration of 5 ng mL⁻¹. The amount of malvidin in each formulation was checked periodically every 30 days for 2 months to determine its stability over the time.

4.2.4 Ex vivo permeation study by Franz diffusion cells

Franz diffusion cells (Copley Scientific, Nottingham, UK) were used to perform

a specific permeation study for topical formulations. This apparatus consisted of ten tailor-made donors and receptors and ten heated chambers. Mixing with a magnetic stirring bar at 300 rpm guaranteed a homogeneous temperature at 37 °C and concentration in the cell solution contents. Porcine ear skin membranes were used to perform the ex vivo permeation study. Briefly, after removing subcutaneous fat, portions of porcine ear skin were carefully cleaned with 0.9% physiological solution before storing them at -20 °C. Before each permeability experiment, tissue specimens were thawed at room temperature in PBS 0.1 M, pH = 7.4, and 5% (m/V) BSA. Thereafter, membranes were mounted in flow-through diffusion cells (exposed area: 1.8 cm²) with the stratum corneum facing the donor compartment and the dermis facing the receptor. The receptor compartment of the cell was filled with the medium chosen (PBS 0.1 M, pH = 7.4, and 5% m/V BSA). A quantity of 1 mL of each NaDES extract was applied to the surface of the skin/membrane in the donor compartment. Aliquots of 200 µL were collected from the receptor side at the designated time intervals (0.5, 1, 2, 4, 6 and 8 h) and immediately replaced by 200 µL of fresh medium solution. The permeated anthocyanin concentration was determined by the LC-mass spectrometry method described above. The cumulative amount permeated per unit area was plotted versus time for the three tested NaDES extracts along with their permeability profiles at 37 °C. The steady state flux (J , µg cm⁻² h⁻¹) and lag time could be estimated by extrapolation. The malvidin amount passing through the porcine ear skin (expressed as µg/cm²) and the steady state flux J are reported for each tested formulation.

The values reported are the means of at least five independent experiments.

4.2.5 3D Keratinocyte cell model

An immortalized keratinocyte cell line from adult human skin (HaCaT cells), kindly gifted by Prof. F. Martini (University of Ferrara), was used for all the experiments. Cells were maintained in DMEM high glucose containing 10% FBS, 2.5 mM L-glutamine, penicillin and streptomycin at 37 °C in an atmosphere of 5% CO₂. To obtain 3D spheroids, HaCaT cells were seeded in the “Ultra-Low Attachment Surface” 96-well black microtiter plate (Corning,

Amsterdam, Netherlands), which consisted of a hydrophilic and neutrally charged hydrogel coating covalently bound with polystyrene surfaces (20,000 cells per well⁻¹). This hydrogel surface naturally inhibits nonspecific interactions of the cells, eliminating unwanted cell attachment and forcing them to rest in suspension, allowing the formation of 3D spheroids. The medium culture was the same as 2D HaCaT cells and it was changed every day before experiments to obtain the spheroids' morphology [12].

4.2.6 Quantification of intracellular H₂O₂ in 3D HaCaT cells

Three days before the experiment, HaCaT cells (20 x 10³ cells well⁻¹) were plated in the "Ultra-Low Attachment Surface" 96-well black microtiter plate with a concave transparent bottom to allow the formation of 3D spheroids. The medium (DMEM high glucose + 10% FBS, 2.5 mM L-glutamine and antibiotic–antimycotic solution) was replaced every day, removing 50 µL and then adding the same volume for optimal cell growth. After 72 h, 50 µL of the dioxetane CL probe working solution (20 µM) was added in each well and then incubated for 20 min at 37 °C to obtain a final concentration of 5 µM/well. After this incubation, 50 µL of standard solutions of menadione were dispensed to induce intracellular H₂O₂ production (final concentration range 5–200 µM) and the CL signal was monitored for 40 min using a Luminoskan™ Ascent luminometric plate reader [13]. Menadione was used as an ROS-generating chemical [14]. The whole assay was performed at 37°C and the dose–response curve was obtained by plotting the CL signal versus the concentration of the pro-oxidant and fitting the experimental data to a straight line using the method of least squares.

4.2.7 Antioxidant activity of red pomace extracts in HaCaT spheroids

Two days before the experiment, HaCaT cells (20 x 10³ cells well⁻¹) were plated in the "Ultra-Low Attachment Surface" 96-well black microtiter plate with a concave transparent bottom to allow the formation of 3D spheroids. The medium (DMEM high glucose + 10% FBS, 2.5 mM L-glutamine and

antibiotic–antimycotic solution) was replaced every day, removing 50 μL and then adding the same volume for optimal cell growth. After 48 h, cells were treated for 24 h with serial dilutions of NaDES, with some containing polyphenolic extracts (range in content of malvidin: 0.05–1.1 $\mu\text{g mL}^{-1}$). On the day of the experiment, the cell medium was collected, then 50 μL of the CL probe working solution of Aquaspark (20 μM) was added and incubated for 20 min at 37 °C to obtain a final concentration in the well of 5 μM in 150 μL . After the incubation, 50 μL of the oxidative stress inductor menadione (200 μM) was added in each well to obtain a final concentration in the well of 50 μM . CL emission signal was monitored using a Luminoskan™ Ascent luminometric plate reader. The temperature was maintained at 37 °C during the measurement [13]. 24 h treatment with malvidin in BET-CA (range of 0.07–0.6 $\mu\text{g mL}^{-1}$) was used as a reference.

4.2.8 Cell cytotoxicity: lactate dehydrogenase release

Lactate dehydrogenase (LDH) release from HaCaT spheroids was monitored by collecting aliquots of the medium using a standard spectrophotometric method [14]. The method is based on a coupled enzymatic reaction in which LDH catalyses the conversion of lactate to pyruvate via NAD^+ reduction to NADH. Diaphorase reduces tetrazolium salt oxidizing NADH in the process to a red formazan product that can be measured at 490 nm. The medium derived from HaCaT spheroids, treated for 24 h with different concentrations of NaDES extracts (range in content of malvidin: 0.05–1.1 $\mu\text{g mL}^{-1}$), was collected and the increase in absorbance between the treatment after 24 h and the control was monitored at 37 °C using an Allsheng FlexA-200 Microplate Reader. Menadione (50 μM for 16 h of treatment) was used as a cytotoxic agent [14].

4.2.9 Spectrophotometric Cell Viability Bioassay

The cell viability was assessed by WST8 [2-(2-methoxy-4-nitrophenyl)-3-(4-nitrophenyl)-5-(2,4-disulfophenyl)-2H-tetrazolium, monosodium salt] (Dojindo Molecular Technologies, Japan), which, in the presence of an electron

mediator, is reduced by dehydrogenases in cells (as a vitality biomarker) to formazan dye, which is soluble in the tissue culture medium. The amount of the formazan dye generated by dehydrogenases in cells is directly proportional to the number of living cells. The decrease in absorbance between the treatment after 24h and the control was monitored at 37 °C at 450 nm using an Allsheng FlexA-200 Microplate Reader [15]. For this set of experiments, BET-CA formulation was added to the medium of human 3D HaCaT spheroids for 24 h (range in content of malvidin: 0.05–1.1 $\mu\text{g mL}^{-1}$). The free radical-generating chemical menadione (50 μM for 16 h of treatment) was used as cytotoxic agent [14]. 24 h treatment with malvidin in BET-CA (range of 0.07–0.6 $\mu\text{g mL}^{-1}$) was used as a reference.

4.2.10 Protein release

Human HaCaT keratinocytes seeded for 48 h into the “Ultra-Low Attachment Surface” 96-well black microtiter plate with a concave transparent bottom were treated with NaDES polyphenolic extracts for 24 h and stimulated with menadione (50 μM for 16 h), as previously reported.

At the end of the treatment, supernatants were collected and centrifuged to remove any cell detritus. Aliquots were stored at -80 °C until use. IL-8 and IL-10 protein levels were then determined using commercially available ELISA (Elabscience, US). 24 h treatment with malvidin in BET-CA (range of 0.07–0.6 $\mu\text{g mL}^{-1}$) was used as a reference. The assay was performed according to the manufacturer’s instructions. Triplicate wells were used for each individual sample.

4.2.11 Statistical analysis

Results are expressed as means \pm SD of at least three independent experiments. GraphPad Prism v. 6.0 (GraphPad Software, Inc., La Jolla, CA, USA) was used to plot the experimental data and for the least-squares fitting of calibration, dose–response curves (for evaluation of IC50 values) and assay comparison graphs.

4.3 Results and discussion

4.3.1 Extraction and characterization of anthocyanins in NaDES extracts

It is well-known that skins from grape pomace are highly enriched in phenolic compounds and the main representatives of this family are anthocyanins [16]. Anthocyanins are extremely unstable and their degradation during processing is influenced by several factors, including pH [17] and light [18], so the extraction process is crucial in maintaining the stability of these compounds. The conventional extraction of polyphenols uses volatile, toxic, and flammable organic solvents and usually mixtures of solvents in a multiple-step process, which can be time-consuming and expose the operator and the overall plant to different levels of risk [19]. In the present work, polyphenols from red grape pomace were extracted with the greener alternative of natural deep eutectic solvents (NaDESs), both as extracting agents and polyphenols carriers, incorporating NaDESs into bioactive formulations. NaDESs have recently been proposed as an excellent platform to enable transdermal delivery of various therapeutics, including proteins and siRNA, with a higher capacity for skin permeation and lower tendency to induce skin irritation compared to conventional chemical permeation enhancer (CPE) molecules [20]. This relatively new approach makes it possible to exploit the peculiarities of these new solvents, which are non-volatile and biocompatible, thus creating novel NaDES-based materials and at the same time improving the bioavailability, diffusion, and transport of polyphenols, as well as maintaining their stability [21]. Moreover, the overall sustainability of the process is increased, thus bypassing the need for downstream purification steps aimed at NaDES removal with consequent solvent consumption. Indeed, NaDESs can be used as vehicles for anthocyanins, making it easy for the process to be scaled-up. Three NaDESs were prepared by mixing betaine, the hydrogen bond acceptor (HBA), and three different hydrogen bond donors (HBDs), namely citric acid (BET-CA), ethylene glycol (BET-EG), and betaine-urea (BET-U). The single components were chosen based on their skin compatibility, being allowed by the European Union for cosmetic products or regularly used as active

materials in cosmetic products: betaine is allowed as an antistatic/viscosity controlling agent [22], urea is allowed as an antistatic/humectant/skin conditioning agent and citric acid is allowed as a buffering/chelating agent, whereas ethylene glycol is allowed as a surfactant, emulsifier and humectant [23]. Moreover, the incorporation of these single components into NaDES mixtures has already been proven to be suitable for the extraction of polyphenols from red grape pomace: while BET-EG exhibited similar performance to hydroalcoholic mixtures, both BET-CA and BET-U had improved extraction capabilities, significantly higher than hydroalcoholic mixtures [4]. Anthocyanin content in the three formulations was determined by HPLC-ESI MS/MS. Analytical calibration curve parameters for quantification of the NaDES extracts, in the range 0.5–100 ng mL⁻¹, were obtained from the plot of the analyte/internal standard peak area ratio versus the analyte concentration using a linear least-square regression analysis. The obtained analytical calibration curve equations were expressed in the form of $Y = (a \pm \delta a) X + (b \pm \delta b)$. Determination coefficients (r^2) of the analytical calibration curves were ≥ 0.990 for all analytes (see the Supplementary Materials). Limit of detection values (LOD) were 0.1 ng mL⁻¹, while limit of quantification values (LOQ) were 0.5 ng mL⁻¹ for all analytes. Variation coefficients and bias percentage, calculated intra- and inter-daily, were less than 5% for all analytes at the three different concentration levels, indicating the appropriate precision and accuracy of the developed method. The evaluation between standard solutions and fortified samples with known amounts of analyte and blank samples showed good selectivity in multiple reaction monitoring (MRM) mode, as no interfering signals potentially able to affect the identification of the target analytes were observed. The matrix effect percentage was evaluated at three concentration levels in all the studied matrices. In all the studies, matrix effect values were negligible, always being below 10% [24]. The results showed that malvidin was the major anthocyanin identified, with a similar content in all the formulations: 56.66 $\mu\text{g mL}^{-1}$ for BET-CA, 52.41 $\mu\text{g mL}^{-1}$ for BET-U and 51.69 $\mu\text{g mL}^{-1}$ for BET-EG. Malvidin-3-O-glucoside and quercetin-3-O-glucoside were not detected in the analysed NaDES extracts.

4.3.2 Skin permeation of anthocyanins derived from NaDES extracts

Anthocyanins are increasing in popularity in the food industry but have been poorly investigated as bioactive molecules in topical formulations. In order to exert their biological effects, they must be released from the developed topical formulations on the skin surface, overcome the barrier function of the stratum corneum (SC) and penetrate into the epidermis and dermis [25]. From the therapeutic point of view, the bioavailability is a crucial parameter allowing their biological effects [26]. Anthocyanins constitute the largest group of water-soluble molecules in plants but have limited bioavailability in skin as they are poor lipophilic compounds. Their skin penetration can be enhanced by a proper formulation that constitutes a complex of the excipients and vehicles used, allowing the partition in the lipid domain of the skin structure [27]. NaDESs show promise as drug carriers in dermal formulations or formulations for local administration in the oral cavity due to their low toxicity, tunability and biodegradability, as well as their solubilizing and stabilizing properties [28]. Since the three NaDES formulations showed similar amounts of malvidin aglycone, we directly focused on the bioavailability using Franz cells as an ex vivo permeation model. As can be seen in the **Table 4.1**, the BET-CA formulation seemed to be the one that had major malvidin permeability through the membrane; therefore, we decided to further analyse only this formulation as the best possible excipient in a cosmetic product for topical use.

Table 4.1: Amounts of malvidin permeated (ng cm^2) for the three tested formulations at 37°C.

Time (Hours)	BET-CA (ng cm^{-2}) \pm SD	BET-U (ng cm^{-2}) \pm SD	BET-EG (ng cm^{-2}) \pm SD
6	8.35 \pm 4.71	0.00	0.00
12	213 \pm 43	28.1 \pm 2.5	49.7 \pm 10.2
24	431 \pm 7	50.4 \pm 14.9	103 \pm 5
Flow J ($\text{ng cm}^{-2} \text{h}^{-1}$)	23.4 \pm 3.1	2.80 \pm 0.48	5.71 \pm 1.14

In **figure 4.2** a graph with the malvidin amounts permeated (ng cm^{-2}) versus time is shown. The difference between BET-CA and the other formulations was significant ($p < 0.01$). Since anthocyanins are more stable at low pH (acidic conditions) [29], we hypothesized that the BET-CA formulation preserved the stability of this molecule.

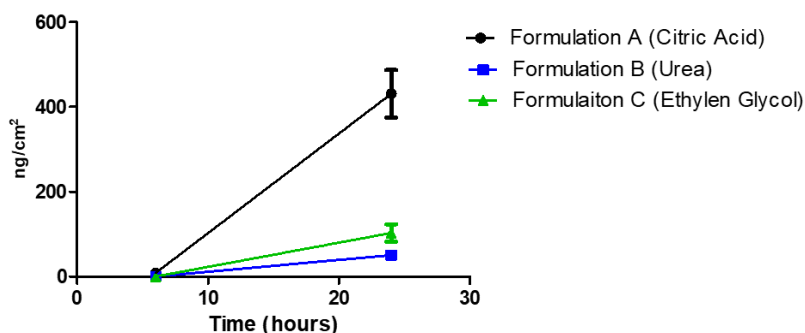


Figure 4.2: Permeation profiles of the three NaDES formulations (24 h experiment). The cumulative amount permeated per unit area was plotted versus time for the three tested NaDES extracts and their permeability profiles at 37 °C. The malvidin amounts passed through the porcine ear skin (expressed as $\mu\text{g}/\text{cm}^2$) and the steady state flux J are reported for each tested formulation at the selected temperature. The values reported are the means of at least five independent experiments.

4.3.3 Safety of NaDES extracts in Vitro in human 3D keratinocytes

Cell-based assays are one of the most appealing tools for the evaluation of a plethora of biological activities in the cosmetic area, since they allow highly human and predictive information that makes it possible to avoid or reduce in vivo experiments in compliance with the guiding principle of the “Three Rs” (replacement, reduction and refinement) concerning the use of animals in scientific research. 3D cell culture systems overcome many of the limitations of conventional 2D cells, more closely mimicking the complex phenotypic heterogeneity that chemical gradients produce during cell growth [10]. In this study, we used low-attachment-based generation of human HaCaT spheroids, as reported by Klicks et al. [10], to evaluate the suitable and safe

concentrations of NaDES formulations and their biological activities. Firstly, the safety of all the formulations was investigated by quantifying the release of lactate dehydrogenase (LDH), a marker for cell death both in vitro and in vivo. HaCaT spheroids were treated with different dilutions of the three formulations (range: 1:50–1:1000 v/v, corresponding to $1.1 \pm 0.1 \mu\text{g mL}^{-1}$ of malvidin), and LDH was quantified in cell culture medium. As shown in **Figure 4.3**, all the formulations tested at the dilution 1:50 v/v significantly increased LDH release ($p < 0.001$), while lower dilutions were not cytotoxic towards the cells and thus considered safe. These data are in line with previous results obtained in 2D HaCat [30], showing good biocompatibility for the tested cells.

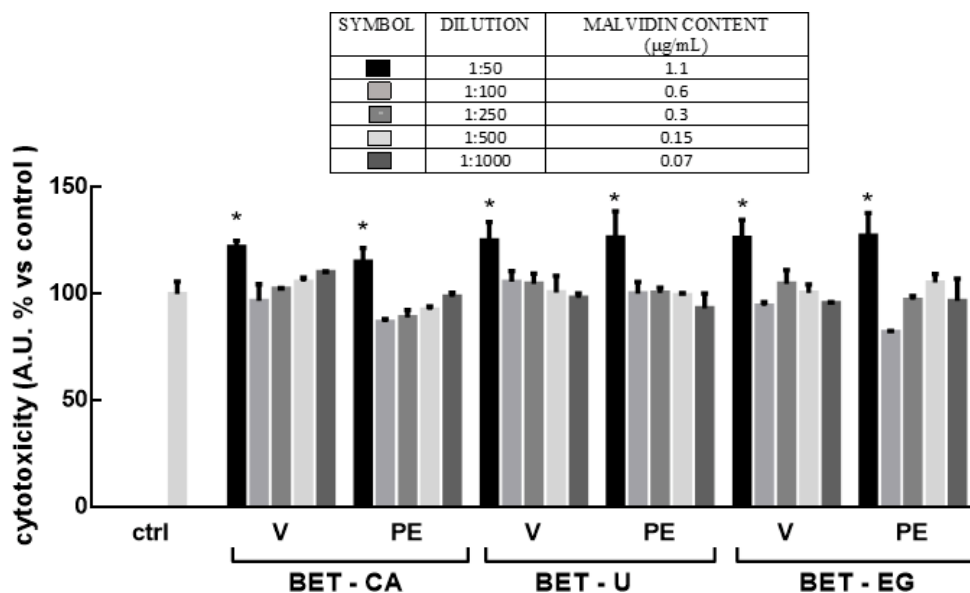


Figure 4.3: HaCaT spheroids were treated with pomace extracts (PE) in NaDES formulations (range in content of malvidin: $0.05\text{--}1.1 \mu\text{g mL}^{-1}$) for 24 h: betaine-citric acid (BET-CA), betaine-urea (BET-U) and betaine-ethylen glycol (BET-EG). Corresponding dilutions of the NaDES mixtures used for extraction, without grape pomace extracts, were utilized as the control (vehicle (V)). LDH activity was spectrophotometrically quantified in a cellular medium as an index of cytotoxicity, as described in the Materials and Methods section. Results are expressed as means \pm SD of three independent experiments, each performed in triplicate. * $p < 0.001$ significantly different from the control (ctrl).

Previously, results obtained by HPLC/ESI MS-MS analysis showed similar malvidin contents in the three formulations, while malvidin in the BET-CA formulation showed the highest bioavailability in the ex vivo permeation studies. We thus further analysed this formulation to determine its antioxidant and anti-inflammatory effects in human 3D keratinocytes, in a range of dilutions related to malvidin contents between 0.6 and 0.07 $\mu\text{g mL}^{-1}$.

4.3.4 Evaluation of intracellular H_2O_2 production in human 3D keratinocytes

The cell-based bioassay recently developed by us to quantify the intracellular production of H_2O_2 in human living cells [13] was employed in 3D keratinocytes cultures upon treatment with the pro-oxidant agent menadione (2-metil-1,4-naftochinone), also known as vitamin K3 [14]. The selectivity against H_2O_2 is due to the salicylaldehyde (the sensing moiety) in the aromatic ring of the aryl-adamantylidene dioxetane CL probe [31]; indeed, upon reaction with H_2O_2 , the salicylaldehyde is oxidized to a catechol, followed by a subsequent ether cleavage to unmask the phenoxy-dioxetane, which further undergoes chemiexcitation to release the chemiluminescent signal at 540 nm [31]. Moreover, the presence of an electron-withdrawing acrylic group in the aromatic ring results in the production of a singlet excited state species that emits light with greater efficiency in aqueous solution, thus increasing CL emission intensity without the use of additional enhancers, allowing the probe to behave as an all-in-one reagent. Finally, the CL probe is able to permeate inside cells without affecting cell viability, thus making it possible to perform experiments in living cells without using any lysing agents [13]. Human HaCat spheroids in the wells of the “Ultra-Low Attachment Surface” 96-well black microtiter plate were incubated for 20 min with the CL probe working solution (5 μM of CL probe in 0.1 M PBS pH 7.4) and then treated with menadione (range 5–200 μM) to measure the intracellular production of H_2O_2 upon the pro-oxidant stimulus. The CL signal of the reaction was monitored for 40 min using a Luminoskan™ Ascent luminometric plate reader. As expected, the CL emission intensity increased with the

concentration of the stimulus (**Fig. 4.4**).

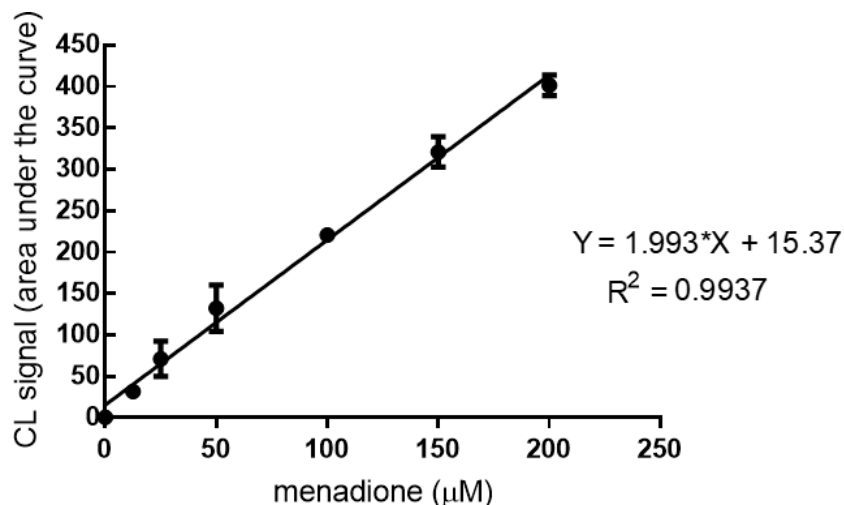


Figure 4.4: Chemiluminescence kinetic profiles obtained for human HaCat spheroids in the presence of the dioxetane CL probe and different concentrations of menadione (range: 5–200 µM).

A good correlation between the CL signal and the concentration of menadione was observed, which reflects the physiological mechanisms of intracellular H₂O₂ production. The concentrations of the pro-oxidant agent menadione required to obtain a detectable increase in the CL signal were in the micromolar range (LOD and LOQ were 6.3 µM and 8.0 µM, respectively).

4.3.5 Antioxidant activity of NaDES extracts toward human HaCaT Spheroids

This CL effect-based bioassay was utilized to evaluate the antioxidant activity of the BET-CA pomace extracts toward human HaCaT spheroids, as this was the formulation that showed more efficient permeation in skin. Oxidative stress is thought to play a central role in initiating and driving the signaling events that lead to cellular response and damage following UV irradiation. Indeed, ROS generated in keratinocytes are rapidly removed by non-enzymatic and enzymatic antioxidant substances to protect the living system from their harmful effects. These factors maintain a pro-oxidant/antioxidant balance, resulting in the stabilization of cell structure. An excess of free

radicals results in a cascade of events mediating progressive deterioration of cellular structure and function, leading to a loss of cellular integrity by modification of DNA and also to abnormal expression of cellular genes [32]. To test the antioxidant efficacy of the BET-CA formulation, HaCaT spheroids were treated for 24 h with increased concentrations of BET-CA, in the range of 0.07–0.6 $\mu\text{g mL}^{-1}$ of malvidin, and then injured with menadione. Specifically, on the day of the experiment, the cell medium containing BET-CA was changed to a fresh one, and cells were challenged with the pro-oxidant menadione (25 μM). The CL signal decreased proportionally to the concentration of malvidin present in the formulation, obtaining an IC₅₀ value of $0.15 \pm 0.02 \mu\text{g mL}^{-1}$. We performed, in parallel, the same experiment but treated cells for 24 h with malvidin in a BET-CA vehicle (range: 0.07–0.6 $\mu\text{g mL}^{-1}$), obtaining an IC₅₀ of $0.20 \pm 0.04 \mu\text{g mL}^{-1}$. These results suggest that the BET-CA formulation can reduce intracellular H₂O₂ production at least in part thanks to malvidin-derived modulation of intracellular pro-oxidant or antioxidant factors.

4.3.6 Protective effects of NaDES extracts on HaCaT spheroids in the presence of the cytotoxic agent menadione

HaCaT spheroids were used to preserve the functionality and responses of human keratinocytes towards the BET-CA formulation since inflammatory responses were initiated in the outer boundary of the skin. The release of pro-inflammatory cytokines and chemokines is one of the adaptive immune responses towards inflammatory stimuli. ROS production derived from exposure to environmental and toxic chemicals, along with UV irradiation, induce keratinocytes to release a wide array of mediators, such as interleukin (IL)-8, -6, -1 β and tumor necrosis factor α (TNF α) [33,34]. Several studies have suggested that nuclear factor kappa B (NF- κ B) and activator protein 1 (AP-1) are redox-regulated transcription factors and that their activation by different agents, including UV light exposure and pro-oxidant factors, is a determinant in promoting the expression of genes related to the inflammatory pathway. Among them, IL-8 plays a pivotal role in cutaneous inflammation

and has been implicated in tumor promotion [34]. **Figure 4.5A** shows that IL-8 release significantly increased ($p < 0.001$) in HaCaT spheroids challenged with menadione (25 μM for 16 h) while pre-treatment with the BET-CA formulation (range of malvidin: 0.15–0.6 $\mu\text{g mL}^{-1}$) partially counteracted IL-8 production ($p < 0.001$).

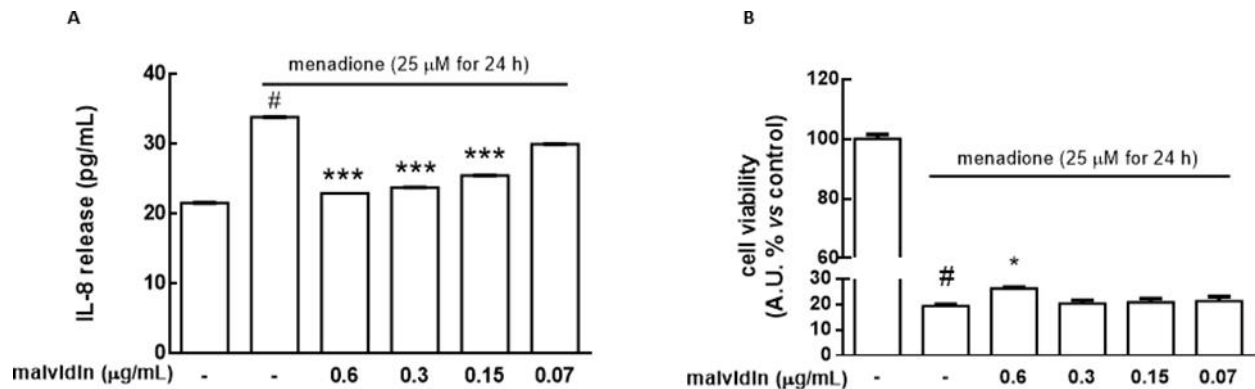


Figure 4.5: *HaCaT spheroids were treated with several dilutions of the BET-CA formulation (range of malvidin: 0.07–0.6 $\mu\text{g mL}^{-1}$) for 24 h, including 16 h in the presence of menadione (25 μM). (A) Release of the proinflammatory cytokine IL-8 (pg mL^{-1}) was determined by ELISA assay. (B) Cell viability was measured by cell counting kit 8, as described in the Materials and Methods section. Untreated HaCat spheroids served as a control (ctrl). Results are expressed as means \pm SD of three independent experiments, each performed in triplicate. * $p < 0.05$, *** $p < 0.001$ significantly different from menadione treatment; # $p < 0.001$ significantly different from the ctrl.*

Finally, we evaluated the ability of the BET-CA formulation to counteract the cyto- toxicity induced by menadione in a concentration range in which it was able to exert its antioxidant activity toward HaCaT spheroids. Cells were treated for 24 h with BET-CA (malvidin content range: 0.6–0.15 $\mu\text{g mL}^{-1}$), including 16 h in the presence of menadione (25 μM). The results showed that menadione treatment (25 μM for 16 h) significantly decreased the cell viability of HaCaT spheroids ($p < 0.001$) and that BET-CA (malvidin content: 0.6 $\mu\text{g mL}^{-1}$) was able to significantly counteract the activity of the cytotoxic agent ($p < 0.05$), suggesting that pomace extract exerts a beneficial,

preventive role in keratinocytes against harmful agents (**Fig. 4.5B**). To better understand if the malvidin in the BET-CA formulation was primarily responsible for the protective effects in IL-8 release and cell viability in HaCaT spheroids, we performed, in parallel, experiments treating cells for 24 h with malvidin with the BET-CA vehicle (range 0.07–0.6 $\mu\text{g mL}^{-1}$), including 16 h in the presence of menadione (25 μM). Supplementary Figures S1 and S2 show that malvidin with the BET-CA treatment was able to significantly counteract IL-8 release and the cytotoxic activity of menadione.

4.4 Conclusions

The sustainable exploitation of grape pomace is a useful strategy for wineries to reduce environmental contamination and as an alternative to reduce the carbon footprint in the whole production process. Its major use is in biogas or compost production, but more valuable routes can be explored. Here, we report an integrated/combined valorization of grape pomace that involved NaDES extraction and bioanalytical analysis to characterize the pomace's content and bioavailability, through HPLC-ESI MS/MS and biological activities, along with the use of smart, highly predictive and effect-based intracellular bioassays in 3D human keratinocytes, for cosmeceutical applications. In this work, NaDES efficiently replaced organic solvents and fulfilled the requirements of the sustainable development concept while maintaining the high-quality standards of safety and beneficial effects that cosmetic products need. In addition, the same cocktail for extraction was directly used as a safe vehicle for the topical formulation proposed. This innovative process can be easily scaled-up to obtain an efficient and sustainable method that can be applied not only for cosmetic purpose but also for oral and genital mucosa applications and in veterinary medicine. The characterization of grape pomace extracts in NaDES formulations and the bioavailability of their bioactive molecules are relevant and key points to increase the economic value of the obtained product. The BET-CA formulation not only exhibited the highest malvidin bioavailability but also

good antioxidant and anti-inflammatory effects at concentrations able to permeate in skin. Studies on the identities and individual concentrations of phenolics recovered after extraction, as well as their biological effects, support the application of extracts in topical preparations [35,36]. We developed a simplified and eco-sustainable process with the aim of making production easier to scale-up, as well cheaper, thus facilitating the valorisation of food waste. Moreover, our findings also support the use of NADES as promising carriers in new drug delivery systems for topical applications, since they can affect the permeation of active molecules. In conclusion, the waste matrices of the wine production chain can represent a promising starting material for the acquisition of active ingredients to be included in topically applied cosmetic products, as they are able to reduce excessive oxidative stress and inflammatory processes, thus preventing cellular aging.

4.5 Acknowledgements

We wish to thank Fernanda Martini (University of Ferrara) for providing HaCaT cells, Donato Calabria for technical support and Biosynth Carbosynth (Staad, Switzerland) for kindly providing the dioxetane CL AquaSpark™ 510 Peroxide Probe.

4.6 References

- [1] Sustainable Development Goals United Nations Home Page. Available online: <https://www.un.org/sustainabledevelopment/> (accessed on 25 May 2021).
- [2] Pomarici, E.; Corsi, A.; Mazzarino, S.; Sardone, R. The Italian Wine Sector: Evolution, Structure, Competitiveness and Future Challenges of an Enduring Leader. *Ital. Econ. J.* 2021, 7, 259–295.
- [3] Schieber, A.; Stintzing, F.; Carle, R. By-products of plant food processing as a source of functional compounds—Recent developments. *Trends Food Sci. Technol.* 2001, 12, 401–413.
- [4] Samorì, C.; Mazzei, L.; Ciurli, S.; Cravotto, G.; Grillo, G.; Guidi, E.; Pasteris, A.; Tabasso, S.; Galletti, P. Urease Inhibitory Potential and Soil Ecotoxicity of Novel “Polyphenols–Deep Eutectic Solvents” Formulations. *ACS Sustain. Chem. Eng.* 2019, 7, 15558–15567.
- [5] Ruesgas-Ramón, M.; Figueroa-Espinoza, M.C.; Durand, E. Application of Deep Eutectic Solvents (DES) for Phenolic Compounds Extraction: Overview, Challenges, and Opportunities. *J. Agric. Food Chem.* 2017, 65, 3591–3601.
- [6] Faggian, M.; Sut, S.; Perissutti, B.; Baldan, V.; Grabnar, I.; Dall’Acqua, S. Natural Deep Eutectic Solvents (NADES) as a Tool for Bioavailability Improvement: Pharmacokinetics of Rutin Dissolved in Proline/Glycine after Oral Administration in Rats: Possible Application in Nutraceuticals. *Molecules* 2016, 21, 1531.
- [7] Hänel, K.H.; Cornelissen, C.; Lüscher, B.; Baron, J.M. Cytokines and the Skin Barrier. *Int. J. Mol. Sci.* 2013, 14, 6720–6745.
- [8] Boukamp, P.; Petrussevska, R.T.; Breitkreutz, D.; Hornung, J.; Markham, A.; Fusenig, N.E. Normal keratinization in a spontaneously immortalized aneuploid human keratinocyte cell line. *J. Cell Biol.* 1988, 106, 761–771.
- [9] Lehmann, B. HaCaT Cell Line as a Model System for Vitamin D3 Metabolism in Human Skin. *J. Investig. Dermatol.* 1997, 108,
- [10] Klicks, J.; von Molitor, E.; Ertongur-Fauth, T.; Rudolf, R.; Hafner, M. In

vitro skin three-dimensional models and their applications.

J. Cell. Biotechnol. 2017, 3, 21–39.

- [11] Panic', M.; Stojkovic', M.R.; Kraljic', K.; Škevin, D.; Redovnikovic', I.R.; Src'ek, V.G.; Radoševic', K. Ready-to-use green polyphenolic extracts from food by-products. *Food Chem.* 2019, 283, 628–636.
- [12] Klicks, J.; Mašlo, C.; Kluth, A.; Rudolf, R.; Hafner, M. A novel spheroid-based co-culture model mimics loss of keratinocyte differentiation, melanoma cell invasion, and drug-induced selection of ABCB5-expressing cells. *BMC Cancer* 2019, 19, 1–14.
- [13] Calabria, D.; Guardigli, M.; Mirasoli, M.; Punzo, A.; Porru, E.; Zangheri, M.; Simoni, P.; Pagnotta, E.; Ugolini, L.; Lazzeri, L.; et al. Selective chemiluminescent TURN-ON quantitative bioassay and imaging of intracellular hydrogen peroxide in human living cells. *Anal. Biochem.* 2020, 600, 113760.
- [14] Klotz, L.-O.; Hou, X.; Jacob, C. 1,4-Naphthoquinones: From Oxidative Damage to Cellular and Inter-Cellular Signaling. *Mol.* 2014, 19, 14902–14918.
- [15] Caliceti, C.; Capriotti, A.L.; Calabria, D.; Bonvicini, F.; Chiozzi, R.Z.; Montone, C.M.; Piovesana, S.; Zangheri, M.; Mirasoli, M.; Simoni, P.; et al. Peptides from Cauliflower By-Products, Obtained by an Efficient, Ecosustainable, and Semi-Industrial Method, Exert Protective Effects on Endothelial Function. *Oxid. Med. Cell. Longev.* 2019, 2019, 1–13.
- [16] Antonioli, A.; Fontana, A.R.; Piccoli, P.; Bottini, R. Characterization of polyphenols and evaluation of antioxidant capacity in grape pomace of the cv. Malbec. *Food Chem.* 2015, 178, 172–178.
- [17] Lee, J.; Durst, R.W.; Wrolstad, R.E.; Eisele, T.; Giusti, M.M.; Hofsommer, H.; Koswig, S.; Krueger, D.A.; Kupina, S.; Martin, S.K.; et al. Determination of Total Monomeric Anthocyanin Pigment Content of Fruit Juices, Beverages, Natural Colorants, and Wines by the pH Differential Method: Collaborative Study. *J. AOAC Int.* 2005, 88, 1269–1278.
- [18] Carlsen, C.; Stapelfeldt, H. Light sensitivity of elderberry extract.

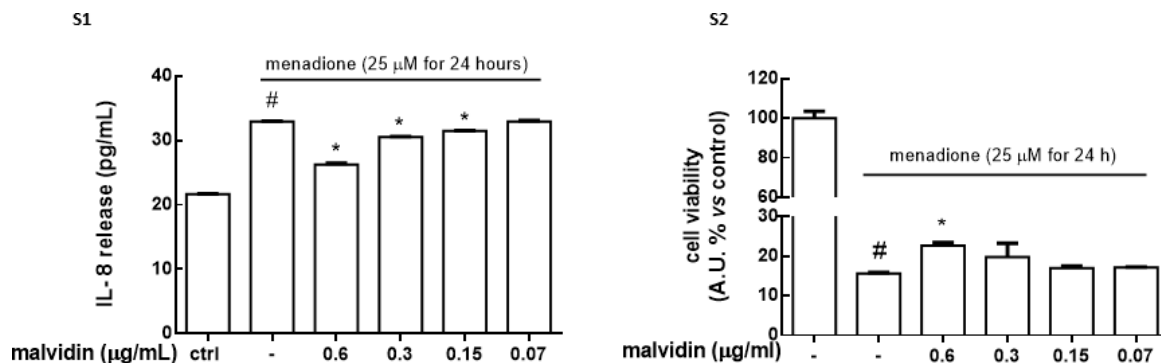
- quantum yields for photodegradation in aqueous solution. *Food Chem.* 1997, 60, 383–387.
- [19] Ignat, I.; Volf, I.; Popa, V.I. A critical review of methods for characterisation of polyphenolic compounds in fruits and vegetables. *Food Chem.* 2011, 126, 1821–1835.
- [20] Qi, Q.M.; Duffy, M.; Curreri, A.M.; Balkaran, J.P.R.; Tanner, E.E.L.; Mitragotri, S. Comparison of Ionic Liquids and Chemical Permeation Enhancers for Transdermal Drug Delivery. *Adv. Funct. Mater.* 2020, 30, 2004257.
- [21] Benvenuti, L.; Sanchez-Camargo, A.D.P.; Zielinski, A.A.F.; Ferreira, S.R.S. NADES as potential solvents for anthocyanin and pectin extraction from *Myrciaria cauliflora* fruit by-product: In silico and experimental approaches for solvent selection. *J. Mol. Liq.* 2020, 315, 113761.
- [22] EUR-Lex, Access to European Union Law. Available online: <http://eur-lex.europa.eu/legal-content/EN/TXT/PDF/?uri=CELEX:32006D0257.pdf> (accessed on 25 May 2021).
- [23] Fruijtier-Pöllöth, C. Safety assessment on polyethylene glycols (PEGs) and their derivatives as used in cosmetic products. *Toxicology* 2005, 214, 1–38.
- [24] Panuwet, P.; Hunter, R.E.; D'Souza, P.E.; Chen, X.; Radford, S.A.; Cohen, J.R.; Marder, M.E.; Kartavenka, K.; Ryan, P.B.; Barr, D.B. Biological Matrix Effects in Quantitative Tandem Mass Spectrometry-Based Analytical Methods: Advancing Biomonitoring. *Crit. Rev. Anal. Chem.* 2016, 46, 93–105.
- [25] Benson, H.A.; Watkinson, A.C. *Topical and Transdermal Drug Delivery: Principles and Practice*, 1st ed.; John Wiley & Sons: Hoboken, NJ, USA, 2012.
- [26] Bharate, S.S.; Vishwakarma, R.A. Impact of preformulation on drug development. *Expert Opin. Drug Deliv.* 2013, 10, 1239–1257.
- [27] Moser, K. Passive skin penetration enhancement and its quantification

in vitro. *Eur. J. Pharm. Biopharm.* 2001, 52, 103–112.

- [28] Nystedt, H.L.; Grønlien, K.G.; Tønnesen, H.H. Interactions of natural deep eutectic solvents (NADES) with artificial and natural membranes. *J. Mol. Liq.* 2021, 328, 115452.
- [29] Liu, Y.; Liu, Y.; Tao, C.; Liu, M.; Pan, Y.; Lv, Z. Effect of temperature and pH on stability of anthocyanin obtained from blueberry. *J. Food Meas. Charact.* 2018, 12, 1744–1753.
- [30] Macário, I.; Oliveira, H.; Menezes, A.C.; Ventura, S.; Pereira, J.L.; Gonçalves, A.M.M.; Coutinho, J.; Gonçalves, F.J.M. Cytotoxicity profiling of deep eutectic solvents to human skin cells. *Sci. Rep.* 2019, 9, 3932.
- [31] Ye, S.; Hananya, N.; Green, O.; Chen, H.; Zhao, A.Q.; Shen, J.; Shabat, D.; Yang, D. A Highly Selective and Sensitive Chemiluminescent Probe for Real-Time Monitoring of Hydrogen Peroxide in Cells and Animals. *Angew. Chem. Int. Ed.* 2020, 59, 14326–14330.
- [32] Kurutas, E.B. The importance of antioxidants which play the role in cellular response against oxidative/nitrosative stress: Current state. *Nutr. J.* 2015, 15, 1–22.
- [33] Mohamadzadeh, M.; Müller, M.; Hultsch, T.; Enk, A.; Saloga, J.; Knop, J.; Müller, M. Enhanced expression of IL-8 in normal human keratinocytes and human keratinocyte cell line HaCaT in vitro after stimulation with contact sensitizers, tolerogens and irritants. *Exp. Dermatol.* 1994, 3, 298–303.
- [34] Park, K.; Lee, J.-H.; Cho, H.-C.; Cho, S.-Y.; Cho, J.-W. Down-regulation of IL-6, IL-8, TNF- α and IL-1 β by glucosamine in HaCaT cells, but not in the presence of TNF- α . *Oncol. Lett.* 2010, 1, 289–292.
- [35] Hubner, A.; Sobreira, F.; Neto, A.V.; Pinto, C.A.S.D.O.; Dario, M.; Díaz, I.; Lourenço, F.R.; Rosado, C.; Baby, A.R.; Bacchi, E.M. The Synergistic Behavior of Antioxidant Phenolic Compounds Obtained from Winemaking Waste's Valorization, Increased the Efficacy of a Sunscreen System. *Antioxidants* 2019, 8, 530.
- [36] Hübner, A.A.; Sarruf, F.D.; Oliveira, C.A.; Neto, A.V.; Fischer, D.C.H.;

Kato, E.T.M.; Lourenço, F.R.; Baby, A.R.; Bacchi, E.M. Safety and Photoprotective Efficacy of a Sunscreen System Based on Grape Pomace (*Vitis vinifera* L.) Phenolics from Winemaking. *Pharmaceutics* 2020, 12, 1148.

4.7 Supplementary material



Supplementary Figures. *HaCaT* spheroids were treated for 24 h with malvidin (range 0.07 – 0.6 μg mL⁻¹) dissolved in BET-CA vehicle, in the presence of menadione (25 μM) for 16 h. 1) Release of the proinflammatory cytokine IL-8 (pg mL⁻¹) was determined by ELISA assay. 2) Cell viability was measured by cell counting kit-8 as described in Materials and Methods Section. *HaCaT* spheroids not treated served as a control (ctrl). Results are expressed as mean ± SD of three independent experiments, each performed in triplicate. **P*<0.05, ****P*<0.001 significantly different from menadione treatment; # *P*<0.001 significantly different from the ctrl.

5

Fermentation of *Vaccinium floribundum* Berries with *Lactiplantibacillus plantarum* Reduces Oxidative Stress in Endothelial Cells and Modulates Macrophages Function

Reproduced from: “Fermentation of *Vaccinium floribundum* Berries with *Lactiplantibacillus plantarum* Reduces Oxidative Stress in Endothelial Cells and Modulates Macrophages Function”

*Luisa Marracino, **Angela Punzo**, Paolo Severi, Rosane Nganwouo Tchoutang, Celia Vargas-De-la-Cruz, Francesca Fortini, Francesco Vieceli Dalla Sega, Alessia Silla, Emanuele Porru, Patrizia Simoni, Valentina Rosta, Alessandro Trentini, Achille Wilfred Ouambo Talla, Silvana Hrelia, Carlo Cervellati, Paola Rizzo and Cristiana Caliceti.*

Nutrients, 2022; 14(8), 1560

Reproduced by permission of MDPI

<https://www.mdpi.com/openaccess>

5.1 Introduction

Oxidative stress is involved in the development of several diseases, including atherosclerosis, the major cause of many cardiovascular diseases (CVDs) [1]. The molecular mechanisms by which oxidative stress contributes to atherosclerosis are well characterized [2-4]. Specifically, the dysregulated production of intracellular reactive oxygen species (ROS) causes phenotypical changes to the endothelial cell surface leading to endothelium dysfunction, which precedes the formation of atherosclerotic plaque [1]. Thus, the maintenance of the endothelium function represents a promising approach to prevent CVDs.

In recent years, the potential role of natural bioactive compounds in preventing and treating disorders where oxidative stress is involved, such as cancers, metabolic diseases (e.g., obesity and diabetes), neurodegenerative, and CVDs, has clearly emerged. Indeed, since natural products exert beneficial biological activities and possess pharmacological properties, they could play a valuable role in drug discovery [5–7].

Epidemiological and clinical studies have reported the beneficial properties of berries in terms of natural antioxidant capabilities and decreased risk of CVDs [8,9]. Berries are significantly enriched in flavonoids and phenolic acids, which are responsible for their protective effects, such as reducing endothelial dysfunction [10] and reducing oxidative stress, and mitochondrial damage [11,12], as well as the anti-inflammatory mediators induction [13]. Both *in vivo* and *in vitro* studies have shown that flavonoids, particularly quercetin and its metabolites, dampen oxidative stress, inflammation, and interfere with atherosclerosis progression [14-21].

Therefore, it is not surprising that berries have been increasingly employed worldwide as components of functional food and dietary supplements. In this regard, there is growing interest in studying the beneficial effects of berries of the *Vaccinium* species from South America, such as bilberry or blueberry, on human health [22]. *Vaccinium floribundum*, commonly known as Pushgay, Mortiño, or Andean blueberry, is a deciduous, spreading shrub, similar to European blueberries, that belongs to the family *Ericaceae*. This species is native to Ecuador and Peru but is also found in other countries of South and Central

America, where it grows at altitudes from 1800 to 3800 m [23]. Local people widely consume these berries as fresh fruit or processed products. Moreover, local communities use the extracts of this plant to treat many pathologies, including diabetes and inflammation [24]. Pushgay berries are rich in quercetin, hydroxycinnamic acids and anthocyanins [25] responsible for their anti-oxidant, anti-inflammatory, and anti-microbial properties [26]. However, the poor bioavailability of the polyphenols present in the berries, mostly influenced by their complex chemical structures, points out their direct effect on human health. None of the studies conducted so far have investigated the potential enhancement of the beneficial effects of Pushgay berries after fermentation.

Traditionally, fermentation has been used to preserve perishable foods. However, this process has attracted significant attention since it leads to the production of health-promoting components that increase the nutritional value of foods. Indeed, the fermentation increases the bioavailability of polyphenols [27], since enzymes present in lactic acid bacteria (LAB) produce changes in both profile and types of bioactive compounds, producing simpler phenolic compounds that may be absorbed in the duodenum. [28,29].

LAB plays an important role not only in improving the antioxidant properties of different foods but also in modulating immune response. Some LAB strains (mainly *Lactobacillus* and *Streptococcus*) and *Bifidobacterium* modulate the innate and adaptive immune response through the induction of pro-inflammatory cytokines, such as TNF α , interferon- γ (IFN- γ), some interleukins (IL) (IL-1 β , IL-6, IL-12) and nitric oxide (NO) [30]. Several studies have shown that LAB-mediated immunomodulation is species-specific: indeed, some strains of *Lactobacillus* reduce the expression levels of pro-inflammatory mediators while others exert opposite effects [31].

This study aimed to evaluate the phytochemical profile and the antioxidant and immunomodulatory activities on endothelial cells and macrophages of Pushgay berries before and after a fermentation process with *Lactiplantibacillus plantarum*. We show that fermentation of Pushgay berries enhances their immunostimulant and antioxidant performance, thus supporting existing studies on the contribution of lactic bacteria fermentation to the health benefits of food (**fig. 5.1**).

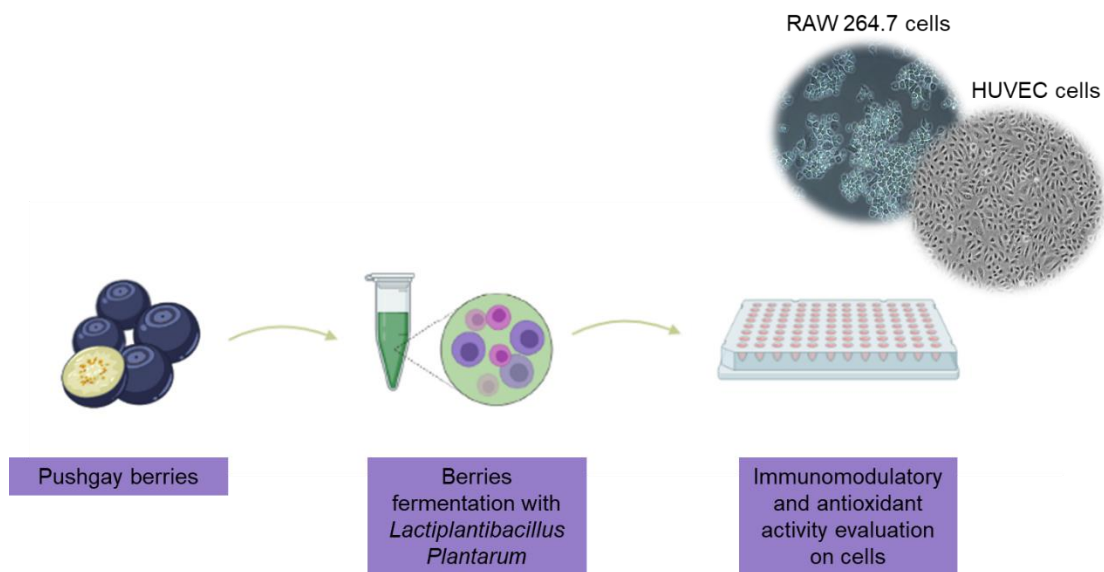


Figure 5.1: Schematic representation of the study.

5.2 Materials and Methods

5.2.1 Reagents

Human umbilical vein endothelial cells (HUVECs), Dulbecco's Modified Eagle's Medium (DMEM), basal medium M200, IFN- γ (100 U/mL in PBS), TNF α (10 μ g/mL in Milli-Q H $_2$ O), Superscript III reverse transcriptase, random primers, dNTPs, and RNaseOut were obtained from Life Technologies (Carlsband, CA, USA). RAW264.7 were obtained from ATCC (Manassas, VA, USA). Fetal bovine serum (FBS) and EGM-2 Endothelial Medium SingleQuot kit were purchased from Lonza (Basel, Switzerland). RNeasy kit for RNA extraction was purchased from Qiagen (Hilden, Germany). Perfecta SYBR Green Supermix for Quantitative RT-PCR was obtained from Quanta Biosciences (Gaithersburg, MD, USA). Oligonucleotides for qRT-PCR were purchased from IDT (Coralville, IA, USA). H $_2$ O $_2$ -CL- 510 probe (AquaSpark™ Peroxide Probe) was provided by Biosynth (Staad, Switzerland). The Cytotoxicity LDH Assay kit and the Cell Counting Kit-8 were purchased from Do-jindo Molecular Technologies (Kumamoto, Japan). *Lactiplantibacillus plantarum* starters were supplied by the American Type Culture Collection (ATCC, Manassas, VA, USA). De Man, Rogosa, and Sharpe (MRS) agar powder and yeast from *Saccharomyces cerevisiae* were purchased from Sigma-Aldrich (St. Louis, MO, USA). Anthocyanins and flavonols standards for HPLC-ESI-MS/MS analysis were bought from Carbosynth (USA, Canada

& South America). Protease inhibitor mix was purchased from SERVA Electrophoresis GmbH (Heidelberg, Germany) and phosphatase inhibitor mix (phosSTOP) from F. Hoffmann–La Roche SA (Basel, Switzerland), The other materials were purchased from Sigma-Aldrich.

5.2.2 Pushgay berries fermentation

Pushgay berries were collected between March and April 2019 in Cajamarca province (Cajamarca, Perú) and their taxonomy was certified by the Herbario San Marcos (National University of San Marcos, Lima, Peru) at the National University of San Marcos (Lima, Peru). Berries were crushed, freeze-dried by a Heto PowerDry LL1500 (Thermo Fisher Scientific, Waltham, MA, USA) finely ground in a mortar, and stored at -20 °C until use [32].

For the fermentation process, *Lactiplantibacillus plantarum* at 5% was grown in 10 mL of MRS agar broth for 16 h at 30 °C under anaerobic conditions, then diluted to 1% with an additional 40 mL MRS agar broth, and allowed to grow for additional 16 h under the same conditions. 200 g of frozen berries were disinfected with sodium hypochlorite 0.5% (w/v), solubilized in 500 mL of distilled water, and placed in a dark bottle. The solution was exposed to a heat shock at 70 °C for 10 min, then cooled in an ice bath until it reached a temperature of 40 °C. Finally, they were heated to 85 °C for 5 min and cooled in an ice bath until they reached a temperature of 25 °C. The solution was divided into sterile flasks, then the inoculum (5×10^7 CFU/mL) and a yeast extract were added (0.01 and 0.4% w/v, respectively). Fermentation was carried out at a temperature of 30 °C for 48 h, in the dark and under constant stirring. The fermentates were lyophilized and stored at -20 °C before being shipped to Italy. Not fermented Pushgay berries were just crushed, freeze-dried by a Heto PowerDry LL1500 (Thermo Fisher), finely ground in a mortar, lyophilized, and stored at -20 °C before being shipped to the laboratories at the University of Bologna, Italy.

5.2.3 Preparation of Pushgay berries solutions

Once in Bologna (Italy), 10 mg of lyophilized Pushgay berries (fermented or not) were solubilized in 1 mL of sterile dimethyl sulfoxide (DMSO) using a sonicator (Soniprep 150 Ultrasonic Disintegrator). Specifically, five sonication cycles were performed while keeping the samples on ice and in the dark, vortexing the samples between the cycles. The solutions obtained were subsequently aliquoted and stored at $-20\text{ }^{\circ}\text{C}$. Samples were briefly centrifuged at a low speed ($700 \times g$) before cell treatment.

5.2.4 Evaluation of total phenolic content

The total phenolic content of lyophilized berries was determined using the Folin–Ciocalteu reagent method described by Ainsworth et al. [33].

Briefly, 100 μL of fermented or non-fermented berries solutions were mixed with a double volume of Folin–Ciocalteu reagent. Then, 800 μL of 700 mM aqueous sodium carbonate was added, and the reaction mixture was incubated for 2 h at room temperature. After the incubation, 200 μL of each sample were transferred into a 96-well microplate. The absorbance was spectrophotometrically read at 765 nm using distilled water as a blank. Gallic acid (range 100–1000 $\mu\text{g}/\text{mL}$) was used as standard, and the total phenolic content was expressed as μg of gallic acid equivalent (GAE)/ μg lyophilized berry.

5.2.5 HPLC-ESI-MS/MS analysis

Liquid chromatography was performed using a 2690 Alliance system (Waters, Milford, MA, USA). Analytical separation was performed using Phenyl-Hexyl 1.7 μm , 150 mm \times 2.1 mm i.d. (Waters, Milford, MA, USA). The mobile phase was constituted as follows: 15 mM ammonium acetate in water adjusted to pH 8.0 with ammonia (solvent A) and methanol 99.9% (solvent B). Chromatographic separation was achieved at a 0.15-mL/min flow rate under gradient elution conditions: 95% A for 5 min, 95–40% A from 5 to 15 min, 40–20% from 15 to 20 min, 20% A from 20 to 25 min, 20–95% A from 25 to 27 min, and 95% A from 27 to 35 min. All the changes in the mobile phase composition were linear. The analytical column was maintained at $30\text{ }^{\circ}\text{C}$. The column effluent was introduced

into the ESI source, operating in positive ionization mode, connected to a triple quadrupole mass spectrometer (Quattro-LC, Micromass) operating in the multiple reaction monitoring (MRM) acquisition mode. Standard solutions of 3 anthocyanins were used to evaluate polyphenols profile of fermented and non-fermented Pushgay berries: malvidin-3-O-glucoside (MAL), quercetin-3-O-glucoside (QUE), and quercetin aglycone (QA). The most abundant signal for each compound in multiple reaction monitoring mode (MRM) was monitored for the quantification [m/z 330.9 \rightarrow 330.9 (quercetin, aglycone), m/z 302.9 \rightarrow 302.9 (quercetin-O-glucoside), m/z 330.9 \rightarrow 330.9 (malvidin-O-glucoside), and m/z 153.6 \rightarrow 125.6 (hydroxytyrosol)]. The analytical method was developed and validated according to ICH guidelines to satisfy high analytical parameters in terms of accuracy and reproducibility. Limit of detection (LOD) and limit of quantification (LOQ) were determined by signal to noise ratio (LOD = 3, LOQ = 10). Recovery and the matrix effect were evaluated for each compound before the sample analysis. Seven point calibration curves (0.5, 1, 2.5, 5, 10, 25, and 50 ng/mL) were used for the quantification of each compound using standard solutions in the mobile phase (phase A: phase B 95:5). Internal standard hydroxytyrosol was used for calibration curves at a fixed concentration of 5 ng/mL. Then, 100 mg of each sample was extracted by sonication with 1 mL of 70% ethanol solution three times. The samples were centrifuged, the supernatants were pooled, and 10 μ L of the sample was injected into the HPLC-MS.

5.2.6 Cell culture

HUVECs were plated on 1.5% gelatin-coated tissue culture dishes and maintained in phenol red-free basal medium M200 containing 2% FBS and EGM-2 at 37 °C with 5% CO₂. HUVECs at passages 2 to 7 were actively proliferating (70–90% of confluency) when they were harvested and analyzed. RAW 264.7 cells (murine monocyte/macrophage cell line) were cultured in DMEM without phenol red containing 4 mM L-glutamine, 4500 mg/L glucose, 10% FBS, 100 IU/mL penicillin, and 100 μ g/mL streptomycin at 37 °C with 5% CO₂; for experiments, cells were used at passages 2 to 7, to avoid possible

changes of cellular phenotype.

5.2.7 Cell viability and proliferation assays

In HUVECs, WST8 (2-(2-methoxy-4-nitrophenyl)-3-(4-nitrophenyl)-5-(2,4-disulfophenyl)-2H-tetrazolium, monosodium salt) was used to determine the cell viability. Indeed, in the presence of an electron mediator, WST8 is reduced to red formazan dye by dehydrogenases present in the cells. The amount of red dye generated is directly proportional to the number of living cells [34].

For the experiments, 1.0×10^4 cells/well HUVECs were seeded in a 96-well plate.

After 80% confluence had been reached, cells were treated with different concentrations of berries solutions: fermented Pushgay (FP) and Pushgay (P) in complete culture medium for 24 h (range 0.25–100 $\mu\text{g/mL}$). The decrease in absorbance between the 24 h treatment (representing t1) and the control (representing t0) was monitored at 37 °C at 450 nm using an AMR-100 Microplate reader (Allsheng, Hangzhou, China).

To determine cell viability in RAW 264.7, cells in the logarithmic growth phase were harvested and seeded in six well-plates (3.0×10^5 cells/well) overnight. Cells were incubated for 24 h with different concentrations of berries solutions (range 2.5–5 and 10 $\mu\text{g/mL}$ in 0.1% DMSO). At the end of incubation, viability was determined with the Burker chamber utilizing the Trypan Blue exclusion test. The evaluation of the effects of berries on cell proliferation/metabolism in RAW 264.7 was investigated through the Trypan Blue and Alamar Blue assays. For Trypan Blue assay, RAW 264.7 cells, harvested in the logarithmic growth phase, were plated in triplicate in 24-well plates (3.0×10^4 cells/well) overnight. Subsequently, cells were grown at 37 °C, 5% CO₂ for 24 h and treated with 10 $\mu\text{g/mL}$ of each berry solution and further incubated for 24 and 72 h. At the end of incubation, cell number was determined with the Burker chamber after staining with Trypan Blue.

For the Alamar Blue assay, RAW 264.7 cells in the logarithmic growth phase were harvested and plated in 24 wells in triplicate (3.0×10^4 cells/well) overnight. Next, cells were grown at 37 °C, 5% CO₂ for 24 h and incubated with 10 $\mu\text{g/mL}$

of each berry solution for 24 and 72 h before adding Alamar Blue solution (5%) in complete cell culture medium. Cells were incubated at 37 °C, 5% CO₂ for 3 h. Next, 100 µL of the medium was transferred from each well to a 96-well plate. The reading was carried out with a spectrophotometer at 570 nm (Thermo Electron Corp., model MultiskanEX, Vantaa, Finland).

5.2.8 Cytotoxicity

In HUVECs, the toxicity of the berries solutions was assessed by lactate dehydrogenase (LDH) release. The enzyme LDH catalyzes the conversion of lactate to pyruvate via NAD⁺ reduction to NADH; next the diaphorase reduces tetrazolium salt, oxidizing NADH, to a red formazan product that can be spectrophotometrically determined at 490 nm. LDH release from HUVECs treated for 24 h with berries solutions was monitored by collecting aliquots of the medium under the same experimental conditions performed above for cell viability assays, as previously reported [35]. The decrease in absorbance between the treatment after 24 h and the control was monitored at 37 °C at 490 nm using an AMR-100 Microplate reader (Allsheng).

5.2.9 RNA extraction

HUVEC cells (1.5×10^5 cells/well) were seeded in six well-plates and incubated with 10 µg/mL of berries solutions, in the presence or absence of H₂O₂ (300 µM), for 24 h. RAW 264.7 cells (4.0×10^5 cells/well) were seeded in six well-plates and incubated with 10 µg/mL of berries solutions, in the presence or absence of IFN-γ 100 U/mL, for 24 h. Total RNA was extracted using the commercial kit RNeasy mini Kit (Qiagen, Hilden, Germany). The concentration and purity of RNA were determined using the Nanodrop 1000 spectrophotometer (Thermo Fisher Scientific).

5.2.10 Reverse Transcriptase-Quantitative PCR

Total RNA (500 ng) was reverse transcribed in a volume of 25 µL using 250 units of SuperScript III reverse transcriptase (Life Technologies, Carlsbad, CA, USA) and 50 ng of random hexamers using the reaction conditions described in [36].

Next, 2 μ L of the cDNA solution were used for the quantitative, real time PCR experiments to measure the amount of transcripts. Real-time PCR reactions were performed on a 7500 Fast Real- Time PCR System (Applied Biosystems, Life Technologies, Carlsbad, CA, USA) using PerfeCta SYBR Green SuperMix with ROX kit (VWR International), according to the manufacturer's protocol, in a final volume of 23 μ L. Primers were purchased from IDT (Coralville, IA, USA). Differences in gene expression levels were determined by the $2^{-\Delta\Delta C_t}$ formula [37], using RPL13A (ribosomal protein L13-A) as the reference gene. HO1 forward 5'-CAACAAAGTGCAAGATTCTG-3', reverse 5'-GATTCACATGGCATAAAG-3'; RPL13A forward 5'-CACCTGGAGGAGAAGAGGA-3', reverse 5'-CCGTAGCCTCATGAGCTGTT-3'. iNOS forward 5'-GGCAGACTGGATTTGGCTGG-3', reverse 5'-CAACATCTCCTGG TGGAACAC-3'; TNF α forward 5'-ACTGAACTTCGGGGTGATCG-3', reverse 5'-CCACTTG GTGGTTTGTGAGTG-3'.

5.2.11 Antioxidant activity of berries solution

The intracellular antioxidant activity of the berries was estimated in HUVECs by using the chemiluminescent (CL) cell-based bioassay previously described [38]. Briefly, two days before the experiment, HUVECs (1.0×10^4 cells/well) were plated in a 96-well black microtiter with clear bottom and on the next day, cells were treated with serial dilutions of FP and P (range 0.25–25 μ g/mL) for 24 h. Then, cell medium was removed and 100 μ L of the H₂O₂-CL probe working solution (10 μ M of CL probe in PBS, pH 7.5, final concentration 5 μ M) was added. After the incubation for 20 min at 37 °C, 100 μ L of the oxidant agent menadione (final concentration 25 μ M in PBS, pH 7.4) was dispensed in each well to induce intracellular H₂O₂ production. CL emission signal was monitored for 40 min using a Luminoskan™ Ascent luminometric plate reader. The temperature was maintained at 37 °C during the measurement and the dose–response curve was obtained by plotting the CL signal versus the actual concentration of the menadione and fitting the experimental data to a straight line using the method

of least squares.

5.2.12 Preparation of cell lysates for enzymatic assay

HUVEC cells (1×10^6 cells/dish) were seeded in a 100 mm Petri dish and incubated with 10 $\mu\text{g/mL}$ of berries solutions, in the presence or absence of H_2O_2 (300 μM), for 24 h. The lysates were obtained by scraping cells in a chilled buffer (PBS containing 1 mM phenylmethanesulfonyl fluoride, protease and phosphatase inhibitors mix according to manufacturer's instructions). The lysates were then incubated at $+4^\circ\text{C}$ for 30 min and subsequently centrifuged at $10,000 \times g$ for 10 min. The protein concentration in the supernatant was determined according to Bradford method [39].

5.2.13 Glutathione Reductase (GR) activity assay

GR activity assay was performed according to Smith and collaborators [40]. The assay is based on the reduction in oxidized glutathione (glutathione disulfide, GSSG) to the reduced form (GSH) performed by GR. GSH, in turn, can react with DTNB [5,5'-dithiobis (2-nitrobenzoic acid)], increasing the absorbance at 412 nm. In brief, 10 μL of cell lysate were added to 240 μL reaction mix composed by 100 mM potassium phosphate buffer, pH 7.4 with 0.141 mM NADPH, 0.75 mM DTNB, and 1.41 mM GSSG. The increase in absorbance was spectrophotometrically monitored at 1 min intervals over 10 min. GR activity was calculated using extinction coefficient $14,150 \text{ M}^{-1} \text{ cm}^{-1}$ and expressed as units per milligram protein.

5.2.14 Glutathione Peroxidase (Gpx) activity assay

Gpx activity assay was performed by indirect spectrophotometric analysis according to the method of Engel et al. [41], based on the oxidation of GSH to GSSG performed by Gpx, and simultaneously reduced again to GSH by GR with the consumption of NADPH. Briefly, 5 μL of cell lysate was added to 145 μL of reaction mix (phosphate-buffered saline, pH 7.4 with 3 U/mL of GR, and 1 mM of GSH) and incubated at 37°C for 10 min. Then, 100 μL of the second reaction mix (phosphate-buffered saline, pH 7.4 with 0.2 mM NADPH, and 0.4 mM tert-

butyl hydroperoxide) were added to the reaction tube. The reduction in NADPH concentration was monitored spectrophotometrically at 340 nM at 30 s intervals over 20 min. Gpx activity was calculated using extinction coefficient $6220 \text{ M}^{-1} \text{ cm}^{-1}$ and expressed as units per milligram protein.

5.2.15 Catalase (CAT) activity assay

CAT assay was performed by indirect spectrophotometric analysis by measuring the absorbance of hydrogen peroxide consumed by CAT. Briefly, 20 μL of cell lysate were added to 230 μL of 50 mM sodium phosphate buffer, pH 7.0 with 12 mM H_2O_2 . One unity of CAT is defined as 1 μmol of H_2O_2 consumed for minute. CAT activity is expressed as units per milligram protein.

5.2.16 Superoxide Dismutase (SOD) activity assay

SOD assay was performed according to the method of Cervellati et al. [42]. Briefly, 10 μL of cell lysate were added to 10 μL of 50 mM phosphate buffer, pH 7.8 with 0.2 U/L of xanthine oxidase. Then, 250 μL of reaction mix (50 mM phosphate buffer, pH 7.8 with 900 μM xanthine, and 85 μM cytochrome C) were added to the reaction tube. The rate of cytochrome C reduction was monitored spectrophotometrically at 550 nm at 10 s intervals over 5 min.

5.2.17 Statistical analysis

Results are expressed as means of at least three independent experiments with SD. Differences between the means were determined by unpaired student's t-test or one-way ANOVA, followed by Bonferroni multiple comparison test using the GraphPad Prism Software, version 6.0 (GraphPad Software, Inc., La Jolla, CA, USA). A p-value ≤ 0.05 is statistically significant.

5.3 Results

5.3.1 Content of polyphenols in berries solutions

The total phenolic content was determined by the Folin–Ciocalteu reagent method obtaining a similar polyphenols concentration in fermented and non-fermented

Pushgay berries (P: 2.38 ± 0.01 and FP: 2.95 ± 0.14 $\mu\text{g GAE}/\mu\text{g}$ lyophilized berry) (**Table 5.1**), in line with previous data [32].

Quercetin glycoconjugates are the major flavonoid compounds in Pushgay berries [24,25] and the analysis of the phenolic profile of FP and P was obtained through untargeted characterization by ultra-high-performance liquid chromatography coupled to high-resolution mass spectrometry (UHPLC-HRMS) [32]. Cerrato et al. [32] showed that glyco-conjugations were mostly hydrolyzed following fermentation, and a higher concentration of free flavonols was found, mainly quercetin (97% of the total flavonol content) [32]. In the untargeted analysis, Cerrato et al. also identified, for the first time, a large number of phenolic acids and their derivatives (≈ 145 compounds) in FP and P; furthermore, anthocyanins in P were almost completely degraded after fermentation in phenolic acids [32].

Table 5.1: Total polyphenol content and quantification of quercetin-3-O-glucoside and quercetin aglycone in lyophilized fermented or not fermented berries.

Berry	Total Polyphenol Content ($\mu\text{g GAE}/\mu\text{g}$ Lyophilized Berry \pm SD)	Quercetin-3-Oglucoside ($\mu\text{g/g} \pm$ SD)	Quercetin Aglycone ($\mu\text{g/g} \pm$ SD)
FP	2.38 ± 0.01	96.0 ± 0.1	1680.0 ± 0.2
P	2.95 ± 0.14	720.0 ± 0.1	<i>n.d.</i>

SD: Standard Deviation. FP: Fermented Pushgay; P: Pushgay; *n.d.*: not determined.

In this study, we performed a targeted/quantitative analysis of quercetin (both the aglycone and glycoconjugate forms) through HPLC-ESI MS/MS (**Table 5.1**). In agreement with published data [32], our results showed that quercetin-3-O-glucoside was present in both FP and P: 96 ± 0.1 $\mu\text{g/g}$ and 720 ± 0.1 $\mu\text{g/g}$, respectively, while quercetin aglycone was identified only in the FP with a concentration of 1680 ± 0.2 $\mu\text{g/g}$. Moreover, in line with previous analysis [32], malvidin-3-O-glucoside was not detected, possibly due to differences in the environment of growth and climate with respect with other Vaccinium berries [25]. Quercetin aglycone significantly increases after fermentation, suggesting that LAB fermentation induces the hydrolysis of glucosides (**Table 5.1**). Quercetin-3-O-glucoside has a higher solubility than the aglycone and is rapidly absorbed through the intestinal sodium-glucose cotransporter, irrespective of the position of the glucose moiety [43]. Nevertheless, quercetin-3-O-glucoside biological activity

is limited due to the presence of the sugar moiety. Specifically, the absence of the sugar molecule on the flavonoids appears to be important for their free radical scavenging and antioxidant activities [44,45] and, consistently, treatment with quercetin aglycone is more effective than quercetin-3-O-glucoside in the induction of antioxidant and detoxifying enzymes, such as heme oxygenase (HO-1), NAD(P)H quinone oxidoreductase (NQO-1), and gamma-glutamylcysteine synthetase (GCLC) through the Nrf2/ARE pathway [44].

5.3.2 Cytotoxicity of berries solutions in HUVECs

HUVECs were treated for 24 h with FP or P solutions (between 0.25 and 25 $\mu\text{g}/\text{mL}$) to investigate their potential cytotoxicity. **Figure 5.2A** shows that treatment does not reduce the cell metabolism at any of the tested concentrations, as indicated by the absence of significant changes in the production of formazan dye in treated cells compared to the control. At the same time, lactate dehydrogenase (LDH) release was quantified in cell culture medium as a biomarker of cytotoxicity. Treatments with berries solutions for 24 h at any of the tested concentrations did not increase the release of LDH in cell medium (**Fig. 5.2B**). Treatment with higher concentrations of FP and P solutions (50 and 100 $\mu\text{g}/\text{mL}$) significantly increased LDH release (data not shown), indicating cytotoxic effects at these concentrations.

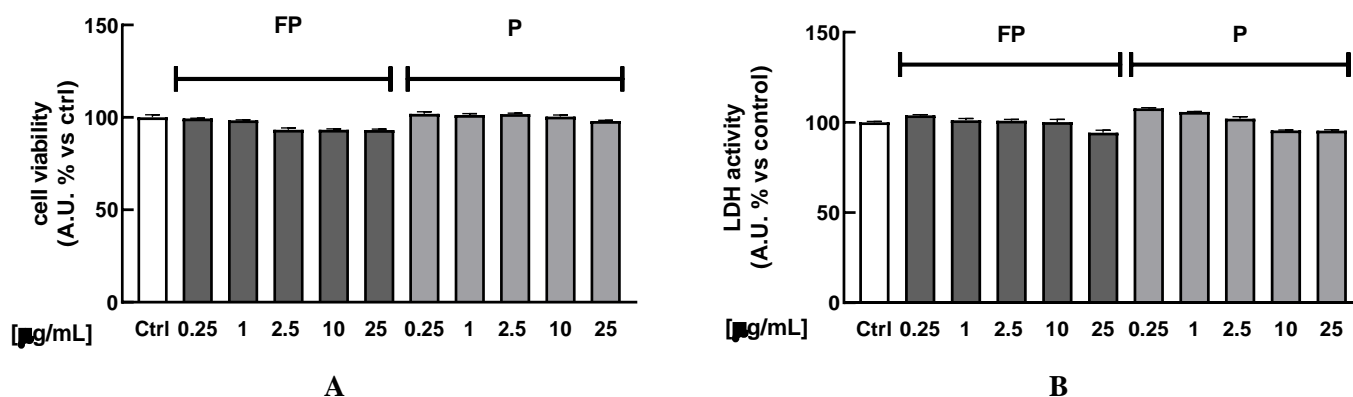


Figure 5.2: HUVECs were treated with fermented Pushgay (FP) or Pushgay (P) berries solutions for 24 h (concentration range: 0.25–25 $\mu\text{g}/\text{mL}$). (A) Cell viability was assessed by measuring red dye production at 490 nm (B) Cytotoxicity was quantified by spectrophotometrically measuring LDH released in cell medium. Ctrl (control,

untreated cells); FP (cells treated with fermented Pushgay solution); P (cells treated with Pushgay solution).

5.3.3 Effect of the fermentation of Pushgay Berries on antioxidant activity in HUVECs

A chemiluminescent (CL) cell-based bioassay was utilized to evaluate the intracellular antioxidant activity of FP or P solutions in HUVECs [38]. Briefly, HUVECs were treated with berries solutions for 24 h (range 0.25–25 $\mu\text{g}/\text{mL}$); the day of the experiment cell medium was changed, and cells were exposed to the oxidant agent menadione (25 μM). As shown in **Figure 5.3A, B**, FP significantly reduces intracellular H_2O_2 production at 2.5, 10, and 25 $\mu\text{g}/\text{mL}$ ($p < 0.05$, $p < 0.01$, and $p < 0.001$, respectively), while treatment with p does not have any significant effect. The IC₅₀ of FP was evaluated by a dose–response curve, obtaining a value of $13.2 \pm 0.6 \mu\text{g}/\text{mL}$ (**Fig. 5.3C**).

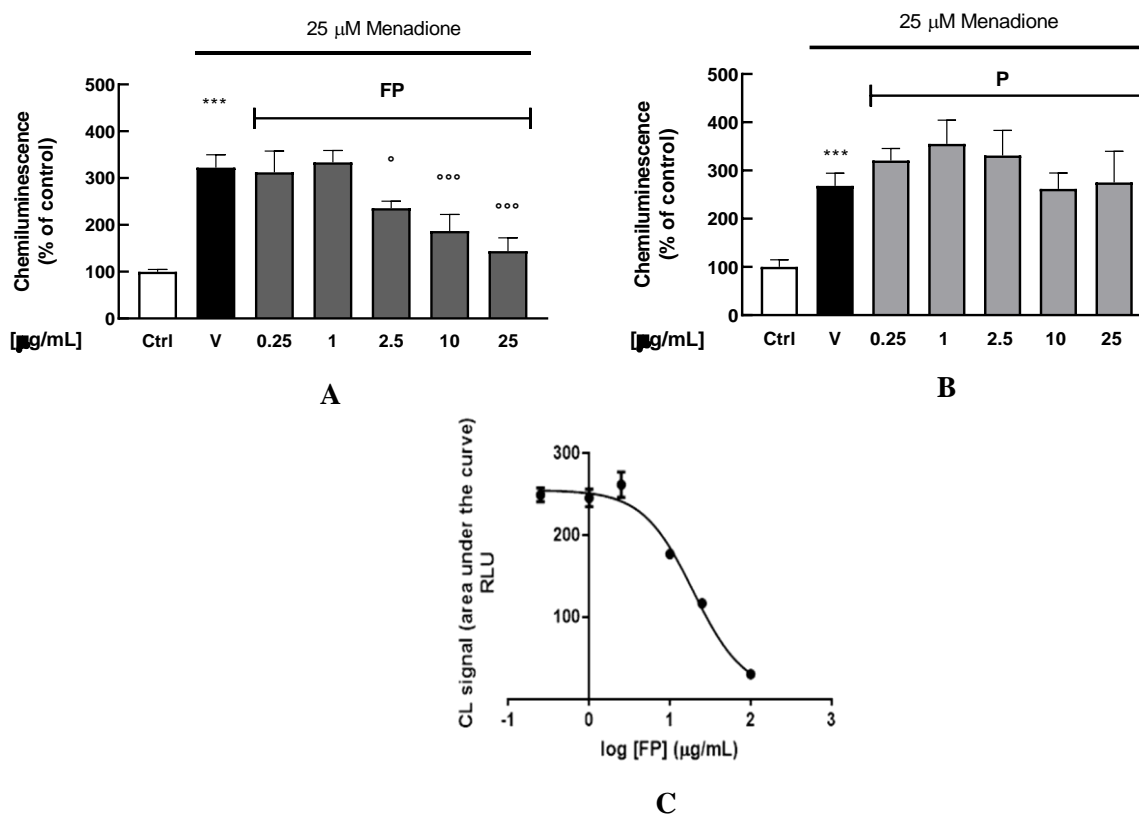


Figure 5.3: HUVECs were treated with fermented Pushgay (FP) (A) and Pushgay (P) (B) solutions for 24 h (concentrations range 0.25–25 $\mu\text{g}/\text{mL}$) and then exposed to the pro-

oxidant agent menadione (25 μM for 40 min). Intracellular H_2O_2 production was measured for 40 min through the CL effect-based bioassay. **(C)** Concentration-response plot of inhibition of intracellular H_2O_2 production in HUVECs treated with FP (range 0.25–25 $\mu\text{g}/\text{mL}$). Results are expressed as mean \pm SD of three independent experiments. *** $p < 0.001$ significantly different from the ctrl. \circ $p < 0.05$ and $\circ\circ$ $p < 0.001$ significantly different from V. Ctrl (control, untreated cells); V (control cells in presence of menadione); FP (cells treated with fermented Pushgay); P (cells treated with Pushgay).

5.3.4 Effect of fermentation of Pushgay berries on H_2O_2 -Induced cell mortality in HUVECs

Trypan Blue was used to determine the viability of HUVECs incubated with H_2O_2 (300 μM) for 24 h, following treatment with FP and P solutions (10 $\mu\text{g}/\text{mL}$) for 24 h. As expected, treatment with H_2O_2 reduced cell viability of HUVECs and FP, but not P, significantly counteracts this effect (**Fig. 5.4**).

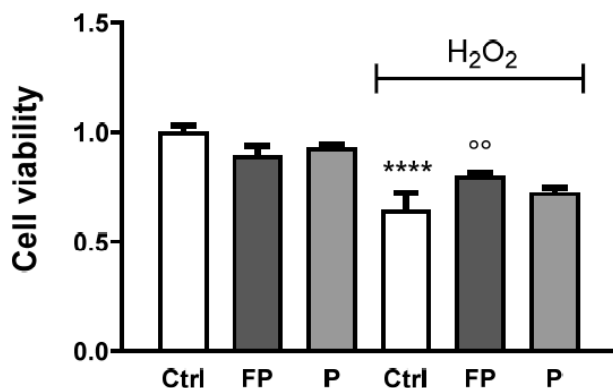


Figure 5.4: HUVECs were plated in six-well plates (1.5×10^5 cells/well) and treated with 10 $\mu\text{g}/\text{mL}$ of FP and P for 24 h followed by treatment with H_2O_2 (300 μM) for 24 h. Cell viability was determined by Trypan Blue staining. Results are expressed as mean \pm SD of at least three experiments. **** $p < 0.0001$ significantly different from the control (ctrl). $\circ\circ$ $p < 0.01$, significantly different from H_2O_2 -treated HUVECs. Ctrl (control, untreated cells); H_2O_2 (cells treated with hydrogen peroxide); FP (cells pretreated with fermented Pushgay); P (cells pretreated with Pushgay).

5.3.5 Effect of fermentation of Pushgay Berries on HO-1 expression in H₂O₂-treated HUVECs

HO-1 gene expression level was determined by qRT-PCR in HUVECs treated with berries solutions (10 µg/mL) for 24 h before treatment with H₂O₂ for 24 h. Data showed that H₂O₂ induces HO-1 expression while pretreatment with FP, but not P, counteracts this effect (Fig. 5.5).

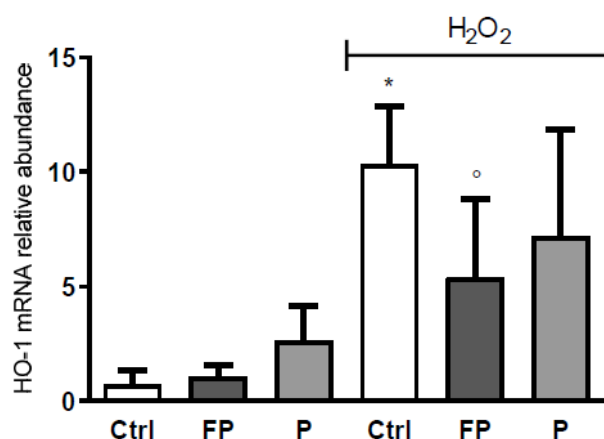


Figure 5.5: HUVECs were plated in 6-well plates (1.5×10^5 cells/well) and treated with 10 µg/mL of FP and P for 24 h followed by injury with H₂O₂ (300 µM) for 24 h. HO-1 gene expression was assessed using qRT-PCR analysis. Gene expression levels were calculated using the $2^{-\Delta\Delta C_t}$ method and RPL13A as reference gene. Results are expressed as mean \pm SD of at least three experiments. * $p < 0.05$ significantly different from the control (ctrl). ° $p < 0.05$, significantly different from H₂O₂-treated HUVECs. Ctrl (control, untreated cells); H₂O₂ (cells treated with hydrogen peroxide); FP (cells pretreated with fermented Pushgay); P (cells pretreated with Pushgay).

5.3.6 Effect of treatment with fermented Pushgay berries on glutathione reductase activity in HUVECs

To investigate the mechanisms underlying the antioxidant capacity of FP, glutathione reductase (GR), glutathione peroxidase (Gpx), catalase (CAT), and superoxide dismutase (SOD) activities were assayed in HUVECs in the presence

or absence of H₂O₂. We found that FP strongly increases GR activity in HUVECs, both in the presence or absence of H₂O₂. No differences were observed for other enzymatic activity (**Fig. 5.6**).

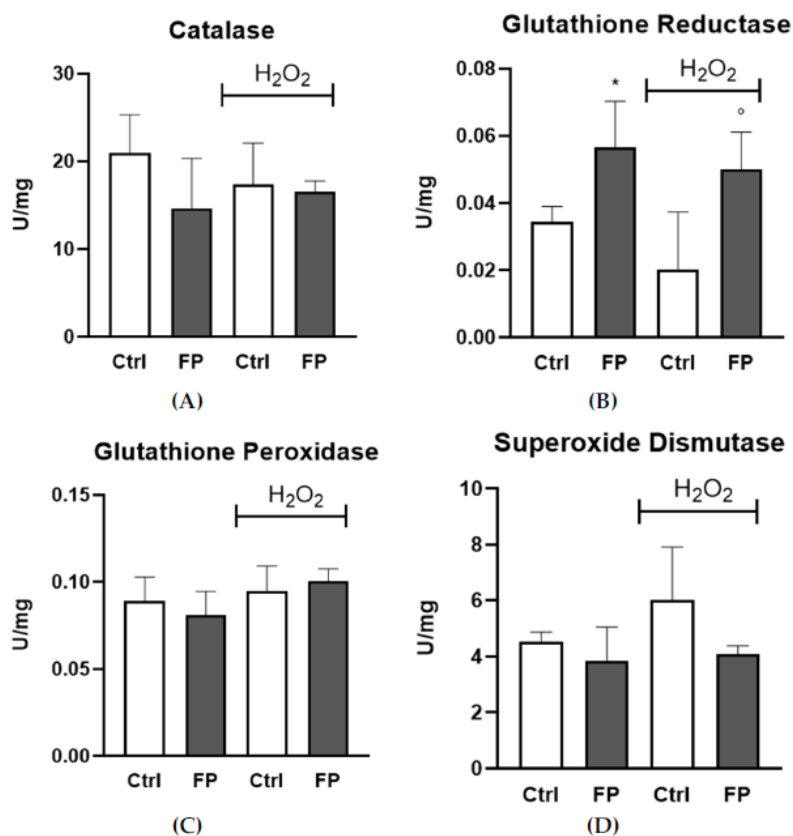


Figure 5.6: HUVECs were plated in 6-well plates (1.5×10^5 cells/well) and treated with 10 $\mu\text{g/mL}$ of FP for 24 h followed by treatment with H₂O₂ (300 μM) for 24 h. (A) CAT, (B) GR, (C) Gpx, and (D) SOD activities were assayed by the methods described in the Methods. Enzyme activity is expressed as units per milligram protein. Results are expressed as mean \pm SD of at least three experiments. * $p < 0.05$ significantly different from the control (ctrl). ° $p < 0.05$, significantly different from H₂O₂-treated HUVECs. Ctrl (control, untreated cells); H₂O₂ (cells treated with hydrogen peroxide); FP (cells pretreated with fermented Pushgay).

5.3.7 Effect of treatment with Pushgay berries on RAW264.7 cells proliferation

Treatments of RAW 264.7 with FP and P for 24 h at different concentrations (range 2.5–10 $\mu\text{g/mL}$) were not toxic (**Fig. 5.7**). Therefore, based on these

experiments, we selected 10 µg/mL concentration for subsequent experiments.

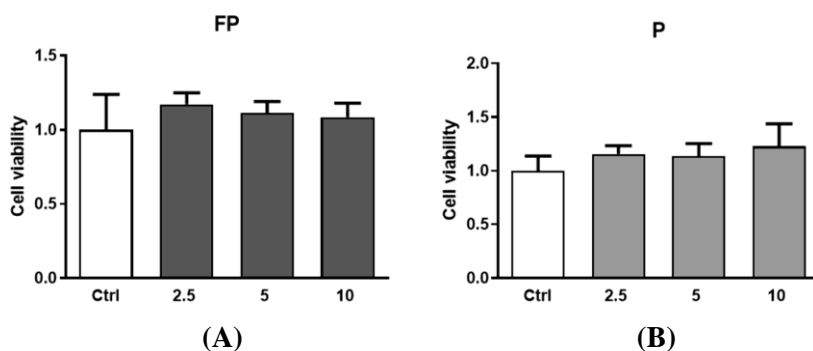


Figure 5.7: RAW 264.7 were plated in 6-well plates (3.0×10^5 cells/well) and treated for 24 h with different concentration of (A) FP and (B) P solutions (2.5, 5 and 10 µg/mL). Cell viability was determined with the Burker chamber utilizing Trypan Blue as a cell dye. Results are expressed as mean \pm SD of at least three experiments. ctrl (control, untreated cells); FP (cells treated with fermented Pushgay); P (cells treated with Pushgay).

5.3.8 Effect of fermentation of Pushgay berries on RAW264.7 cells growth

The effects of berries on RAW 264.7 growth were evaluated by Alamar Blue staining after treatment of cells with FP and P solutions for 24 and 72 h. We found an increase in Alamar Blue staining after 72 h of treatment with P or FP, compared to control cells, but no effect was observed after 24 h of treatment (**Fig. 5.8A**). Since the Alamar Blue staining increase can indicate either stimulation of metabolism or increased cell proliferation, to discriminate between these two effects, we used Trypan Blue to assess changes in the number of cells following treatment with berries solutions for 24 and 72 h. We found a significant increase in the number of cells following 72 h of treatment with P or FP (**Fig. 5.8B**), indicating stimulation of cell growth by either P and FP.

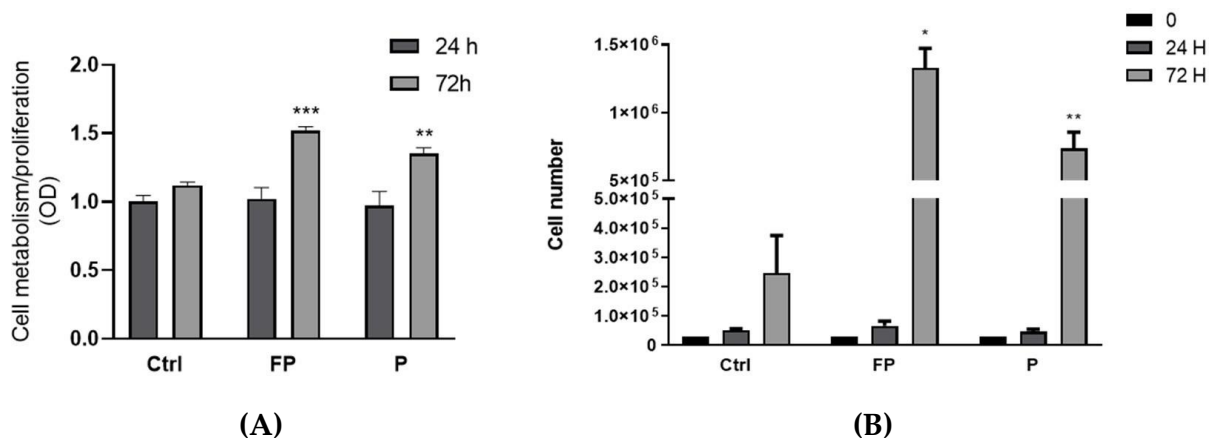


Figure 5.8: (A) RAW 264.7 cells were plated in 24-wells plates (3.0×10^4 cells/well), treated with $10 \mu\text{g/mL}$ of FP or P and further incubated for 24 and 72 h. At the end of treatment cells were incubated at 37°C , 5% CO_2 for 3 h with Alamar Blue solution. Optical density (OD) was determined with a spectrophotometer at 570 nm. (B) RAW 264.7 cells were seeded in 24-well plates (3.0×10^4 cells/well) and treated with $10 \mu\text{g/mL}$ of FP and P and further incubated for 24 and 72 h. At the end of incubation, cell number was determined with the Burker chamber utilizing Trypan Blue as a cell dye. Results are expressed as mean \pm SD of at least three experiments. * $p < 0.05$ ** $p < 0.01$ *** $p < 0.001$ significantly different from the control at 72 h (ctrl). Ctrl (control, not treated cells); FP (cells treated with fermented Pushgay); P (cells treated with Pushgay).

5.3.9 Effects of Pushgay berries on the expression of iNOS and TNF α in RAW264.7 cells

To evaluate the immunomodulatory activity of berries solutions, the mRNA levels of inducible nitric oxide synthase (iNOS) and Tumor Necrosis Factor α (TNF α) were evaluated by qRT-PCR in RAW 264.7 treated with FP or P at $10 \mu\text{g/mL}$ for 24 h in the presence or absence of Interferon γ (IFN γ) (100 U/mL). We found that treatment with FP, but not P, leads to a significant raise in the levels of iNOS mRNA in the absence of IFN- γ (Fig. 5.9A). Treatment with P did not significantly increase TNF α expression, while FP treatment showed a slight increase, which was not statistically significant (Fig. 5.9B).

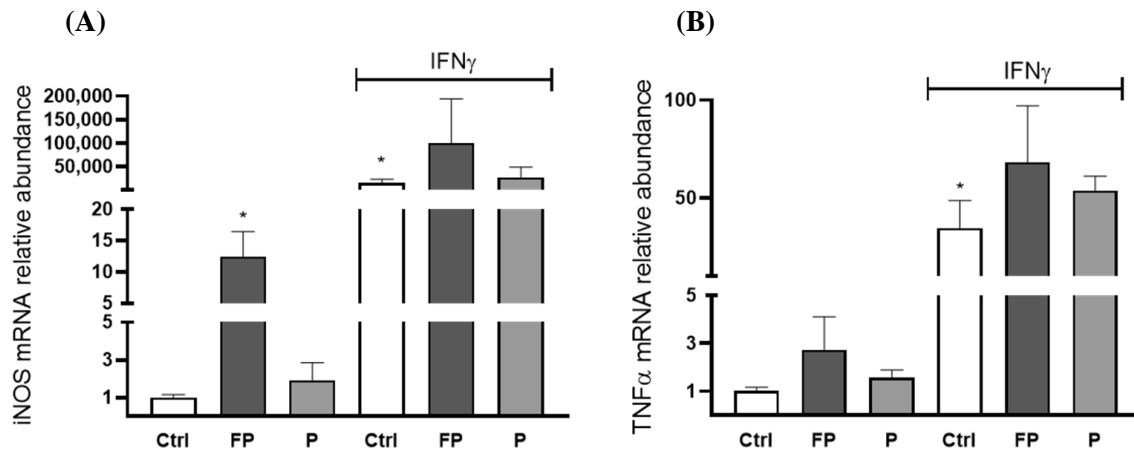


Figure 5.9: RAW 264.7 (4.0×10^5 /well) were seeded in six wells and incubated with 10 μ g/mL of FP or P in the presence or absence of 100 U/mL of IFN- γ for 24 h. (A) iNOS and (B) TNF α genes expression was assessed using qRT-PCR analysis. Differences in gene expression were calculated using the $2^{-\Delta\Delta Ct}$ formula and RPL13A as reference gene. Results are expressed as mean \pm SD of at least three experiments. * $p < 0.05$. significantly different from the ctrl. Ctrl (control, untreated cells); FP (cells treated with fermented Pushgay); P (cells treated with Pushgay); IFN- γ (cells treated with IFN γ).

5.4 Discussion

The European vision of the Joint Programming Initiative “a healthy diet for a healthy life” (JPI HDHL) establishes that by 2030, all citizens will have the motivation, the ability, and the opportunity to consume a healthy diet from a variety of foods (including functional foods and supplements) to stay healthy and reduce the onset of food-related diseases. Epidemiological studies have shown that the intake of natural products, rich in antioxidants polyphenolic compounds, is related with a reduction in the risk of developing CVDs and cancer [46,47]. There is clear evidence that certain flavonoids, such as quercetin, can attenuate endothelial dysfunction [48], the first step toward atherosclerosis. Furthermore, it has been shown that bacterial strains used as probiotics, such as *Lactiplantibacillus plantarum*, may enhance the beneficial activity of phenolic compounds present in food, protecting endothelial cells from oxidative stress [49] and modulating the production of cytokines and other pro-inflammatory mediators (TNF α and iNOS) in macrophages [50]. A variety of fermented foods, such as milk, meat, fish, vegetables, cereal, and fruits, are part of human nutrition around

the world, and the consumption of fermented food has been linked to reduced risk of hypertension, diabetes, obesity, and high cholesterol [51]. Variations in the antioxidant activity of fruits after lactic fermentation have often been observed, possibly due to the release of bioactive molecules from phenolic conjugated phytochemicals [52].

So far as we know, this is the first study that compares the antioxidant and immunostimulant properties of Pushgay berries before and after fermentation with *Lactiplantibacillus plantarum*. We report that treatment with Pushgay berries fermented with *Lactiplantibacillus plantarum* reduces oxidative stress induced by menadione and protects HUVECs against H₂O₂-induced cell toxicity more effectively than treatment with unfermented Pushgay berries. We also found that, after fermentation with *Lactiplantibacillus plantarum*, Push- gay berries promote proliferation and iNOS mRNA synthesis in mouse macrophages RAW 264.7.

Our results are in contrast with others reporting that unfermented berries, due to their high levels of polyphenolic compounds, can reduce oxidative stress [53–55], decrease inflammation [56], protect endothelial cells from H₂O₂-induced cell death [57], attenuate endothelial dysfunction, and regulate cholesterol accumulation and trafficking, along with potentially influencing gut microbiota [58]. It is possible these contrasting results are due to environmental conditions of growth or to our extraction procedures, leading to low levels of polyphenolic compounds in the non-fermented Pushgay berries under investigation in our study. Consistently with this hypothesis, it has been shown that *Lonicera caerulea* berries have a higher antioxidant capacity than blueberries because they are enriched in anthocyanins, such as anidin, peonidin, and delphinidin, which are not present in other berries [59,60]. Additionally, the content of polyphenols of *L. caerulea* may differ based on differences in the extraction approach [59]. Polyphenol contents can also be influenced by altitude [61]. Cell culture conditions used could also explain these contrasting results. It would be of interest to investigate whether treatment with non-fermented Pushgay extract has an effect on human artery endothelial cells grown in the presence of fluid shear stress to mimic the effect of blood flow, which plays a major role in endothelial cell functions [62]. As described for other berries, FP gained the ability to interfere with H₂O₂ production following menadione

treatment [63]. Furthermore, consistent with previous studies on fermented berries [64], FP berries treatment increased HUVECs viability in the presence of H₂O₂, confirming that fermentation interferes with oxidative stress-induced cell damages. This is consistent with other studies that have shown that fermented blueberries have great scavenging ability against hydroxyl radicals [65–67]. Furthermore, we found that H₂O₂-treated cells, pre-treated with FP, express a lower amount of HO-1 mRNA than cells treated with H₂O₂ in the absence of FP. Since HO-1 synthesis is a cell response against damages caused by oxidative stress [68], these data provide more evidence that FP berries treatment reduces oxidative stress in the cell.

Although HO-1 induction promotes a protection against oxidative stress in various cell and animal models, high HO-1 levels may even sensitize the cell to oxidative stress, e.g., through the release of reactive iron [68]. In addition, it has been reported that an uncontrolled and exaggerated up-regulation of HO-1 has pro-oxidant effects [69–71], and thus, berries treatment could protect the cell by limiting its up-regulation.

In order to gain, at least in part, insight into the mechanism underlying the protective activity of FP, we investigated the activity of well-known antioxidant enzymes that could be stimulated by berries treatment such as CAT, SOD, and enzymes involved in the glutathione (GSH) cycle, such as Gpx and GR [72]. Our results show the specific effect of FP on GR activity but not on the other enzymes. Similarly, ginseng extract protects HUVECs against H₂O₂-induced damage by regulating the redox state of the cell, particularly increasing the activity of GR [73], and peptide T8 ameliorate HUVECs resistance against H₂O₂-induced oxidative damage by increasing GR activity [74]. Fruit-derived polyphenols may differentially affect each antioxidant enzyme, and the ability of FP to increase GR activity is of particular importance due to the critical role of GSH in endothelial function [75] and to the ability of GR in maintaining GSH supply, fundamental in the cellular control of reactive oxygen species.

Our study also showed that treatment with FP modulates innate immunity, as indicated by increased RAW 264.7 macrophages proliferation. Furthermore, treatment of these cells with FP increased basal and IFN- γ -induced levels of

iNOS.

We found that Pushgay berries are enriched in quercetin and fermentation enhances their quercetin aglycone content, in line with previous data [32], and increases their intra- cellular antioxidant activity. Indeed, it has been previously reported that the fermentation process promotes the almost complete degradation of anthocyanins in phenolic acids, the hydrolysis of glycol-conjugates, and, in turn, higher concentrations of free flavonoids [32].

Moreover, FP exhibited higher cell-free antioxidant activity compared to the fresh berries following fermentation [32], in agreement with our results. It is known that the bioavailability of berry polyphenols is very low [8], but it is positively influenced by glucosidases during fermentation, thereby increasing in situ ROS scavenging, as well as stimulating natural antioxidant body panel [76,77]. The biotransformation of berries during the fermentation process increases the hydrolysis of phenolic compounds, thus their bioavailability [78].

Even if Hollman et al. suggested that quercetin glucoside has a higher bioavailability than the free form in ileostomized patients [79], it is plausible that the relatively high absorption of quercetin glycosides is not due to glycosylation, but rather to factors present in complex foodstuff matrices. Moreover, it would be important to investigate the role of gut microbiota in influencing the bioactivity and the permeation of dietary (poly)phenols. Indeed, the microbial bioavailability of unabsorbed bioactive compounds in the gut represents a fundamental step in the presumed bioactivity associated with (poly)phenol intake [80].

Finally, the contribution of phenolic acids in FP, which may exert an additive or synergistic effect with the quercetin aglycone within cells, must be carefully considered due to their greater bioavailability in comparison to larger phenolic molecules and their beneficial activities. More studies will be performed to clarify their possible beneficial effects in human cell models on vascular and immune system function.

5.5 Conclusions

We report that fermentation strongly increases the content of quercetin aglycone (present only in the FP, and not in P, with a concentration of $1680 \pm 0.2 \mu\text{g/g}$) and promotes the antioxidant activity of Pushgay berries. One of the possible mechanisms underlying the antioxidant activity of FP could be the increased activity of GR, an enzyme responsible for the maintenance of GSH supply, which acts as an important player in controlling the cellular levels of ROS [75]. Fermentation also enhanced the immunomodulatory properties of Pushgay berries. Our findings are in agreement with previous studies showing that fermented berries reduce oxidative stress and the levels of pro-inflammatory cytokines [81]. Overall, many studies have shown the health beneficial effects of fermented fruits. However, this evidence has been generated mainly from in vitro and in vivo studies, while clinical studies are scarce in this field. Therefore, the potential role of fermented plant products in human health must be confirmed through randomized controlled clinical trials.

5.6 Acknowledgements

We thank Aldo Roda for experimental suggestions and Francesca D'Alessandro for revising the manuscript.

5.7 References

- [1] Khosravi, M.; Poursaleh, A.; Ghasempour, G.; Farhad, S.; Najafi, M. The effects of oxidative stress on the development of atherosclerosis. *Biol. Chem.* 2019, *400*, 711–732.
- [2] Fortini, F.; Sega, F.V.D.; Caliceti, C.; Lambertini, E.; Pannuti, A.; Peiffer, D.S.; Balla, C.; Rizzo, P. Estrogen-mediated protection against coronary heart disease: The role of the Notch pathway. *J. Steroid Biochem. Mol. Biol.* 2019, *189*, 87–100.
- [3] Marracino, L.; Fortini, F.; Bouhamida, E.; Camponogara, F.; Severi, P.; Mazzoni, E.; Patergnani, S.; D’Aniello, E.; Campana, R.; Pinton, P.; et al. Adding a “Notch” to Cardiovascular Disease Therapeutics: A MicroRNA-Based Approach. *Front. Cell Dev. Biol.* 2021, *9*, 695114.
- [4] Fortini, F.; Sega, F.V.D.; Marracino, L.; Severi, P.; Rapezzi, C.; Rizzo, P.; Ferrari, R. Well-Known and Novel Players in Endothelial Dysfunction: Updates on a Notch(ed) Landscape. *Biomedicines* 2021, *9*, 997.
- [5] Chen, T.-H.; Tseng, H.-P.; Yang, J.-Y.; Mao, S.J. Effect of antioxidant in endothelial cells exposed to oxidized low-density lipoproteins. *Life Sci.* 1998, *62*, 277–282.
- [6] Geng, J.; Xu, H.; Yu, X.; Xu, G.; Cao, H.; Lin, G.; Sui, D. Rosuvastatin protects against oxidized low-density lipoprotein-induced endothelial cell injury of atherosclerosis in vitro. *Mol. Med. Rep.* 2019, *19*, 432–440.
- [7] Malaguti, M.; Angeloni, C.; Hrelia, S. Nutraceutical Bioactive Compounds Promote Healthspan Counteracting Cardiovascular Diseases. *J. Am. Coll. Nutr.* 2015, *34* (Suppl. 1), 22–27.
- [8] Basu, A.; Rhone, M.; Lyons, T.J. Berries: Emerging impact on cardiovascular health. *Nutr. Rev.* 2010, *68*, 168–177.
- [9] Aquila, G.; Marracino, L.; Martino, V.; Calabria, D.; Campo, G.; Caliceti, C.; Rizzo, P. The Use of Nutraceuticals to Counteract Atherosclerosis: The Role of the Notch Pathway. *Oxid. Med. Cell. Longev.* 2019, *2019*, 5470470.
- [10] Engler, M.M.; Engler, M.B.; Malloy, M.J.; Chiu, E.Y.; Scholletter, M.C.; Paul, S.M.; Stuehlinger, M.; Lin, K.Y.; Cooke, J.P.; Marrow, J.D.; et al.

- Antioxidant vitamins C and E improve endothelial function in children with hyperlipidemia: Endothelial Assessment of Risk from Lipids in Youth (EARLY) Trial. *Circulation* 2003, 108, 1059–1063.
- [11] Shafi, S.; Ansari, H.R.; Bahitham, W.; Aouabdi, S. The Impact of Natural Antioxidants on the Regenerative Potential of Vascular Cells. *Front. Cardiovasc. Med.* 2019, 6, 28.
- [12] Chang, X.; Zhang, W.; Zhao, Z.; Ma, C.; Zhang, T.; Meng, Q.; Yan, P.; Zhang, L.; Zhao, Y. Regulation of Mitochondrial Quality Control by Natural Drugs in the Treatment of Cardiovascular Diseases: Potential and Advantages. *Front. Cell Dev. Biol.* 2020, 8, 616139.
- [13] Hung, C.-H.; Chan, S.-H.; Chu, P.-M.; Tsai, K.-L. Quercetin is a potent anti-atherosclerotic compound by activation of SIRT1 signaling under oxLDL stimulation. *Mol. Nutr. Food Res.* 2015, 59, 1905–1917.
- [14] Bhaskar, S.; Kumar, K.S.; Krishnan, K.; Antony, H. Quercetin alleviates hypercholesterolemic diet induced inflammation during progression and regression of atherosclerosis in rabbits. *Nutrition* 2013, 29, 219–229.
- [15] Phie, J.; Krishna, S.; Moxon, J.V.; Omer, S.M.; Kinobe, R.; Golledge, J. Flavonols reduce aortic atherosclerosis lesion area in apolipoprotein E deficient mice: A systematic review and meta-analysis. *PLoS ONE* 2017, 12, e0181832.
- [16] Hayek, T.; Fuhrman, B.; Vaya, J.; Rosenblat, M.; Belinky, P.; Coleman, R.; Elis, A.; Aviram, M. Reduced progression of atherosclerosis in apolipoprotein E-deficient mice following consumption of red wine, or its polyphenols quercetin or catechin, is associated with reduced susceptibility of LDL to oxidation and aggregation. *Arterioscler. Thromb. Vasc. Biol.* 1997, 17, 2744–2752.
- [17] Angeloni, C.; Hrelia, S. Quercetin Reduces Inflammatory Responses in LPS-Stimulated Cardiomyoblasts. *Oxid. Med. Cell. Longev.* 2012, 2012, 837104.
- [18] Angeloni, C.; Leoncini, E.; Malaguti, M.; Angelini, S.; Hrelia, P.; Hrelia, S. Role of quercetin in modulating rat cardiomyocyte gene expression profile. *Am. J. Physiol. Heart Circ. Physiol.* 2008, 294, H1233–H1243.

- [19] Derlindati, E.; Dall'Asta, M.; Ardigò, D.; Brighenti, F.; Zavaroni, I.; Crozier, A.; Del Rio, D. Quercetin-3-O-glucuronide affects the gene expression profile of M1 and M2a human macrophages exhibiting anti-inflammatory effects. *Food Funct.* 2012, 3, 1144–1152.
- [20] Liu, P.L.; Liu, J.-T.; Kuo, H.-F.; Chong, I.-W.; Hsieh, C.-C. Epigallocatechin gallate attenuates proliferation and oxidative stress in human vascular smooth muscle cells induced by interleukin-1 β via heme oxygenase-1. *Mediators Inflamm.* 2014, 2014, 523684.
- [21] Ohara, K.; Wakabayashi, H.; Taniguchi, Y.; Shindo, K.; Yajima, H.; Yoshida, A. Quercetin-3-O-glucuronide induces ABCA1 expression by LX $\text{R}\alpha$ activation in murine macrophages. *Biochem. Biophys. Res. Commun.* 2013, 441, 929–934.
- [22] Del Bo, C.; Martini, D.; Porrini, M.; Klimis-Zacas, D.; Riso, P. Berries and oxidative stress markers: An overview of human intervention studies. *Food Funct.* 2015, 6, 2890–2917.
- [23] National Research Council. *Popenoe, Lost Crops of the Incas*; National Academies Press: Washington, DC, USA, 1989.
- [24] Prencipe, F.P.; Bruni, R.; Guerrini, A.; Rossi, D.; Benvenuti, S.; Pellati, F. Metabolite profiling of polyphenols in *Vaccinium* berries and determination of their chemopreventive properties. *J. Pharm. Biomed. Anal.* 2014, 89, 257–267.
- [25] Vasco, C.; Riihinen, K.; Ruales, J.; Kamal-Eldin, A. Chemical composition and phenolic compound profile of mortiño (*Vaccinium floribundum* Kunth). *J. Agric. Food Chem.* 2009, 57, 8274–8281.
- [26] Llivisaca, S.; Manzano, P.; Ruales, J.; Flores, J.; Mendoza, J.; Peralta, E. Chemical, antimicrobial, and molecular characterization of mortiño. *Food Sci. Nutr.* 2018, 6, 934–942. [
- [27] Rodríguez, L.G.R.; Gasga, V.M.Z.; Pescuma, M.; Van Nieuwenhove, C.; Mozzi, F.; Burgos, J.A.S.; Cevallos-Cevallos, J.M. Fruits and fruit by-products as sources of bioactive compounds. Benefits and trends of lactic acid fermentation in the development of novel fruit-based functional beverages. *Food Res. Int.* 2021, 140, 109854.

- [28] Vатtem, D.A.; Shetty, K. Ellagic acid production and phenolic antioxidant activity in cranberry pomace (*Vaccinium macrocarpon*) mediated by *Lentinus edodes* using a solid-state system. *Process Biochem.* 2003, 39, 367–379.
- [29] Hur, S.J.; Lee, S.Y.; Kim, Y.-C.; Choi, I.; Kim, G.-B. Effect of fermentation on the antioxidant activity in plant-based foods. *Food Chem.* 2014, 160, 346–356.
- [30] Perdigón, G.; Vintiñi, E.; Alvarez, S.; Medina, M.; Medici, M. Study of the Possible Mechanisms Involved in the Mucosal Immune System Activation by Lactic Acid Bacteria. *J. Dairy Sci.* 1999, 82, 1108–1114.
- [31] Oh, N.S.; Joung, J.Y.; Lee, J.Y.; Kim, Y. Probiotic and anti-inflammatory potential of *Lactobacillus rhamnosus* 4B15 and *Lactobacillus gasseri* 4M13 isolated from infant feces. *PLoS ONE* 2018, 13, e0192021.
- [32] Cerrato, A.; Piovesana, S.; Aita, S.E.; Cavaliere, C.; Felletti, S.; Laganà, A.; Montone, C.M.; Vargas-De-La-Cruz, C.; Capriotti, A.L. Detailed investigation of the composition and transformations of phenolic compounds in fresh and fermented *Vaccinium floribundum* berry extracts by high-resolution mass spectrometry and bioinformatics. *Phytochem. Anal.* 2022.
- [33] Ainsworth, E.A.; Gillespie, K.M. Estimation of total phenolic content and other oxidation substrates in plant tissues using Folin–Ciocalteu reagent. *Nat. Protoc.* 2007, 2, 875–877. [
- [34] Caliceti, C.; Rizzo, P.; Ferrari, R.; Fortini, F.; Aquila, G.; Leoncini, E.; Zambonin, L.; Rizzo, B.; Calabria, D.; Simoni, P. Novel role of the nutraceutical bioactive compound berberine in lectin-like OxLDL receptor 1-mediated endothelial dysfunction in comparison to lovastatin. *Nutr. Metab. Cardiovasc. Dis.* 2017, 27, 552–563.
- [35] Caliceti, C.; Capriotti, A.; Calabria, D.; Bonvicini, F.; Zenezini Chiozzi, R.; Montone, C.; Piovesana, S.; Zangheri, M.; Mirasoli, M.; Simoni, P. Peptides from cauliflower by-products, obtained by an efficient, ecosustainable, and semi-industrial method, exert protective effects on endothelial function. *Oxid. Med. Cell. Longev.* 2019, 2019, 1046504.

- [36] Caliceti, C.; Aquila, G.; Pannella, M.; Morelli, M.B.; Fortini, C.; Pinton, P.; Bonora, M.; Hrelia, S.; Pannuti, A.; Miele, L.; et al. 17 β -Estradiol Enhances Signalling Mediated by VEGF-A-Delta-Like Ligand 4-Notch1 Axis in Human Endothelial Cells. *PLoS ONE* 2013, 8, e71440.
- [37] Aquila, G.; Morelli, M.B.; Segal, F.V.D.; Fortini, F.; Nigro, P.; Caliceti, C.; Ferracin, M.; Negrini, M.; Pannuti, A.; Bonora, M.; et al. Heart rate reduction with ivabradine in the early phase of atherosclerosis is protective in the endothelium of ApoE-deficient mice. *J. Physiol. Pharmacol.* 2018, 69, 35–52.
- [38] Calabria, D.; Guardigli, M.; Mirasoli, M.; Punzo, A.; Porru, E.; Zangheri, M.; Simoni, P.; Pagnotta, E.; Ugolini, L.; Lazzeri, L.; et al. Selective chemiluminescent TURN-ON quantitative bioassay and imaging of intracellular hydrogen peroxide in human living cells. *Anal. Biochem.* 2020, 600, 113760.
- [39] Bradford, M.M. A rapid and sensitive method for the quantitation of microgram quantities of protein utilizing the principle of protein-dye binding. *Anal. Biochem.* 1976, 72, 248–254. [
- [40] Smith, I.K.; Vierheller, T.L.; Thorne, C.A. Assay of glutathione reductase in crude tissue homogenates using 5,5'-dithiobis(2-nitrobenzoic acid). *Anal. Biochem.* 1988, 175, 408–413.
- [41] Engel, H.J.; Domschke, W.; Alberti, M.; Domagk, G.F. Protein structure and enzymatic activity II. Purification and properties of a crystalline glucose-6-phosphate dehydrogenase from *Candida utilis*. *Biochim. Biophys. Acta Enzym.* 1969, 191, 509–516.
- [42] Cervellati, C.; Sticozzi, C.; Romani, A.; Belmonte, G.; De Rasmio, D.; Signorile, A.; Cervellati, F.; Milanese, C.; Mastroberardino, P.G.; Pecorelli, A.; et al. Impaired enzymatic defensive activity, mitochondrial dysfunction and proteasome activation are involved in RTT cell oxidative damage. *Biochim. Biophys. Acta Mol. Basis Dis.* 2015, 1852, 2066–2074. [
- [43] Olthof, M.R.; Hollman, P.C.H.; Vree, T.B.; Katan, M.B. Bioavailabilities of Quercetin-3-Glucoside and Quercetin-4'-Glucoside Do Not Differ in Humans. *J. Nutr.* 2000, 130, 1200–1203.

- [44] Lee, S.; Lee, J.; Lee, H.; Sung, J. Relative protective activities of quercetin, quercetin-3-glucoside, and rutin in alcohol-induced liver injury. *J. Food Biochem.* 2019, *43*, e13002. [
- [45] De Araújo, M.E.; Moreira Franco, Y.E.; Alberto, T.G.; Aves Sobreiro, M.; Aurélio Conradoa, M.; Gonçalves Priollia, D.; Frankland Sawaya, A.C.H.; Ruiz, A.L.T.G.; de Carvalho, J.E.; de Oliveira Carvalho, P. Enzymatic de-glycosylation of rutin improves its antioxidant and antiproliferative activities. *Food Chem.* 2013, *141*, 266–273.
- [46] Kris-Etherton, P.M.; Hecker, K.D.; Bonanome, A.; Coval, S.M.; Binkoski, A.E.; Hilpert, K.F.; Griel, A.E.; Etherton, T.D. Bioactive compounds in foods: Their role in the prevention of cardiovascular disease and cancer. *Am. J. Med.* 2002, *113*, 71–88.
- [47] Yahfoufi, N.; Alsadi, N.; Jambi, M.; Matar, C. The immunomodulatory and anti-inflammatory role of polyphenols. *Nutrients* 2018, *10*, 1618.
- [48] Loke, W.M.; Proudfoot, J.M.; Hodgson, J.M.; McKinley, A.; Hime, N.; Magat, M.; Stocker, R.; Croft, K.D. Specific Dietary Polyphenols Attenuate Atherosclerosis in Apolipoprotein E–Knockout Mice by Alleviating Inflammation and Endothelial Dysfunction. *Arter. Thromb. Vasc. Biol.* 2010, *30*, 749–757.
- [49] Li, Z.; Teng, J.; Lyu, Y.; Hu, X.; Zhao, Y.; Wang, M. Enhanced Antioxidant Activity for Apple Juice Fermented with *Lactobacillus plantarum* ATCC14917. *Molecules* 2018, *24*, 51.
- [50] Milani, R.V.; Lavie, C.J.; Mehra, M.R.; Ventura, H.O. Impact of Exercise Training and Depression on Survival in Heart Failure Due to Coronary Heart Disease. *Am. J. Cardiol.* 2011, *107*, 64–68.
- [51] Şanlıer, N.; Gökçen, B.B.; Sezgin, A.C. Health benefits of fermented foods. *Crit. Rev. Food Sci. Nutr.* 2019, *59*, 506–527.
- [52] Septembre-Malaterre, A.; Remize, F.; Poucheret, P. Fruits and vegetables, as a source of nutritional compounds and phytochemicals: Changes in bioactive compounds during lactic fermentation. *Food Res. Int.* 2018, *104*, 86–99.
- [53] Rojas-Ocampo, E.; Torrejón-Valqui, L.; Muñoz-Astecker, L.D.; Medina-

- Mendoza, M.; Mori-Mestanza, D.; Castro-Alayo, E.M. Antioxidant capacity, total phenolic content and phenolic compounds of pulp and bagasse of four Peruvian berries. *Heliyon* 2021, 7, E07787.
- [54] Vargas-Ramella, M.; Lorenzo, J.M.; Zamuz, S.; Valdés, M.E.; Moreno, D.; Balcázar, M.C.; Fernández-Arias, J.M.; Reyes, J.F.; Franco, D. The Antioxidant Effect of Colombian Berry (*Vaccinium meridionale* Sw.) Extracts to Prevent Lipid Oxidation during Pork Patties Shelf-Life. *Antioxidants* 2021, 10, 1290.
- [55] Ziemlewska, A.; Zagórska-Dziok, M.; Nizioł-Łukaszewska, Z. Assessment of cytotoxicity and antioxidant properties of berry leaves as by-products with potential application in cosmetic and pharmaceutical products. *Sci. Rep.* 2021, 11, 3240.
- [56] Cheng, A.; Yan, H.; Han, C.; Wang, W.; Tian, Y.; Chen, X. Polyphenols from blueberries modulate inflammation cytokines in LPS-induced RAW264.7 macrophages. *Int. J. Biol. Macromol.* 2014, 69, 382–387.
- [57] Caliceti, C.; Urao, N.; Rizzo, P.; Giuliano, M. New Trends in Antioxidant Compounds: A Precise Nutraceutical in Cardiometabolic Disorders. *Oxid. Med. Cell. Longev.* 2019, 2019, 4794563.
- [58] Wu, X.; Wang, T.T.Y.; Prior, R.L.; Pehrsson, P.R. Prevention of Atherosclerosis by Berries: The Case of Blueberries. *J. Agric. Food Chem.* 2018, 66, 9172–9188.
- [59] Myjavcová, R.; Marhol, P.; Krřen, V.; Šimánek, V.; Ulrichová, J.; Palíková, I.; Papoušková, B.; Lemr, K.; Bednár, P. Analysis of anthocyanin pigments in *Lonicera (Caerulea)* extracts using chromatographic fractionation followed by microcolumn liquid chromatography-mass spectrometry. *J. Chromatogr. A* 2010, 1217, 7932–7941.
- [60] Palíková, I.; Heinrich, J.; Bednár, P.; Marhol, P.; Krřen, V.; Cvak, L.; Valentová, K.; Ruzicka, F.; Hola, V.; Kolár, M.; et al. Constituents and Antimicrobial Properties of Blue Honeysuckle: A Novel Source for Phenolic Antioxidants. *J. Agric. Food Chem.* 2008, 56, 11883–11889.
- [61] Suleiman, M.H.A.; Ali ALaerjani, W.M.; Ahamed Mohammed, M.E.

- Influence of altitudinal variation on the total phenolic and flavonoid content of *Acacia* and *Ziziphus* honey. *Int. J. Food Prop.* 2020, 23, 2077–2086.
- [62] Chakraborty, A.; Chakraborty, S.; Jala, V.R.; Thomas, J.M.; Sharp, M.K.; Berson, R.E.; Haribabu, B. Impact of Bi-Axial Shear on Atherogenic Gene Expression by Endothelial Cells. *Ann. Biomed. Eng.* 2016, 44, 3032–3045.
- [63] Punzo, A.; Porru, E.; Silla, A.; Simoni, P.; Galletti, P.; Roda, A.; Tagliavini, E.; Samorì, C.; Caliceti, C. Grape Pomace for Topical Application: Green NaDES Sustainable Extraction, Skin Permeation Studies, Antioxidant and Anti-Inflammatory Activities Characterization in 3D Human Keratinocytes. *Biomolecules* 2021, 11, 1181.
- [64] Shahbazi, R.; Sharifzad, F.; Bagheri, R.; Alsadi, N.; Yasavoli-Sharahi, H.; Matar, C. Anti-Inflammatory and Immunomodulatory Properties of Fermented Plant Foods. *Nutrients* 2021, 13, 1516.
- [65] Zhou, H.; Zhuang, X.; Zhou, C.; Ding, D.; Li, C.; Bai, Y.; Zhou, G. Effect of fermented blueberry on the oxidative stability and volatile molecule profiles of emulsion-type sausage during refrigerated storage. *Asian Australas. J. Anim. Sci.* 2019, 33, 812–824.
- [66] Oh, B.-T.; Jeong, S.-Y.; Velmurugan, P.; Park, J.-H.; Jeong, D.-Y. Probiotic-mediated blueberry (*Vaccinium corymbosum* L.) fruit fermentation to yield functionalized products for augmented antibacterial and antioxidant activity. *J. Biosci. Bioeng.* 2017, 124, 542–550. [
- [67] Su, M.-S.; Chien, P.-J. Antioxidant activity, anthocyanins, and phenolics of rabbiteye blueberry (*Vaccinium ashei*) fluid products as affected by fermentation. *Food Chem.* 2007, 104, 182–187.
- [68] Bauer, M.; Bauer, I. Heme Oxygenase-1: Redox Regulation and Role in the Hepatic Response to Oxidative Stress. *Antioxidants Redox Signal.* 2002, 4, 749–758.
- [69] Sorrenti, V. Editorial of Special Issue “Protective and Detrimental Role of Heme Oxygenase-1”. *Int. J. Mol. Sci.* 2019, 20, 4744.
- [70] Waza, A.A.; Hamid, Z.; Ali, S.; Bhat, S.A.; Bhat, M.A. A review on heme

- oxygenase-1 induction: Is it a necessary evil. *Agents Actions* 2018, 67, 579–588.
- [71] Ryter, S.W.; Tyrrell, R.M. The heme synthesis and degradation pathways: Role in oxidant sensitivity: Heme oxygenase has both pro- and antioxidant properties. *Free Radic. Biol. Med.* 2000, 28, 289–309.
- [72] Rossino, M.G.; Casini, G. Nutraceuticals for the Treatment of Diabetic Retinopathy. *Nutrients* 2019, 11, 771.
- [73] Kwok, H.-H.; Ng, W.Y.; Yang, M.S.M.; Mak, N.K.; Wong, R.N.S.; Yue, P.Y.K. The ginsenoside protopanaxatriol protects endothelial cells from hydrogen peroxide-induced cell injury and cell death by modulating intracellular redox status. *Free Radic. Biol. Med.* 2010, 48, 437–445.
- [74] Qin, D.; Yang, F.; Hu, Z.; Liu, J.; Wu, Q.; Luo, Y.; Yang, L.; Han, S.; Luo, F. Peptide T8 isolated from yak milk residue ameliorates H₂O₂-induced oxidative stress through Nrf2 signaling pathway in HUVEC cells. *Food Biosci.* 2021, 44, 101408.
- [75] Espinosa-Díez, C.; Miguel, V.; Vallejo, S.; Sánchez, F.J.; Sandoval, E.; Blanco, E.; Cannata, P.; Peiro, C.; Sánchez-Ferrer, C.F.; Lamas, S. Role of glutathione biosynthesis in endothelial dysfunction and fibrosis. *Redox Biol.* 2018, 14, 88–99.
- [76] Escudero-López, B.; Calani, L.; Fernández-Pachón, M.-S.; Ortega, Á.; Brighenti, F.; Crozier, A.; Del Rio, D. Absorption, metabolism, and excretion of fermented orange juice (poly)phenols in rats. *BioFactors* 2013, 40, 327–335.
- [77] Michlmayr, H.; Kneifel, W. β -Glucosidase activities of lactic acid bacteria: Mechanisms, impact on fermented food and human health. *FEMS Microbiol. Lett.* 2014, 352, 1–10.
- [78] Zhang, Y.; Liu, W.; Wei, Z.; Yin, B.; Man, C.; Jiang, Y. Enhancement of functional characteristics of blueberry juice fermented by *Lactobacillus plantarum*. *LWT* 2021, 139, 110590.
- [79] Hollman, P.C.; De Vries, J.H.; Van Leeuwen, S.D.; Mengelers, M.J.; Katan, M.B. Absorption of dietary quercetin glycosides and quercetin in healthy ileostomy volunteers. *Am. J. Clin. Nutr.* 1995, 62, 1276–1282.

- [80] Manach, C.; Morand, C.; Demigné, C.; Texier, O.; Régéat, F.; Rémésy, C. Bioavailability of rutin and quercetin in rats. *FEBS Lett.* 1997, *409*, 12–16.
- [81] Vuong, T.; Mallet, J.-F.; Ouzounova, M.; Rahbar, S.; Hernandez-Vargas, H.; Herceg, Z.; Matar, C. Role of a polyphenol-enriched preparation on chemoprevention of mammary carcinoma through cancer stem cells and inflammatory pathways modulation. *J. Transl. Med.* 2016, *14*, 13.

6

Treatment with PCSK9 inhibitor Evolocumab improves vascular oxidative stress and arterial stiffness in hypercholesterolemic patients with high cardiovascular risk

Reproduced from: “Treatment with PCSK9 Inhibitor Evolocumab Improves Vascular Oxidative Stress and Arterial Stiffness in Hypercholesterolemic Patients with High Cardiovascular Risk”

*Alessia Silla, Federica Fogacci, **Angela Punzo**, Silvana Hrelia, Patrizia Simoni, Cristiana Caliceti and Arrigo F.G. Cicero.*

Antioxidants, 2023, 12(3), 578.

Reproduced by permission of MDPI

<https://www.mdpi.com/openaccess>

6.1 Introduction

Cardiovascular diseases (CVD) are the leading causes of death worldwide, being also associated with oxidative stress. Increased reactive oxygen species (ROS) accumulation and inflammation are involved in the CV functional and structural damage underlying all CVD and CV risk factors [1]. For example, it is well known that oxidative stress is increased in hypertension [2]. Furthermore, an increased ROS production in arteries have also been shown to promote atherosclerotic plaque formation [3].

Familial hypercholesterolemia (FH) is an autosomal dominant disorder characterized by high circulating levels of low-density lipoprotein cholesterol (LDL-C). Monogenic mutation in the LDL-receptor (LDL-R) gene may suppress protein synthesis, and consequently its translocation to the cell surface, in reducing its turnover. Additional mechanisms include mutations affecting the apolipoprotein B (ApoB), the key structural component of LDL-C and the gene of pro-protein convertase subtilisin-Kexin type 9 (PCSK9), which promotes the LDL-R internalization and elimination in hepatocytes [4].

High serum level of LDL-C represents a very well-known risk factor for atherosclerotic CVD (ASCVD) [5]. LDL-C proteins are highly susceptible to being modified by the oxidative milieu found inside the vascular wall. In fact, the “oxidative modification hypothesis of atherosclerosis” is based on the evidence that modified oxidized LDL-C proteins are retained in atherosclerotic plaques and their uptake by scavenger receptors on phagocytes leads to foam cell formation [6]. Indeed, detrimental effects of FH on lipid metabolism led to an increased mortality rate even in young patients, which is largely due to ASCVD [7] moreover, FH promotes the generation of ROS which is another key mechanism involved in atherosclerosis development and progression [8].

Evolocumab, a new lipid-lowering drug, is a fully human monoclonal antibody against PCSK9, able to prevent the hepatic LDL-R degradation induced by PCSK9, finally reducing the risk of ASCVD and limb events[9].

In several clinical trials, treatment with Evolocumab lowered LDL-C levels and reduced the risk of CV events, also in FH patients [10,11]. Recent reports also suggest that therapy with PCSK9 inhibitors (iPCSK9) promotes an improvement in

arterial stiffness [12,13], even though the underlying molecular mechanism has not already been fully explained. This may be related to PCSK9 expression also in the arterial site and its possible involvement in certain mechanisms driving ASCVD development and progression.

Indeed, emerging evidence points out the role of PCSK9 as a vascular inflammation regulator, by contributing to cytokines release, inflammatory cell recruitment, and atherosclerotic plaque formation [14]. In line with these findings, in vitro and in vivo experimental studies have shown that PCSK9 overexpression is positively related to an up-regulation of the TLR4 (toll-like receptor 4)/NF- κ B (nuclear factor-kappa B) proinflammatory pathway, thus contributing to vascular inflammation and endothelial dysfunction [15]. Moreover, recent experimental evidence underlines the contribution of PCSK9 also in the oxidative state within the arterial wall [16].

Interestingly, investigational results have shown that Evolocumab pre-treatment significantly protects endothelial cells from H₂O₂-induced mortality by increasing antioxidant capacity and reducing hydroperoxides, malondialdehyde, and lipid peroxide levels [17].

According to these findings, further investigation of oxidative stress involvement may be the link in unveiling the pleiotropic effects of iPCSK9s in vascular homeostasis, beyond low-density lipoprotein cholesterol lowering.

Based on the crucial role that ROS play within the CV system and more generally in CVD, monitoring ROS levels in human patients would be important for both prognostic and diagnostic purposes (changes in oxidative stress level parallel the progression of the pathological condition) as well as to evaluate the response to treatment. In this regard, a major disadvantage is represented by the limited availability of tissue samples from both heart and blood vessels. To overcome this problem, circulating markers of CV stress condition could be used as a novel approach. Notably, several studies performed over the last 15 years have identified circulating leukocytes as a suitable indicator of systemic CV stress conditions requiring minimal invasive intervention [18].

Peripheral blood mononuclear cells (PBMCs), i.e. blood lymphocytes and monocytes, are one of the primary contributors to systemic ROS, playing a key

role not only in the immune system but also in the development of inflammation (cytokine production), endothelial dysfunction (endothelium adhesion molecule production), an CVD [19,20]. Interestingly, reports consistently demonstrate a reduced mitochondrial respiratory chain oxidative capacity related to the degree of CVD severity and to an increased ROS production by PBMCs [21,22], possibly due to other pro-oxidant pathways such as the nicotinamide adenine dinucleotide phosphate (NADPH) oxidase enzyme family (NOXs) [23] activated by different stimuli (i.e., cytokines, growth factors, angiotensin II and oxLDL) [24].

Indeed, CVDs (i.e., coronary artery failure), can be considered as a systemic alteration, and understanding the eventual implication of circulating blood cells peripheral blood mononuclear cells (PBMCs) and ROS production in patients with cardiac impairments, appears worthwhile.

In this report, we present data from patients with high or very high CV risk who experienced 2-month treatment with the iPCSK9 Evolocumab. Since PBMCs can be considered one of the main sources of ROS in the vasculature, we tested the hypothesis that higher H_2O_2 production in PBMCs is associated with variable improvements in arterial stiffness depending on patients' background lipid-lowering treatment (patients were receiving ezetimibe and maximum tolerated statin treatment at baseline) (**fig 6.1**). Results showed a significant improvement in BP-adjusted cfPWV, which was associated with a significant decrease in PBMCs- derived H_2O_2 .

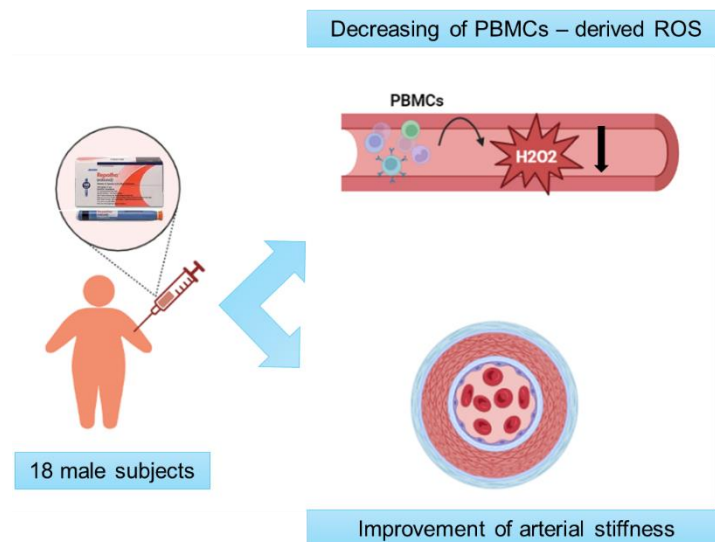


Figure 6.1: Schematic representation of the study.

6.2 Material and methods

6.2.1 Chemicals

The dioxetane CL probe (AquaSpark™ Peroxide Probe) was kindly provided by Biosynth (Staad, Switzerland). A 10 mM stock solution was prepared by dissolving the probe in DMSO (the CL probe solution is stable for months when stored at 4 °C and protected from light).

Phosphate-buffered saline (PBS) tabs (giving a 137 mM NaCl, 2.7 mM KCl and 10 mM phosphate buffer solution, pH 7.4), H₂O₂ solution, pro-oxidant agent phorbol myristate acetate (PMA) were purchased from Sigma-Aldrich (St Louis, MO, USA).

Ficoll-Paque™ PLUS was purchased from GE Healthcare (Boston, MA, US).

Dulbecco's Modified Eagle Medium (DMEM) high glucose and MEM Non-Essential Amino Acids solution 100X were purchased from Microgem (Naples, Italy). Antibiotic solution 100X (10,000 U/mL penicillin and 10 mg/mL streptomycin) was purchased from Sigma-Aldrich.

Cytotoxicity LDH Assay kit was purchased from Dojindo Molecular Technologies (Rockville, MD, USA).

All other chemicals and solvents were of the highest analytical grade.

Stock solutions of the pro-oxidant phorbol myristate acetate (PMA, 10 mM) was prepared by dissolving the compounds in DMSO.

6.2.2 Study population

The study was approved by the Local Ethics Committee and followed the Declaration of Helsinki and its later amendments.

Whole blood was collected from 18 hypercholesterolemic volunteers who were recruited at the Lipid Clinic of the S. Orsola-Malpighi University Hospital, Bologna, Italy. Enrolled patients were eligible for treatment with PCSK9 inhibitor in agreement with the European Society of Cardiology (ESC) / European Atherosclerosis Society (EAS) clinical guidance recommendations [25] and the criteria released by the Italian regulatory agency AIFA [26]. Additional inclusion criteria were ≥ 18 years of age, male sex and being on oral lipid-lowering therapy (statin and/or ezetimibe) for ≥ 6 months before enrollment, with no planned dose

change during study participation. Individuals with underlying diseases potentially interfering with the interpretation of the study's findings were excluded.

6.2.3 Treatment

Enrolled patients were evaluated anamnestically and by the execution of physical examination, non-invasive vascular tests, and laboratory analyses before and after two months of treatment with 140 mg Evolocumab every 2 weeks. All laboratory and instrumental measurements were carried out by trained staff who followed standardized protocols.

6.2.4 Assessments

6.2.4.1 Clinical assessments

Patients' personal history was evaluated paying particular attention to ASCVD, smoking habit and ongoing pharmacological treatments. Height and weight were measured by standard procedures [27].

6.2.4.2 Clinical chemistry analyses

Biochemical analyses were carried out on venous blood, withdrawn from the basilic vein after at least 12 hours of fasting. Plasma was obtained by the addition of disodium ethylenediaminetetraacetate (Na₂EDTA) (1 mg/mL) and blood centrifugation at 3000 RPM for 15 min at room temperature.

Immediately after centrifugation, laboratory analyses were performed in accordance with standardized methods by trained personnel [28], to assess total cholesterol (TC), high-density lipoprotein-cholesterol (HDL-C), triglycerides (TG), lipoprotein(a) (Lp(a)), apolipoprotein B (apoB), fasting glucose (FPG), serum uric acid (SUA), creatinine (Cr), estimated glomerular filtration rate (eGFR), total and fractionated bilirubin, alanine transaminase (ALT), aspartate transaminase (AST), creatinine phosphokinase (CPK) and thyroid-stimulating hormone (TSH). LDL-C was calculated by the Friedewald formula.

6.2.4.3 Blood pressure measurements

Systolic and diastolic blood pressure (SBP and DBP) measurements were

performed using a validated oscillometric device in individuals at rest in the supine position, with a cuff of the appropriate size applied on the right upper arm. To improve detection accuracy, three BP readings were sequentially obtained at 3-min intervals. The first one was discarded, and the average between the second and the third was recorded [29].

6.2.4.4 Non-invasive vascular tests

Arterial stiffness and ankle brachial index (ABI) were noninvasively evaluated by the Vicorder® apparatus (Skidmore Medical Ltd, Bristol, UK), which is a validated cuff-based oscillometric device. Carotid-femoral pulse wave velocity (cfPWV) consists in the measurement of the pulse wave transmission through the arteries and is considered a reliable and early marker of arterial stiffness, as well as a predictor of CV risk [30]. The theoretical basis of cfPW is explained with the equation of Moens–Korteweg [31], and it is calculated as the length between two measurement sites divided by the time the pulse wave needs to cover that distance (m/s) [32].

During this study, cfPWV has been calculated with simultaneous measurement of carotid and femoral BP. A neck pad with a photoplethysmographic detector has been placed around the neck and a cuff has been positioned around the patient's thigh. The distance between the suprasternal notch and the thigh cuff represents the distance covered by the pulse wave in its carotid–femoral path and has been used by the Vicorder® apparatus to establish the cfPWV value [33].

ABI measurement followed the American Heart Association (AHA) guidelines and the ESC/ European Society of Hypertension (ESH) guidelines [29,34] and has been assessed using Vicorder® on the right and left sides, standing the patients supine. Hokanson SC10 cuffs have been positioned on the upper arms and lower legs (above the ankles) and photoplethysmography sensors have been clipped bilaterally to the end of the middle finger and the big toe. The cuffs have been inflated up to 180 mmHg occluding the brachial and tibial arteries simultaneously. BP has been taken at the point of the pulse returning at both sites as the cuffs slowly deflated.

In agreement with the international guidelines, ABI has been calculated in each

leg dividing the highest pressure between posterior tibial and dorsalis pedis arteries by the highest arm pressure. The lowest ABI among the legs has been considered as a study variable [35].

6.2.5 H₂O₂ bioassay procedure

6.2.5.1 PBMCs collection

Fresh PBMCs were isolated from whole blood by Ficoll-Paque density gradient centrifugation [36], and resuspended in DMEM high glucose containing 10% FBS to a target concentration of 2×10^6 cells mL⁻¹. The protocol foresees different steps: the whole blood (about 20mL) was diluted 1:2 with PBS, then about 40 mL of diluted blood was gently layered over 15 mL of Ficoll-Paque medium. Gradients were centrifuged at $400 \times g$ for 30 min at 20°C in a swinging-bucket rotor without the brake applied. The PBMCs interface was carefully removed by pipetting, the PBMCs were washed with 50mL of PBS and centrifuged at $200 \times g$ for 15 min removing the supernatant. This step was repeated twice. Finally, PBMCs pellets were suspended in DMEM using 25 cm² cell culture flasks and incubated at 37°C in a humidified atmosphere of 5% CO₂. Cell counts and viability were assessed by Countess Automated Cell Counter (Thermo Fisher Scientific).

6.2.5.2 Quantification of intracellular H₂O₂ in PBMCs

One hundred microliters of suspension of freshly isolated PBMCs were plated in the wells of a 96-well black microtiter plate (2.0×10^5 – 0.25×10^5 cells well⁻¹) and incubated for 20 min with 50 µL of the dioxetane CL probe working solution. Then, 50 µL of working solution of the pro-oxidant PMA (25 µM final concentration in well) was added to induce intracellular H₂O₂ production and the CL emission was monitored for 60 min using a Luminoskan™ Ascent luminometric plate reader (PBS was used as the negative control). The whole assay was conducted at 37 °C. The integrated CL emission in the time interval between 40 and 60 min upon addition of PMA was used as the CL analytical signal. The experimental results were analyzed by plotting the CL analytical signal versus the PBMCs concentration and fitting the experimental data to a straight line using the method of least squares. The slope of the line was taken as an index of H₂O₂ production

by PBMCs under pro-oxidant stimulus.

6.2.6 Cell viability assay

The cell viability was assessed by WST8 [2-(2-methoxy-4-nitrophenyl)-3-(4-nitrophenyl)-5-(2,4-disulfophenyl)-2H-tetrazolium, monosodium salt] (Dojindo Molecular Technologies, Japan) that, in the presence of an electron mediator is reduced by dehydrogenases in cells (as a vitality biomarker) to formazan dye which is soluble in the tissue culture medium. The amount of the formazan dye generated by dehydrogenases in cells is directly proportional to the number of living cells [39]. The absorbance signal between the beginning and the end of each experiment was monitored at 37 °C at 450 nm using a Varioskan™ Flash Multimode Reader.

6.2.7 Data analysis

Baseline characteristics of the patients were reported as percentage frequencies for categorical variables and mean \pm standard deviation (SD) for continuous variables. The normality distribution of the variables was tested using the D'agostino-Pearson omnibus normality test. A paired-sample T-test and 1-way ANOVA were used to compare values obtained before and after treatment. Multiple variable analyses were carried out by analyzing the constructed correlation matrix using Pearson's coefficient with blood-pressure adjusted cfPWV as the dependent variable, and H₂O₂, age, BMI, SUA, eGFR and pre-post treatment variation in LDL-C as potential predictors. Then, a stepwise univariate correlation analysis was carried out between blood-pressure adjusted cfPWV and H₂O₂, in both study sub-cohorts. The correlation between two variables was analyzed as a function of p-value: P-values < 0.05 were always regarded as statistically significant. Furthermore, a correlation coefficient $\geq 0,7$ was considered as the threshold for determining strong correlation, while a correlation coefficient $\geq 0,4$ as at least moderate correlation.

Data was analyzed using GraphPad Prism v. 6.05 (GraphPad Software, Inc., La Jolla, CA, USA) was used to plot the experimental data and for the least-squares fitting of CL signal/PBMCs concentration graphs.

6.3 Results and discussion

Patients started treatment with Evolocumab between March 2019 and November 2019. In the overall study population, the mean age was 65.7 years. Demographic and clinical characteristics of the patients at baseline were reported in **Table 5.1**. Heterozygous FH (HeFH) affected 53.3% of the patients and preexisting CVD and/or peripheral obliterative arterial disease were present in 60%. A total of 60% of the patients had a story of statin intolerance and 26.7% were receiving high-dose statin treatment (20 or 40 mg rosuvastatin per day). The mean baseline LDL-C level was 154.49 ± 67.84 mg/dL.

All patients in the intention-to-treat population completed the clinical study through 2-month follow-up.

Table 5.1: *Baseline clinical characteristics of the study cohort.*

Characteristics	Statin and ezetimibe (N= 8)	Ezetimibe (N= 10)
Age – years	63.2 ± 7.3	69.4 ± 4.9
Active smokers - %	37.5	10
Heterozygous FH - %	62.5	30
Primary cardiovascular prevention - %	25	40
Secondary cardiovascular prevention - %	75	60
Cardiovascular disease - %	75	40
Cerebrovascular disease - %	0	10
Peripheral obliterative arterial disease- %	12.5	20
Type 2 diabetes - %	0	20
Hypertension - %	50	70
History of statin intolerance - %	50	80
Low-dose* statin treatment - %	50	0
High-dose [§] statin treatment - %	50	0
n-3 PUFA - %	25	0
Urate-lowering treatment - %	12.5	10

*defined as 5 or 10 mg Rosuvastatin; [§]defined as 20 or 40 mg Rosuvastatin.

FH= Familial hypercholesterolemia; PUFA= Poly-unsaturated fatty acids

6.3.1 Evolocumab treatment decreases intracellular H₂O₂ production in PBMCs

For the first primary endpoint, a significant decrease in H₂O₂ production by PBMCs from baseline to 2-month follow-up was observed (P-value = 0.02).

Thanks to a recently developed rapid and selective bioassay able to quantify a very small intracellular amount of H₂O₂ in human living cells [40], we monitored the cellular production of H₂O₂ in freshly isolated PBMCs. The bioassay employed an adamantylidene-1,2-dioxetane lipophilic probe containing an arylboronate moiety, which upon reaction with H₂O₂ is converted to the correspondent phenol, leading to probe decomposition and formation of an excited-state fragment that emits light. We first evaluated the H₂O₂ production of PBMCs obtained from healthy volunteer staff members upon treatment with PMA. **Figure 6.2A** shows a representative example of the correlation between CL signal and cell concentration. As expected, the CL emission intensity linearly increased with the concentration of cells up to 2×10^5 cells well⁻¹. We were particularly interested in the possibility of sensitively detecting the H₂O₂ produced by a small number of PBMCs, in order to be able in the near future to perform the assay using painless not-invasive blood sampling tools such as HemoLink [41]. Next, the dioxetane CL probe was employed to compare the intracellular production of H₂O₂ in freshly isolated PBMCs from 18 hypercholesterolemic subjects before (t₀) and after two-month treatment with Evolocumab (t₁). As an example, **figure 6.2B** shows a statistically significant decrease (P-value < 0.0001) in the slope of the CL signal/PBMCs concentration graph obtained using PBMCs isolated from a patient at t₀ and t₁, indicating that H₂O₂ production from PBMCs decreased after Evolocumab treatment. When considering all the subjects enrolled in the study, it can be observed that, despite the small number of subjects (n = 18), a ratio paired-sample t-test indicated that treatment with Evolocumab significantly reduced the production of H₂O₂ from PBMCs (P-value = 0.02), suggesting a possible beneficial effect in endothelial dysfunction (**Fig. 6.2C**). Notably, we monitored PBMCs viability before and after each experiment obtaining no significant differences (data not shown), thus confirming that Evolocumab treatment significantly reduces H₂O₂ production from PBMCs. Interestingly, we compared the slope values of all

the 18 subjects pre and after Evolocumab treatment, observing both in study sub-cohorts a significant tendency to decrease (Ezetimibe group, P-value=0.04; Ezetimibe+statin group, P-value=0.009), mainly when the slope value is higher than 0.08 threshold (**Fig. 6.2D / supplementary Fig. S1**). The numerous efforts made over the last decades to develop tools able to monitor the oxidative stress level in patients affected by CVD rely on the need to gain information on the disease state. Among others, the isolation of circulating leukocytes to measure their oxidant level offers a valid, noninvasive challenge that has been tested in few pathological contexts, including hypertension, atherosclerosis and its clinical manifestations, and heart failure. Since leukocytes circulate in the bloodstream, it is expected that they might reflect quite closely both systemic and cardiovascular oxidative stress and provide useful information on the pathological condition [42]. Moreover, the measurement of leukocyte oxidant activities may reveal the importance also to monitor the effectiveness of specific therapies, such as antihypertensive drugs [43]. Several studies support the concept that dysfunctional circulating PBMCs can act as an amplifier of oxidative stress and cell/tissue damage, ultimately contributing to the progression of the HF condition [44] and atherosclerosis [45]. Consequently, it is not surprising that PBMCs-derived ROS level predicts hospital readmission in chronic HF [46].

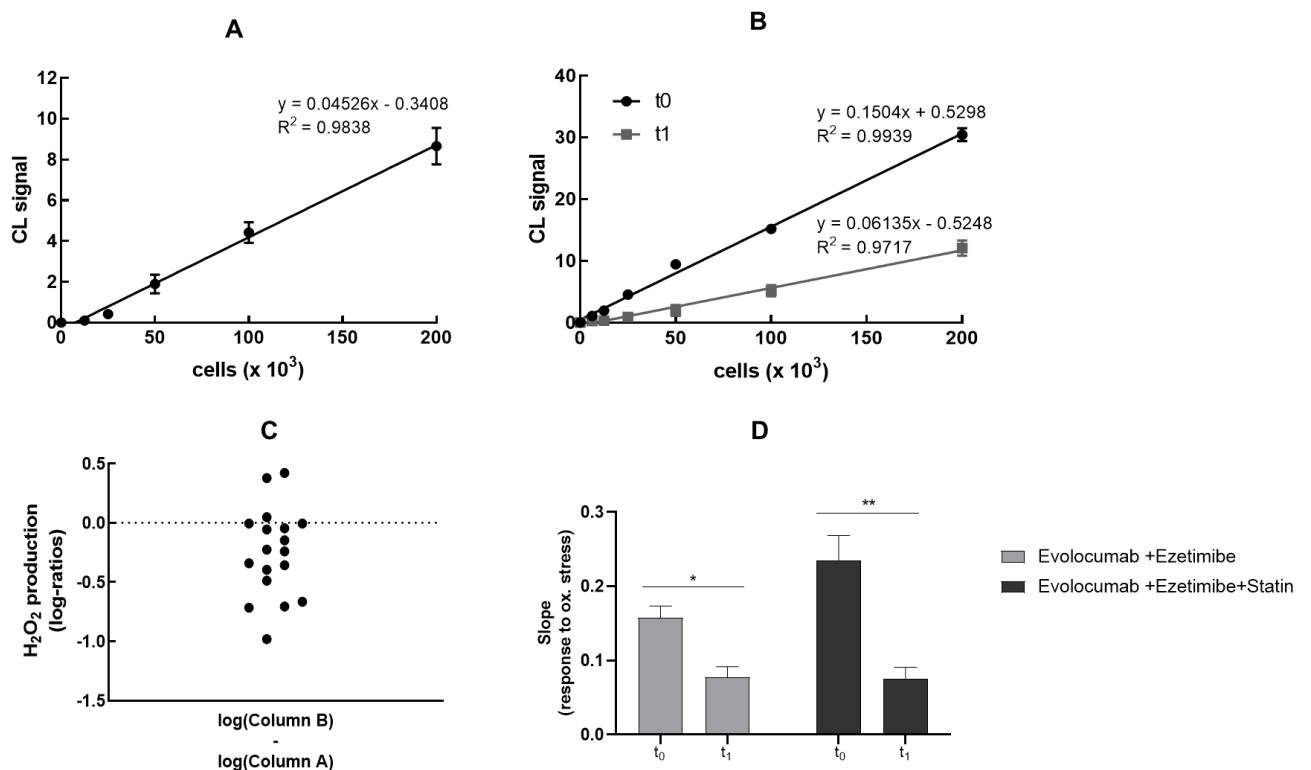


Figure 6.2: (A) Dose-response graph showing the correlation between the CL signal and the concentration of freshly isolated PBMCs from a healthy volunteer (range 0 – 2×10^5 cells). Each point represents the mean \pm SD of three independent measurements. (B) Dose-response graph showing the correlation between the CL signal and the concentration of freshly isolated PBMCs from a hypercholesterolemic subject before (t_0) and after (t_1) two-month treatment with Evolocumab. Each point represents the mean \pm SD of three independent measurements. (C) Changes of H_2O_2 production (as log-ratios) by PBMCs isolated from 18 hypercholesterolemic subjects observed after two-month treatment with Evolocumab (H_2O_2 production was evaluated as the slope of the CL signal versus PBMCs concentration graphs). (D) Slope values before and after Evolocumab treatment (the slope was calculated from the calibration curve obtained correlating the CL signal versus PBMCs concentration pre- and post-treatment). * $p < 0.05$, ** $p < 0.01$ significantly different from t_0 values.

6.3.2 Arterial stiffness improvement in Evolocumab- treated patients in association with Ezetimibe and Ezetimibe+ statin

For the second primary endpoint, cfPWV significantly improved in both study sub-cohorts (Ezetimibe group, P-value=0.015; Ezetimibe+statin group, P-value=0.0046) (**Table 6.2 and Fig. 6.3**).

Obviously, patients treated with PCSK9 inhibitors also experienced significant improvements in serum levels after treatment (**Table 6.3**).

cfPWV is a benchmark clinical measure of large elastic arterial stiffness and has been found to be a powerful predictor of CVD in the aging population. It is now well established that increased vascular stiffness, as can be measured using PWV, signifies declining vascular function and is associated with elevated cardiovascular risk.

For example, changes in the arterial wall, including increased collagen deposition and degradation of elastin, have been associated with changes in mechanical properties of the artery.

Table 6.2: Pre- and post-treatment data of enrolled patients.

Parameters	Statin and ezetimibe (N= 8)		Ezetimibe (N= 10)	
	Baseline	Follow-up	Baseline	Follow-up
Fasting plasma glucose - mg/dL	94.13±5.08	93.4±8	93.6±10.04	99.6±14.48
Creatinine - mg/dL	0.81±0.13	0.78±0.15	0.95±0.16	1±0.18
eGFR - mL/min/1.73 m ²	89.16±17.11	90.63±18.52	73.78±15.34	68.11±16.09
Serum uric acid - mg/dL	5.05±0.93	4.61±0.85*	5.86±0.91	6±0.98
Total cholesterol - mg/dL	212.88±35.92	111.75±12.15*	247.4±85.19	138.3±60.73*
Triglyceride - mg/dL	137.75±93.23	106.5±64.36*	138.7±66.67	153±150.69
HDL-cholesterol - mg/dL	58±13.22	58±11.87	56.2±12.47	55.2±13.58
Non-HDL-cholesterol - mg/dL	154.88±32.99	53.75±8.88*	191.2±78.63	83.1±52.84*
LDL-cholesterol - mg/dL	132.54±35.94	33.4±12.92*	163.46±78.16	52.5±55.33*
VLDL-cholesterol - mg/dL	28.03±20.09	21.31±13.9*	28.16±14.07	32.07±31.59
Apolipoprotein-B - mg/dL	147.2±47.8	53±20.48*	148±41.12	53.63±33.62*
Lipoprotein(a) - mg/dL	95.72±92.62	67.06±58.42	42.05±54.45	30.79±42.15*
Total bilirubin - mg/dL	0.5±0.07	0.54±0.12	0.64±0.18	0.58±0.21
Direct bilirubin - mg/dL	0.13±0.04	0.16±0.09	0.11±0.03	0.13±0.05*
Indirect bilirubin - mg/dL	0.37±0.05	0.37±0.06	0.54±0.15	0.46±0.17
Aspartate aminotransferase - U/L	25.71±7.7	26.71±8.73	33.2±24.79	31.9±26.59
Alanine aminotransferase - U/L	24.13±10.26	23.5±9.93	27.4±14.97	24.6±16.15
Gamma-glutamyl transferase - U/L	36±51.8	45.13±82.16	32.5±23.63	29.8±13.74
Creatine phosphokinase - U/L	125.25±78.04	150.38±95.58	393.8±392.8	361.2±398.3
Thyroid-stimulating hormone - µU/mL	1.92±1.09	2.06±1.2	2.44±0.77	2.03±0.38

eGFR= Estimated glomerular filtration rate; HDL= High-density lipoprotein; LDL= Low-density lipoprotein; VLDL= Very-low density lipoprotein. * P<0.05 versus baseline.

Table 6.3: Pre- and post-treatment hemodynamical data of enrolled patients.

Parameters	Statin and ezetimibe (N= 8)		Ezetimibe (N= 10)	
	Baseline	Follow-up	Baseline	Follow-up
Heart rate – bpm	67.13±13	68.75±8.19	62.8±7.18	64.1±10.04
Systolic blood pressure – mmHg	135.13±14.29	148.13±17.76*	142.3±20.87	153±14.31
Diastolic blood pressure – mmHg	70.5±10.3	71.1±10.5	70.1±11.1	75.4±8.1
Pulse wave velocity - m/s	11.39±1.26	4.91±2.7**	11.5 ± 1.9	6.77 ± 2.71*
Ankle brachial index right	1.06 ± 0.06	1.1 ± 0.15	0.91 ± 0.23	1.08 ± 0.07
Ankle brachial index left	1.02 ± 0.18	1.06 ± 0.21	0.98 ± 0.19	1.1 ± 0.2

* $P < 0.05$ versus baseline; ** $P < 0.01$ versus baseline.

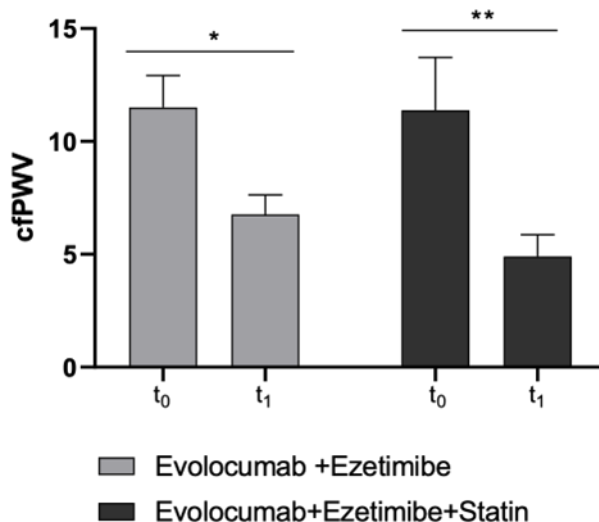


Figure 6.3: Changes in cfPWV values before and after Evolocumab treatment in study sub-cohorts (Ezetimibe group and Ezetimibe+statin group). * $P < 0.05$ and ** $P < 0.01$ significantly different versus t₀ values.

6.3.3 H₂O₂ decrease correlates with arterial stiffness improvement

In the multiple correlation model, change in 2-month BP-adjusted cfPWV was significantly associated with a change in H₂O₂ (Pearson coefficient R= 0,65, P-value= 0,004), though neither with age, BMI, eGFR, and SUA levels at baseline

nor with the percentage change in LDL-C at 2-month follow-up (P-values > 0.05 for all the considered variables). In the univariate analysis, the improvement of cfPWV in both sub-cohorts correlated with the reduction in H₂O₂ production (R=0,77 p-value=0.02 and R=0.56 p-value=0.05 in Ezetimibe+statin sub-cohort and Ezetimibe, respectively).

Recently, Maulucci and co-workers showed that two months of treatment with 140 mg Evolocumab could improve endothelial function in subjects with increased cardiovascular risk, being the improvement proportional to LDL-C reduction [47]. On the other hand, it has recently been reported that two iPCSK9-treated patients experienced a cfPWV improvement despite the increase in LDL-C suggesting that the iPCSK9s could independently exert a beneficial impact on vasomotor function [12]. This may contribute to cardiovascular disease risk reduction independent of changes in serum lipoprotein concentrations [48].

In the past, short-term effects of statins in ameliorating arterial stiffness have been attributed at least [49] in part, to their pleiotropic antioxidant and anti-inflammatory effects, so the strong correlation between cfPWV decrease and H₂O₂ production in Ezetimibe + statin sub-cohort can be derived by the combination of PCSK9 and statin treatments. Our results suggest that the effect on arterial stiffness could be not only attributed to LDL-C change but also to a decreased vascular oxidative stress.

6.4 Conclusions

In conclusion, cfPWV and PBMCs-derived H₂O₂ production profiles in hypercholesterolemic subjects significantly improved after short-term treatment of the iPCSK9 Evolocumab. Our results appear to be consistent with the beneficial role of this novel, lipid-lowering therapy in hypercholesterolemic subjects. There are several limitations to our study: firstly, the study population size was relatively small; then, other parameters regarding the evaluation of cardiovascular risk in hypercholesterolemic patients, including oxidized LDL-C, were not available and were not taken into consideration.

Of course, these preliminary findings should be further confirmed in an adequately powered long-term placebo-controlled randomized clinical trial to evaluate the

effect of iPCSK9 on arterial stiffness and oxidative stress in a selected clinical setting through proper statistical means; however, we were able to show a significant improvement of cfPWV and PBMCs derived- H₂O₂ production profile after Evolocumab treatment both in Ezetimibe and Ezetimibe+statin study cohorts. Moreover, a genomic fingerprint of PBMCs derived from high CV-risk patients will be also assessed in the near future to better characterize the effect of Evolocumab treatment in the gene expression profile differences associated with the health status of a human subject.

6.5 Acknowledgements

We wish to thank Biosynth (Staad, Switzerland) for kindly providing the dioxetane CL probe AquaSpark™ Peroxide Probe. We would thank also Proff. Aldo Roda and Antonio Pannuti for their supervision.

6.6 References

- [1] Touyz, R.M.; Rios, F.J.; Alves-Lopes, R.; Neves, K.B.; Camargo, L.L.; Montezano, A.C. Oxidative Stress: A Unifying Paradigm in Hypertension. *Can J Cardiol* **2020**, *36*, 659–670, doi:10.1016/j.cjca.2020.02.081.
- [2] Roger, V.L.; Go, A.S.; Lloyd-Jones, D.M.; Benjamin, E.J.; Berry, J.D.; Borden, W.B.; Bravata, D.M.; Dai, S.; Ford, E.S.; Fox, C.S.; et al. Heart Disease and Stroke Statistics—2012 Update. *Circulation* **2012**, *125*, doi:10.1161/CIR.0b013e31823ac046.
- [3] Martin-Ventura, J.; Rodrigues-Diez, R.; Martinez-Lopez, D.; Salaices, M.; Blanco-Colio, L.; Briones, A. Oxidative Stress in Human Atherothrombosis: Sources, Markers and Therapeutic Targets. *Int J Mol Sci* **2017**, *18*, 2315, doi:10.3390/ijms18112315.
- [4] Benn, M.; Watts, G.F.; Tybjaerg-Hansen, A.; Nordestgaard, B.G. Mutations Causative of Familial Hypercholesterolaemia: Screening of 98 098 Individuals from the Copenhagen General Population Study Estimated a Prevalence of 1 in 217. *Eur Heart J* **2016**, *37*, 1384–1394, doi:10.1093/eurheartj/ehw028.
- [5] Presta, V.; Figliuzzi, I.; Miceli, F.; Coluccia, R.; Fogacci, F.; Cicero, A.F.G.; Ferrucci, A.; Borghi, C.; Volpe, M.; Tocci, G.; et al. Achievement of Low Density Lipoprotein (LDL) Cholesterol Targets in Primary and Secondary Prevention: Analysis of a Large Real Practice Database in Italy. *Atherosclerosis* **2019**, *285*, 40–48, doi:10.1016/j.atherosclerosis.2019.03.017.
- [6] Steinberg, D. The LDL Modification Hypothesis of Atherogenesis: An Update. *J Lipid Res* **2009**, *50*, S376–S381, doi:10.1194/jlr.R800087-JLR200.
- [7] Marks, D.; Thorogood, M.; Neil, H.A.W.; Humphries, S.E. A Review on the Diagnosis, Natural History, and Treatment of Familial Hypercholesterolaemia. *Atherosclerosis* **2003**, *168*, 1–14, doi:10.1016/S0021-9150(02)00330-1.

- [8] Mollazadeh, H.; Carbone, F.; Montecucco, F.; Pirro, M.; Sahebkar, A. Oxidative Burden in Familial Hypercholesterolemia. *J Cell Physiol* **2018**, *233*, 5716–5725, doi:10.1002/jcp.26466.
- [9] Shapiro, M.D.; Tavori, H.; Fazio, S. PCSK9. *Circ Res* **2018**, *122*, 1420–1438, doi:10.1161/CIRCRESAHA.118.311227.
- [10] Sabatine, M.S.; Giugliano, R.P.; Keech, A.C.; Honarpour, N.; Wiviott, S.D.; Murphy, S.A.; Kuder, J.F.; Wang, H.; Liu, T.; Wasserman, S.M.; et al. Evolocumab and Clinical Outcomes in Patients with Cardiovascular Disease. *N Engl J Med* **2017**, *376*, 1713–1722, doi:10.1056/NEJMoa1615664.
- [11] Raal, F.J.; Stein, E.A.; Dufour, R.; Turner, T.; Civeira, F.; Burgess, L.; Langslet, G.; Scott, R.; Olsson, A.G.; Sullivan, D.; et al. PCSK9 Inhibition with Evolocumab (AMG 145) in Heterozygous Familial Hypercholesterolaemia (RUTHERFORD-2): A Randomised, Double-Blind, Placebo-Controlled Trial. *The Lancet* **2015**, *385*, 331–340, doi:10.1016/S0140-6736(14)61399-4.
- [12] Cicero, A.F.G.; Toth, P.P.; Fogacci, F.; Viridis, A.; Borghi, C. Improvement in Arterial Stiffness after Short-Term Treatment with PCSK9 Inhibitors. *Nutr Metab Cardiovasc Dis* **2019**, *29*, 527–529, doi:10.1016/j.numecd.2019.01.010.
- [13] Mandraffino, G.; Scicali, R.; Rodríguez-Carrio, J.; Savarino, F.; Mamone, F.; Scuruchi, M.; Cinquegrani, M.; Imbalzano, E.; di Pino, A.; Piro, S.; et al. Arterial Stiffness Improvement after Adding on PCSK9 Inhibitors or Ezetimibe to High-Intensity Statins in Patients with Familial Hypercholesterolemia: A Two-Lipid Center Real-World Experience. *J Clin Lipidol* **2020**, *14*, 231–240, doi:10.1016/j.jacl.2020.01.015.
- [14] Punch, E.; Klein, J.; Diaba-Nuhoho, P.; Morawietz, H.; Garelnabi, M. Effects of PCSK9 Targeting: Alleviating Oxidation, Inflammation, and Atherosclerosis. *J Am Heart Assoc* **2022**, *11*, doi:10.1161/JAHA.121.023328.
- [15] Tang, Z.-H.; Peng, J.; Ren, Z.; Yang, J.; Li, T.-T.; Li, T.-H.; Wang, Z.; Wei, D.-H.; Liu, L.-S.; Zheng, X.-L.; et al. New Role of PCSK9 in

- Atherosclerotic Inflammation Promotion Involving the TLR4/NF-KB Pathway. *Atherosclerosis* **2017**, *262*, 113–122, doi:10.1016/j.atherosclerosis.2017.04.023.
- [16] Cammisotto, V.; Baratta, F.; Simeone, P.G.; Barale, C.; Lupia, E.; Galardo, G.; Santilli, F.; Russo, I.; Pignatelli, P. Proprotein Convertase Subtilisin Kexin Type 9 (PCSK9) Beyond Lipids: The Role in Oxidative Stress and Thrombosis. *Antioxidants* **2022**, *11*, 569, doi:10.3390/antiox11030569.
- [17] Safaeian, L.; Mirian, M.; Bahrizadeh, S. Evolocumab, a PCSK9 Inhibitor, Protects Human Endothelial Cells against H₂O₂-Induced Oxidative Stress. *Arch Physiol Biochem* **2022**, *128*, 1681–1686, doi:10.1080/13813455.2020.1788605.
- [18] Swirski, F.K.; Nahrendorf, M. Leukocyte Behavior in Atherosclerosis, Myocardial Infarction, and Heart Failure. *Science (1979)* **2013**, *339*, 161–166, doi:10.1126/science.1230719.
- [19] Rubattu, S.; Forte, M.; Raffa, S. Circulating Leukocytes and Oxidative Stress in Cardiovascular Diseases: A State of the Art. *Oxid Med Cell Longev* **2019**, *2019*, 1–9, doi:10.1155/2019/2650429.
- [20] De Mello, V.D.F.; Kolehmanien, M.; Schwab, U.; Pulkkinen, L.; Uusitupa, M. Gene Expression of Peripheral Blood Mononuclear Cells as a Tool in Dietary Intervention Studies: What Do We Know so Far? *Mol Nutr Food Res* **2012**, *56*, 1160–1172, doi:10.1002/mnfr.201100685.
- [21] Shirakawa, R.; Yokota, T.; Nakajima, T.; Takada, S.; Yamane, M.; Furihata, T.; Maekawa, S.; Nambu, H.; Katayama, T.; Fukushima, A.; et al. Mitochondrial Reactive Oxygen Species Generation in Blood Cells Is Associated with Disease Severity and Exercise Intolerance in Heart Failure Patients. *Sci Rep* **2019**, *9*, 14709, doi:10.1038/s41598-019-51298-3.
- [22] Alfatni, A.; Riou, M.; Charles, A.-L.; Meyer, A.; Barnig, C.; Andres, E.; Lejay, A.; Talha, S.; Geny, B. Peripheral Blood Mononuclear Cells and Platelets Mitochondrial Dysfunction, Oxidative Stress, and Circulating

- MtDNA in Cardiovascular Diseases. *J Clin Med* **2020**, *9*, 311, doi:10.3390/jcm9020311.
- [23] Wenzel, P.; Knorr, M.; Kossmann, S.; Stratmann, J.; Hausding, M.; Schuhmacher, S.; Karbach, S.H.; Schwenk, M.; Yogev, N.; Schulz, E.; et al. Lysozyme M-Positive Monocytes Mediate Angiotensin II-Induced Arterial Hypertension and Vascular Dysfunction. *Circulation* **2011**, *124*, 1370–1381, doi:10.1161/CIRCULATIONAHA.111.034470.
- [24] Forte, M.; Nocella, C.; de Falco, E.; Palmerio, S.; Schirone, L.; Valenti, V.; Frati, G.; Carnevale, R.; Sciarretta, S. The Pathophysiological Role of NOX2 in Hypertension and Organ Damage. *High Blood Press Cardiovasc Prev* **2016**, *23*, 355–364, doi:10.1007/s40292-016-0175-y.
- [25] Catapano, A.L.; Graham, I.; de Backer, G.; Wiklund, O.; Chapman, M.J.; Drexel, H.; Hoes, A.W.; Jennings, C.S.; Landmesser, U.; Pedersen, T.R.; et al. 2016 ESC/EAS Guidelines for the Management of Dyslipidaemias. *Rev Esp Cardiol (Engl Ed)* **2017**, *70*, 115, doi:10.1016/j.rec.2017.01.002.
- [26] AIFA (Italian Medicines Agency). Classificazione del medicinale per uso umano «Repatha», ai sensi dell'art. 8, comma 10, della legge 24 dicembre 1993, n. 537. (Determina n. 172/2017). Available online: <http://https://www.gazzettaufficiale.it/eli/id/2017/02/07/17A01047/s#:~:text=%C2%ABRepatha%C2%BB%20e%20indicato%20nei,C%20target%20con%20la%20dose> (accessed on 2 December 2022).
- [27] Cicero, A.F.G.; Fogacci, F.; Veronesi, M.; Strocchi, E.; Grandi, E.; Rizzoli, E.; Poli, A.; Marangoni, F.; Borghi, C. A Randomized Placebo-Controlled Clinical Trial to Evaluate the Medium-Term Effects of Oat Fibers on Human Health: The Beta-Glucan Effects on Lipid Profile, Glycemia and Intestinal Health (BELT) Study. *Nutrients* **2020**, *12*, 686, doi:10.3390/nu12030686.
- [28] Cicero, A.F.G.; Fogacci, F.; Giovannini, M.; Grandi, E.; D'Addato, S.; Borghi, C. Interaction between Low-Density Lipoprotein-Cholesterolaemia, Serum Uric Level and Incident Hypertension. *J Hypertens* **2019**, *37*, 728–731, doi:10.1097/HJH.0000000000001927.

- [29] Williams, B.; Mancia, G.; Spiering, W.; Agabiti Rosei, E.; Azizi, M.; Burnier, M.; Clement, D.L.; Coca, A.; de Simone, G.; Dominiczak, A.; et al. 2018 ESC/ESH Guidelines for the Management of Arterial Hypertension. *Eur Heart J* **2018**, *39*, 3021–3104, doi:10.1093/eurheartj/ehy339.
- [30] van Bortel, L.M.; Laurent, S.; Boutouyrie, P.; Chowienczyk, P.; Cruickshank, J.K.; de Backer, T.; Filipovsky, J.; Huybrechts, S.; Mattace-Raso, F.U.S.; Protogerou, A.D.; et al. Expert Consensus Document on the Measurement of Aortic Stiffness in Daily Practice Using Carotid-Femoral Pulse Wave Velocity. *J Hypertens* **2012**, *30*, 445–448, doi:10.1097/HJH.0b013e32834fa8b0.
- [31] Marque, V.; van Essen, H.; Struijker-Boudier, H.A.J.; Atkinson, J.; Lartaud-Idjouadiene, I. Determination of Aortic Elastic Modulus by Pulse Wave Velocity and Wall Tracking in a Rat Model of Aortic Stiffness. *J Vasc Res* **2001**, *38*, 546–550, doi:10.1159/000051090.
- [32] Hirata, K.; Kawakami, M.; O'Rourke, M.F. Pulse Wave Analysis and Pulse Wave Velocity A Review of Blood Pressure Interpretation 100 Years After Korotkov. *Circulation* **2006**, *70*, 1231–1239, doi:10.1253/circj.70.1231.
- [33] Hickson, S.S.; Butlin, M.; Broad, J.; Avolio, A.P.; Wilkinson, I.B.; McEniery, C.M. Validity and Repeatability of the Vicorder Apparatus: A Comparison with the SphygmoCor Device. *Hypertens Res* **2009**, *32*, 1079–1085, doi:10.1038/hr.2009.154.
- [34] Aboyans, V.; Criqui, M.H.; Abraham, P.; Allison, M.A.; Creager, M.A.; Diehm, C.; Fowkes, F.G.R.; Hiatt, W.R.; Jönsson, B.; Lacroix, P.; et al. Measurement and Interpretation of the Ankle-Brachial Index. *Circulation* **2012**, *126*, 2890–2909, doi:10.1161/CIR.0b013e318276fbcf.
- [35] Samba, H.; Guerchet, M.; Ndamba-Bandzouzi, B.; Kehoua, G.; Mbelesso, P.; Desormais, I.; Aboyans, V.; Preux, P.-M.; Lacroix, P. Ankle Brachial Index (ABI) Predicts 2-Year Mortality Risk among Older Adults in the Republic of Congo: The EPIDEMCA-FU Study.

- Atherosclerosis* **2019**, *286*, 121–127, doi:10.1016/j.atherosclerosis.2019.05.013.
- [36] Bua, G.; Manaresi, E.; Bonvicini, F.; Gallinella, G. Parvovirus B19 Replication and Expression in Differentiating Erythroid Progenitor Cells. *PLoS One* **2016**, *11*, e0148547, doi:10.1371/journal.pone.0148547.
- [37] Hananya, N.; Shabat, D. Recent Advances and Challenges in Luminescent Imaging: Bright Outlook for Chemiluminescence of Dioxetanes in Water. *ACS Cent Sci* **2019**, *5*, 949–959, doi:10.1021/acscentsci.9b00372.
- [38] Green, O.; Gnaim, S.; Blau, R.; Eldar-Boock, A.; Satchi-Fainaro, R.; Shabat, D. Near-Infrared Dioxetane Luminophores with Direct Chemiluminescence Emission Mode. *J Am Chem Soc* **2017**, *139*, 13243–13248, doi:10.1021/jacs.7b08446.
- [39] Caliceti, C.; Rizzo, P.; Ferrari, R.; Fortini, F.; Aquila, G.; Leoncini, E.; Zambonin, L.; Rizzo, B.; Calabria, D.; Simoni, P.; et al. Novel Role of the Nutraceutical Bioactive Compound Berberine in Lectin-like OxLDL Receptor 1-Mediated Endothelial Dysfunction in Comparison to Lovastatin. *Nutr Metab Cardiovasc Dis* **2017**, *27*, 552–563, doi:10.1016/j.numecd.2017.04.002.
- [40] Calabria, D.; Guardigli, M.; Mirasoli, M.; Punzo, A.; Porru, E.; Zangheri, M.; Simoni, P.; Pagnotta, E.; Ugolini, L.; Lazzeri, L.; et al. Selective Chemiluminescent TURN-ON Quantitative Bioassay and Imaging of Intracellular Hydrogen Peroxide in Human Living Cells. *Anal Biochem* **2020**, *600*, 113760, doi:10.1016/j.ab.2020.113760.
- [41] ClinLab navigator. HemoLink Blood Collection Device.
- [42] Yasunari, K.; Watanabe, T.; Nakamura, M. Reactive Oxygen Species Formation by Polymorphonuclear Cells and Mononuclear Cells as a Risk Factor of Cardiovascular Diseases. *Curr Pharm Biotechnol* **2006**, *7*, 73–80, doi:10.2174/138920106776597612.
- [43] Yasunari, K.; Maeda, K.; Nakamura, M.; Watanabe, T.; Yoshikawa, J. Benidipine, a Long-Acting Calcium Channel Blocker, Inhibits Oxidative Stress in Polymorphonuclear Cells in Patients with Essential

- Hypertension. *Hypertension Research* **2005**, *28*, 107–112, doi:10.1291/hypres.28.107.
- [44] IJsselmuiden, A.J.; Musters, R.J.; de Ruiter, G.; van Heerebeek, L.; Alderse-Baas, F.; van Schilfgaarde, M.; Leyte, A.; Tangelder, G.-J.; Laarman, G.J.; Paulus, W.J. Circulating White Blood Cells and Platelets Amplify Oxidative Stress in Heart Failure. *Nat Clin Pract Cardiovasc Med* **2008**, *5*, 811–820, doi:10.1038/ncpcardio1364.
- [45] Leu, H.-B.; Lin, C.-P.; Lin, W.-T.; Wu, T.-C.; Lin, S.-J.; Chen, J.-W. Circulating Mononuclear Superoxide Production and Inflammatory Markers for Long-Term Prognosis in Patients with Cardiac Syndrome X. *Free Radic Biol Med* **2006**, *40*, 983–991, doi:10.1016/j.freeradbiomed.2005.10.047.
- [46] Song, B.; Li, T.; Chen, S.; Yang, D.; Luo, L.; Wang, T.; Han, X.; Bai, L.; Ma, A. Correlations between MTP and ROS Levels of Peripheral Blood Lymphocytes and Readmission in Patients with Chronic Heart Failure. *Heart Lung Circ* **2016**, *25*, 296–302, doi:10.1016/j.hlc.2015.09.004.
- [47] Maulucci, G.; Cipriani, F.; Russo, D.; Casavecchia, G.; di Staso, C.; di Martino, L.; Ruggiero, A.; di Biase, M.; Brunetti, N.D. Improved Endothelial Function after Short-Term Therapy with Evolocumab. *J Clin Lipidol* **2018**, *12*, 669–673, doi:10.1016/j.jacl.2018.02.004.
- [48] Vlachopoulos, C.; Aznaouridis, K.; Terentes-Printzios, D.; Ioakeimidis, N.; Stefanadis, C. Prediction of Cardiovascular Events and All-Cause Mortality With Brachial-Ankle Elasticity Index. *Hypertension* **2012**, *60*, 556–562, doi:10.1161/HYPERTENSIONAHA.112.194779.
- [49] Oesterle, A.; Laufs, U.; Liao, J.K. Pleiotropic Effects of Statins on the Cardiovascular System. *Circ Res* **2017**, *120*, 229–243, doi:10.1161/CIRCRESAHA.116.308537.

6.7 Supplementary material

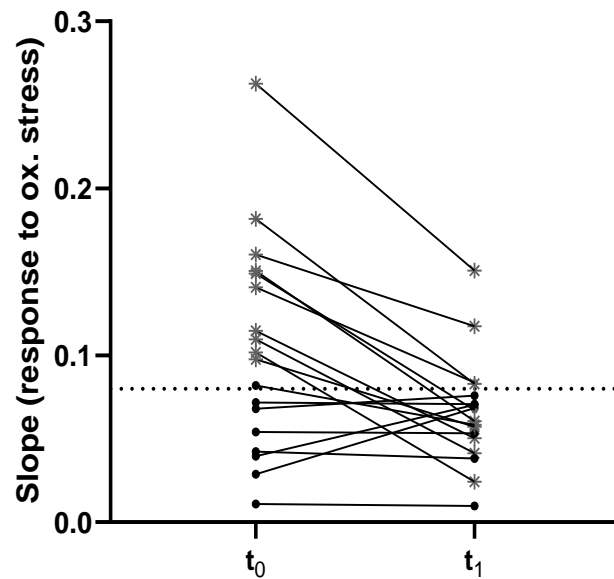


Figure S1: Changes of H_2O_2 production by PBMCs isolated from 18 hypercholesterolemic subjects observed before (t_0) and after (t_1) two-month treatment with Evolocumab (H_2O_2 production is expressed as the slope of the curve derived by CL signal versus PBMCs concentration graphs).

7

Jagged1-Fluc: a bioluminescent recombinant protein as potential diagnostic tool for the high-throughput screening of colorectal cancer

Adapted from: “New Insights into Bile Acids Related Signaling Pathways in the Onset of Colorectal Cancer”

Cristiana Caliceti, Angela Punzo, Alessia Silla, Patrizia Simoni, Giulia Roda and Silvana Hrelia.

Nutrients, 2022; 14(14), 2964

Reproduced by permission of MDPI

<https://www.mdpi.com/openaccess>

7.1 Introduction

Colorectal cancer (CRC) ranks as the fourth most common cancer and the second cause of cancer in men and the third in women. The International Agency for Research on Cancer (IARC) estimated 1.9 million new cases in 2020, with more than 900,000 deaths, and this rate might increase by 60% over the next 10 years [1]. These data are troublesome considering that CRC could be successfully treated if diagnosed in the early stages. To date, the guaiac-based test of fecal occult blood (FOBT), although not very sensitive, is used in most CRC screening programs, eventually followed by endoscopic assessment and prophylactic surgical resection in cases of high-grade dysplasia [2]. This rapid growth in cases may reflect both increased lifespan, genetic predisposition, such as positive family history (almost 20% of all patients), and other genetic syndromes, such as Lynch and Gardner syndromes, and familial adenomatous polyposis (FAP), as well as environmental factors [3]. The cancer gradual progression offers an opportunity to detect it before the malignant changes; studies have shown that over 90% of all CRC results from colon–rectal adenomas and just the metastatic phases are related to a high mortality rate and 5-year survival of below 10% [4]. The CRC progression is a multi-step process that involves a series of events from adenoma to carcinoma. The stepwise accumulation of genetic and epigenetic alteration leads to a generalized disorder of stem and epithelial cell replication and differentiation, thus causing aberrant proliferation of cells within crypts that may progress to adenomas with different grades of dysplasia and may even become more invasive leading to carcinoma [5]. There are several mechanisms underlying tumorigenic development, such as the activation of oncogenes and the inactivation of tumor suppressors. In the hereditary CRC forms, there have been frequent reports of a mutation in the adenomatous polyposis coli (APC) gene, which plays a key role in the Wnt/ β -catenin signaling pathway, and mutations in the family of mismatch repair genes (MMR), which preserve genomic integrity. Instead, in sporadic CRC, which accounts for nearly 85% of all CRC cases, a plethora of mutations which can lead the oncogenic events have been identified. No single pathway is considered to be responsible for colorectal cancer but several pathways, such as Wnt/ β -catenin, the mitogen-activated protein kinase (MAPK), the phosphatidylinositol 3-kinase (PI3K)/protein kinase B (AKT), the

transforming growth factor- β (TGF- β), have been frequently reported to be dysregulated in the CRC [6]. Indeed, recent studies suggest a pivotal role of “abnormal” Notch signaling activation in CRC, partially due to cross-talks of Notch with the other pathways mentioned above [7- 9]. Notch signaling controls various cellular processes including stem cell self-renewal, cell fate specification, and differentiation [10]. The pathway, in brief, consists of five ligands (Jagged 1,2 - Dll 1,3,4), and four receptors (Notch1, Notch2, Notch3, and Notch4) and it is activated upon the interaction of the ligand with the receptor in adjacent cells [11]. Notch family receptor is a single-pass transmembrane molecule composed of extracellular (ECD) and (ICD) intracellular domains. The ECD domain appears to function primarily as regulatory region involved with ligand binding [12].

It is well known that the deregulation of Notch signaling results in developmental deficits in humans such as Alagille Syndrome and different types of neoplasia [13]. Notch was first described as an oncogene by Ellisen et al. in acute lymphoblastic leukemia (T-ALL) [14]. Subsequently, altered activation of the Notch pathway was discovered in several cancers such as breast cancer, lung adenocarcinoma, ovarian cancer, and colorectal cancer [15,16]. In particular, it has been recently shown that positive Notch3 protein expression is an unfavorable prognostic factor for disease-free survival (DFS) and overall survival (OS) in CRC patients [17].

In an APC-deficient mouse model the depletion of Jagged1 (Jag1) in tumor-initiating cells resulted in a dramatic reduction in the proliferation activity of intestinal tumors and disruption of stem cell niche formation, suggesting that the growth of these tumors is highly dependent on Jag1 [18]. Experimental and clinical evidence shows that Jag1 empowers Notch signaling activity promoting Notch3/Jag1 auto-sustaining loop that supports the survival, proliferation, and invasion of cancer cells in several tumors, such as T-ALL and breast cancer [19, 20]. However, little is known about the role of Jag1 in the onset of CRC. In order to elucidate the role of Jag1 in human CRC, we developed a recombinant protein derived from the extracellular domain of the Notch high affinity mutated form of the ligand Jag1 [21] fused to a red emitting firefly luciferase (Fluc) (**Fig. 7.1**), to understand if Jag1-Fluc binding correlates with Notch expression and Notch signaling activation in CRC progression.

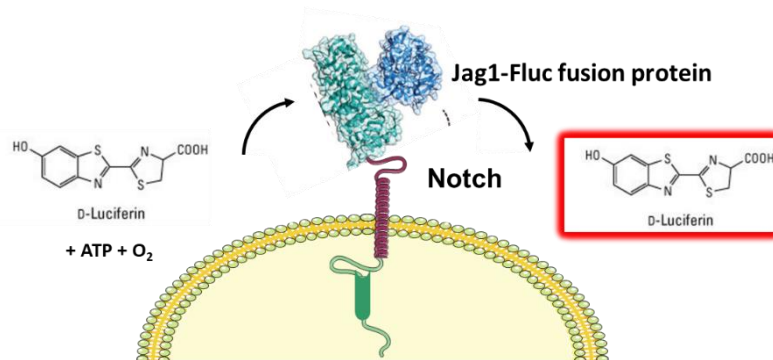


Figure 7.1: Schematic representation of probe mechanism of action.

7.2 Material and Methods

7.2.1 Reagents and kits

Phosphate-buffered saline (PBS) tabs (giving a 137 mM NaCl, 2.7 mM KCl and 10 mM phosphate buffer solution, pH 7.4), LB broth powder (Lennox), Agar powder, dimethylsulfoxide (DMSO), sodium and potassium chloride, tris base, acetic acid, EDTA, trypsin-EDTA, Antibiotic solution 100X (10,000 U/mL penicillin and 10 mg/mL streptomycin) methanol, protease inhibitor cocktail, kanamycin sulfate, ampicillin (sodium salt) isopropyl β -D-1- thiogalactopyranoside (IPTG), β -mercaptoethanol, Tween 20, Bovine Serum Albumin (BSA), H_2O_2 solution and Triton X-100 were purchased from Sigma-Aldrich (St Louis, MO, USA). Dulbecco's Modified Eagle Medium (DMEM), high glucose Non-Essential Amino Acids solution (NEAA), Roswell Park Memorial Institute (RPMI) 1640 medium, Hanks' balanced Salt solution (10X) and Fetal Bovine Serum (FBS) were purchased from Microgem (Naples, Italy). JAG1 ORF Vector (Human) was purchased from ABM (Canada) while the pIDTsmart (Amp) for JAG1_Mut_High_Affinity (320 bp) from IDT (Coralville, Iowa, US). pCMVRed FLuc, Pierce Firefly Luc One-Step glow assay kit as BL substrate, Bac-to-Bac™ HBM TOPO™ Secreted Expression System, MAX Efficiency™ DH10Bac Competent Cells, ExpiFectamine™ Sf Transfection Reagent, One Shot™ TOP10 Chemically Competent E. coli, Phusion Site-Directed Mutagenesis Kit, Maxima Sybr Green QPCR, Pure Link™ HiPure Plasmid Miniprep kit, Ni-NTA Purification System, BacPAK™ qPCR Titration Kit, Zero Blunt® TOPO® PCR Cloning Kit, restriction enzymes, Phusion U Hot Start PCR Master Mix and Pierce BCA Protein Assay Kit were purchased from Thermo Fischer Scientific

(Waltham, MA, USA). PCR extraction kit, and gel Purification Kit were obtained from Qiagen(Hilden, Germany). High glucose Dulbeccos' Modified Eagle Medium (DMEM), were purchased from Gibco/Life Technologies (Grand Island, NY, USA). Laemmli sample buffer, Protein Markers and Mini-Protean TGX (4–20%) gels were obtained from Bio-Rad (Hercules, CA, USA). Mouse-anti-His mAb was purchased from GenScript (Piscataway, NJ, US). Recombinant Human Jagged 1 Fc Chimera Protein was purchased by Biotechne (Minneapolis, MN, USA).

7.2.2 Fusion gene design, transformation, and protein expression

The coding region for the extracellular domain (ECD) of JAG1_WT gene was cloned in pTOPO, and next, a fragment containing S32L, R68G, D72N, T87R mutations (see supplementary materials **Fig. S1** JAG1_Mut_Minigene) that confer a higher binding strength for Notch receptors [21] was inserted in the end terminal part of JAG1_WT, obtaining the resulting plasmid pTopo_JAG1_Mut, according to the manufacturer's instructions.

Then JAG1mut and R-Firefly luciferase (Fluc) coding genes were combined in a single fusion construct which was inserted into the pFast-Bac expression vector to generate pFast-Bac JAG1mut_Fluc (see the map in supplementary **Fig. S2**). Following the insertion of pFast-Bac JAG1mut_Fluc into a Bacmid, the resulting construct was transfected in Sf9 insect cells. The High five insect cells were infected with the recombinant Baculovirus to produce the JAG1mut_Fluc soluble protein (according to the manufacturer's instruction, Bac-to-Bac® TOPO® Cloning Kits Thermo Fisher Scientific, Waltham, MA, USA). Then JAG1mut-Fluc protein was isolated from cell lysates using immobilized metal affinity chromatography (Ni-NTA). Analysis by SDS-PAGE and Western Blot indicated that isolated JAG1mut_Fluc exhibited an approximate size of 150 kDa, in accordance to the predictive size (supplementary materials, **Fig. S3** and **S4**).

7.2.3 Study population

The study was approved by the Local Ethics Committee (14/03/2019) and followed the Declaration of Helsinki and its later amendments. This is an

exploratory, controlled, single-center, *in vitro* human tissue study with three groups of subjects: 10 subjects with hyperplastic polyps, 20 with low- and high-grade adenomatous polyps, and 10 subjects with colon cancer were enrolled in the trial. The study is non-interventional. Subjects will be treated according to clinical practice in accordance with the judgment of the physician. Specifically, the specimens analyzed will be fragments taken from polyps removed by endoscopic polypectomy during the normal course of care or a portion of the removed tissue from surgical resections. 5 ml of blood was also taken from each subject during the normal course of care.

Inclusion criteria:

- Males and females aged between 18 and 75 years belonging to one of the following groups:

Group A: patients with benign hyperplastic polyps at first diagnosis,

Group B: patients with dysplastic adenomatous polyps at first diagnosis or with familial adenomatous polyposis in endoscopic follow-up,

Group C: patients with established colorectal cancer who will have to undergo intestinal resection surgery.

- Subjects for whom colonoscopy or surgical bowel resection is indicated as part of the normal care pathway (groups A and B) or subjects with CRC who must undergo bowel resection surgery (group C)

- Obtaining written, signed and dated informed consent prior to admission to the study.

Exclusion criteria:

- Patients with infectious colitis

- Patients already undergoing surgery/endoscopy for neoplastic disease of the colon and in endoscopic follow-up after surgery

- Patients with contraindications to performing a colonoscopy.

7.2.4 Insect cell culture

Commercially available serum-free insect cell lines *Spodoptera frugiperda* (Sf)-9 and High Five™ (BTI-TN-5BI-4 from *Trichoplusia ni*) were acquired from Thermo Fisher Scientific (Waltham, MA, USA) and maintained in Sf900-II media

with continuous shaking at 120 rpm at 27 °C. For expression culture, High Five™ cells were grown in Grace's Insect Cell Culture Medium unsupplemented (Thermo Fisher Scientific, Waltham, MA, US) and incubated at 27 °C prior to infection.

7.2.5 Human cell culture

Human colorectal adenocarcinoma cells (Caco-2), obtained from the American Type Culture Collection (ATCC), were grown in DMEM high glucose, supplemented with 10% heat-inactivated FBS, 1% Non-Essential Amino Acids solution (NEAA), 2.5 mM L-glutamine and 1% penicillin/streptomycin at 37°C in an atmosphere of 5% CO₂. Michigan cancer foundation-7 (MCF-7) cells, a breast cancer cell line, were kindly gifted by Prof. Natalia Calonghi (Department of Pharmacy and Biotechnology-FABIT, University of Bologna). Cells were maintained in RPMI 1640 containing 10% heat-inactivated FBS and 1% penicillin/streptomycin. Both cell lines were selected because already been reported in studies to investigate the Notch pathway [22-24].

7.2.6 Calibration curve of Jag1-Fluc in a cell-free system

The bioluminescence spectrum of Jag1-Fluc was obtained using Spectramax iD3 setting bandpass filters ranging from 580 to 800 nm, for 1000 ms. The spectrum was collected after the addition of BL substrate cocktail.

Different dilutions of Jag1-Fluc starting from 10 ug/mL (range: 0,25-10 ug/mL) were prepared by diluting the 400 µg/mL stock solution with a working solution made of PBS, FBS 2%, and 100 µg/mL of CaCl₂. 100 µL of each different concentration (working solution for the blank) were dispensed in the wells of a 96-well black microtiter plate, then the reaction was triggered by adding 100 µL of substrate cocktail containing luciferin, Mg²⁺, and ATP, and the resulting BL emission was monitored for 90 min using a luminometric plate reader (Thermo Fisher Scientific). The calibration curve was obtained by plotting the BL signal versus the different concentrations of Jag1-Fluc and fitting the experimental data to a straight line using the method of least squares. The limits of detection (LOD) and quantification (LOQ) of the assay were evaluated as the concentrations of Jag1-Fluc giving BL signals corresponding to those of the blank plus three and ten times its standard deviation, respectively.

7.2.7 Cell-based calibration curve of Jag1-Fluc in fixed and living human colorectal adenocarcinoma cells (Caco-2)

The day before the experiment, Caco-2 (1×10^5 cells well⁻¹) were plated in the wells of a 96-well black microtiter plate for 24 hours at 37 °C with 5% CO₂. The day after the cell medium (DMEM high glucose + 10% FBS, 2.5 mM L-glutamine, and antibiotic–antimycotic solution) was removed, the cells were washed twice with cold PBS, incubated with 100 µL of a blocking solution (PBS, BSA 5% and 100 µg/mL of CaCl₂) for 1h, and fixed with cold EtOH 70%. Then, 100 µL of Jag1-Fluc (range: 5-50 µg/mL) were incubated overnight. The following day, after the protein removal, the cells were washed twice with PBS at room temperature, and subsequently, 100 µL of the substrate solution was added. BL emission was monitored for 90 min using a Luminoskan™ Ascent luminometric plate reader. The dose-response curve was obtained by plotting the BL signal versus Jag1-Fluc concentrations and fitting the experimental data to a straight line using the method of least squares. The same assay was performed also using living cells. One day before the experiment Caco-2 cells (1×10^5 cells well⁻¹) were seeded in a 96-well black microtiter plate. The day after cell medium was removed and cells were washed twice with PBS and incubated with the different concentrations of Jag1-Fluc (range: 5-50 µg/mL) in a solution made of HBSS and BSA 0,1% for 30 minutes. BL emission signal was monitored using a Luminoskan™ Ascent luminometric plate reader. The temperature was maintained at 37 °C during the measurement.

7.2.8 Jag1-Fluc selectivity vs Notch receptors in fixed cells

The day before the experiment, Caco-2 (1×10^5 cells well⁻¹), expressing Notch3 [25], and MCF-7 (5×10^4 cells well⁻¹) cells, expressing all Notch receptors [26], [27], were plated in a 96-well black microtiter plate for 24 hours. The day after the cell medium was removed, the cells were washed twice with cold PBS, incubated with 100 µL of a blocking solution for 1h (PBS, BSA 5%, and 100 µg/mL of CaCl₂), and fixed with cold EtOH 70%. Then cells were treated overnight with serial dilutions of human soluble Jagged 1 chimera (range 0,1-25 µg/mL) able to bind Notch receptors. The day of the experiment 100 µL of Jag1-Fluc (50 µg/mL) were added to each well. After ~8 hours of incubation, the well

supernatant was removed, and the cells were washed twice with PBS at room temperature. BL emission signal was monitored after the substrate addition using a Luminoskan™ Ascent luminometric plate reader.

7.2.9 In Vitro Cell-based Imaging

Imaging experiments were performed using an Olympus IX73 inverted microscope (Olympus Corporation, Tokyo, Japan) equipped with an ultrasensitive EM-CCD camera (ImagEM X2, Hamamatsu Photonics KK, Shizuoka, Japan) controlled by the proprietary software HCImage v.4.2.6.1 and enclosed in a dark box to prevent interference from ambient light. Caco-2 cells (1×10^5 cells well⁻¹) were grown in a 96-well black microtiter plate for 24 hours at 37 °C with 5%CO₂. After 24 hours, cells were fixed with EtOH 70% as described above and incubated overnight with three different concentrations of Jag1-Fluc (400, 200, 50 µg/mL). Before each imaging session, Jag1-Fluc was gently removed, and cells were washed twice with PBS. Images of Caco-2 cells were acquired using a 10X objective with an integration time of 5, 8, and 12 min, at a gain level set to 200, after the addition of 100 µL of substrate cocktail to trigger the BL reaction. All experiments were performed in triplicate and repeated at least three times. Image processing was performed using the freely available Java-based software ImageJ v. 1.52d.

7.2.10 Bioluminescence imaging (BLI) on *ex-vivo* human biopsies

Bioluminescence imaging (BLI) was performed on formalin-fixed, paraffin-embedded colorectal cancer samples from a single patient as a proof-of-concept since a clinical study with a limited number of patients enrolled (10 subjects with CRC, 20 with low or high-grade adenomas and 10 with benign/hyperplastic polyps) is ongoing at the Sant'Orsola-Malpighi University Hospital in Bologna (Italy). Tissue sections were deparaffinized in xylene and rehydrated through graded ethanol. Antigen retrieval was carried out by heating sections in 95°C water for 25 min in the presence of 1X IHC select citrate buffer pH 6.0. Sections were treated with a solution made of 3% H₂O₂ at 4°C for 30 min to inhibit the peroxidases, and then for the blocking step with a solution containing horse serum and Triton 100X (0,1 final in PBS) for 1h at room temperature. Then the

samples were incubated with Jag1-Fluc 50 µg/mL in a humidified chamber overnight at 4°C (negative control: only with PBS). The day of the experiment Jag1-Fluc was removed, and the samples were washed twice with PBS. After substrate addition, BLI images were taken using the IVIS Spectrum (PerkinElmer) with the following acquisition conditions: open for total bioluminescence, exposure time = 1, 10, 20, 30, 40, 50, 60, 120 sec, binning = medium: 8, field of view = 12.6 × 12.6 cm, and f/stop = 1. Analysis of BLI images was performed with Living Image 4.3 software (PerkinElmer).

7.2.11 Data analysis

GraphPad Prism v. 6.05 (GraphPad Software, Inc., La Jolla, CA, USA) was used to plot the experimental data and for the least-squares fitting of calibration, and dose-response curves (for evaluation of IC50 values).

7.3 Results and Discussion

7.3.1 Characterization of Jag1-Fluc light output in a cell-free system

Once confirming the BL emission signal at 610 nm (see emission spectra in **Fig. 7.2A**), the correlation between the BL emission and the concentration of Jag1-FLuc was investigated in a cell-free system to test the performance of the protein and for setting the best experimental conditions.

BL measurements were carried out for 90 min after the addition of the BL substrate cocktail and the integrated BL emission in this time interval was used as the analytical signal.

The same signal integration period was used in cell-based experiments, thus making the calibration curve suitable for the evaluation of the binding of Jag1-Fluc.

The calibration curve showed a good linear correlation between the BL signal and the concentration of the bioluminescent recombinant protein up to 10 µg/mL (**Fig. 7.2B**) with a LOD and LOQ of 0.20 ± 0.03 and 0.50 ± 0.03 µg/mL respectively.

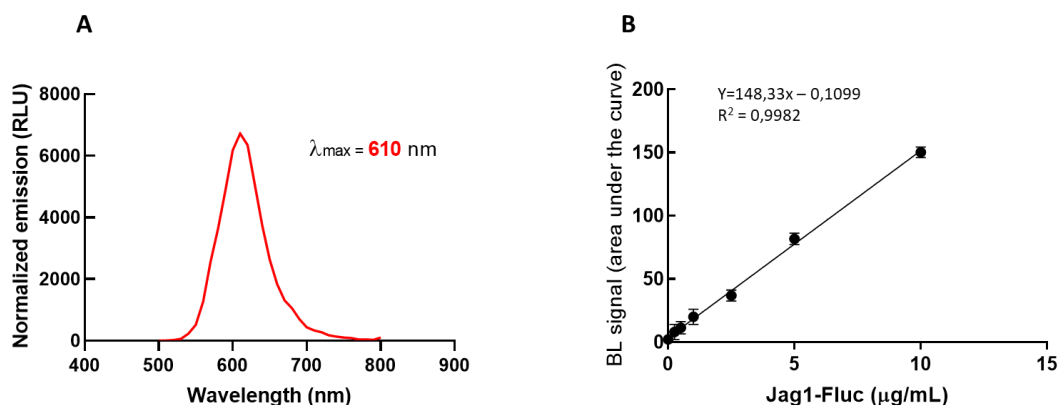


Figure 7.2: (A) Normalized bioluminescence emission spectra of Jag1-Fluc. (B) Calibration curve showing the correlation between BL signal and concentration of the Jag1-Fluc protein in a cell-free model.

On the basis of these results, we were confident that the BL recombinant protein would be able to generate a detectable BL signal also in human cell models.

7.3.2 Evaluation of Jag1-Fluc BL emission in fixed and living human colorectal adenocarcinoma cells (Caco-2)

Once successfully demonstrated the BL emission of Jag1-Fluc in a cell-free system we moved on to a cell model to test its performance. Since we know that human colorectal adenocarcinoma cells (Caco-2) express different Notch receptors and in particular high levels of the isoform Notch 3, [25, 28] these cells were selected for *in vitro* experiments.

BL intensities were measured in Caco-2 cells fixed with EtOH 70% following the addition of the substrate. The BL signal exhibits an increased luminescence in presence of higher concentration of Jag1-Fluc until 50 µg/mL obtaining a LOD and LOQ of 0.8 ± 0.2 µg/mL and 6.0 ± 0.2 µg/mL respectively (see supplementary **fig. S5**). The same experiment was performed on living Caco-2 cells to setup a faster and easier procedure. Moreover, avoiding the fixing step, a clear “picture” of the human living cells is allowed without any possible interferent. Data obtained showed a good correlation between the BL signal and the concentration of Jag1-Fluc (**Fig. 7.3A**) as observed for the fixed cells, obtaining a LOD and LOQ of 0.4 ± 0.2 µg/mL and 3.0 ± 0.2 µg/mL respectively. These results suggest

that the probe could bind to the ECD of Notch receptors expressed on cells surface.

7.3.3 Human soluble Jagged 1 chimera as competitor of Notch receptors in Caco-2 and MCF-7

To be sure that Jag1-Fluc didn't bind to the cells in a non-specific way the probe selectivity was checked using a soluble Jag1-IgG1 Fc chimera as competitor. Characterization of soluble forms of Notch ligands has been reported in several studies [29, 30]. After testing the probe on Caco-2 cells as a model we decided to try it also on MCF-7, a breast cancer cell line that expressed high levels of all Notch receptors [31,32]. Fixed cells were firstly incubated with increased concentrations of the human soluble Jag1 chimera in the range of 0,1-25 µg/mL overnight and then Jag1-Fluc was added to reach a concentration of 50 µg/mL, then the incubation was prolonged for 8 hours. After two PBS washes and the substrate addition, we observed that the BL signal decreased proportionally in the presence of the competitor Jag1 soluble with an IC₅₀ of 0.55 ± 0.06 µg/mL and 0.45 ± 0.04 µg/mL in Caco-2 (**Fig. 7.3B**) and MCF-7 (supplementary **fig. S6**), respectively. These results suggest that Jag1-Fluc can selectively bind to ECD of Notch receptors since in the presence of high concentrations of human soluble Jag1 chimera we had a low BL signal (**Fig. 7.3C**).

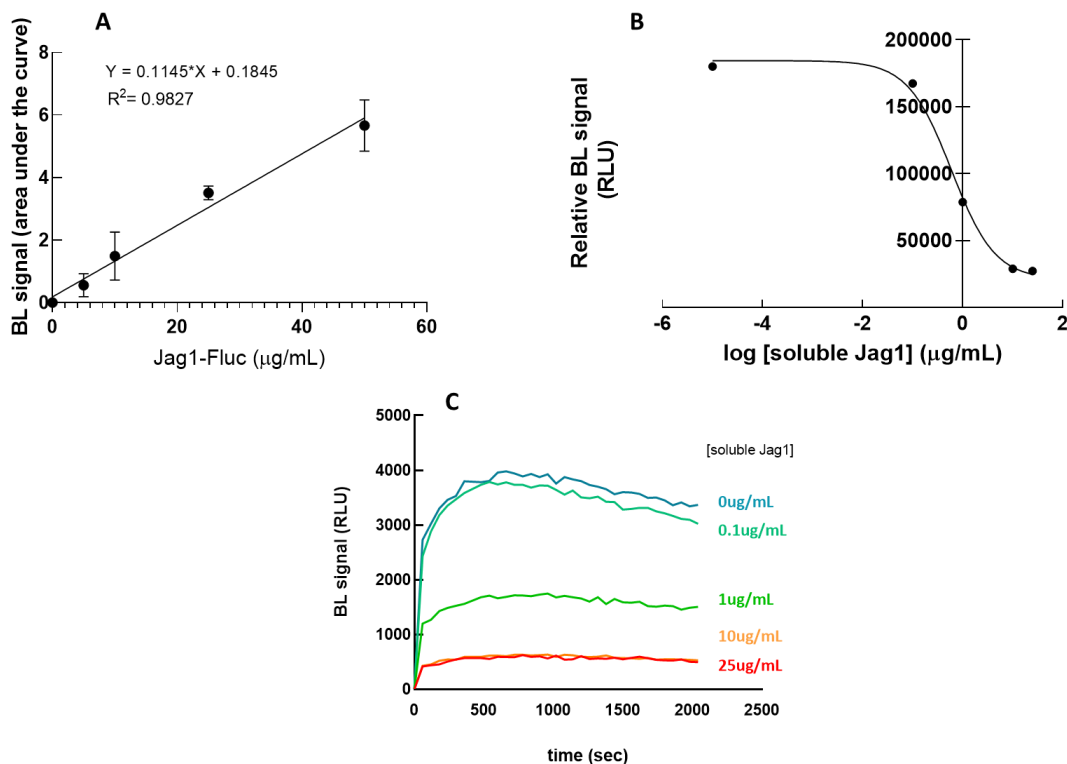


Figure 7.3: (A) Calibration curve showing the correlation between the BL signal and the concentration of Jag1-Fluc in Caco-2 living cells. Each point represents the mean \pm SD of three independent measurements. (B) IC50 graph of fixed Caco-2 cell line (1×10^5 cells well⁻¹) treated with the human soluble Jagged-1 chimera (range 0,1-25 $\mu\text{g}/\text{mL}$) and Jag1-Fluc at fixed concentration (50 $\mu\text{g}/\text{mL}$). (C) Bioluminescence kinetic profiles for fixed Caco-2 cells (1×10^5 cells well⁻¹) obtained in presence of human soluble Jag-1 chimera (range 0,1-25 $\mu\text{g}/\text{mL}$) and Jag1-Fluc at fixed concentration (50 $\mu\text{g}/\text{mL}$).

7.3.4 BL imaging on fixed Caco-2 cells

To fully confirm the ability of Jag1-Fluc to bind the ECD of Notch receptors expressed on cell membranes, BL imaging of fixed Caco-2 cells (1×10^5 cells/well⁻¹) was performed. Cells were grown as a monolayer for 24 hours, fixed with EtOH 70% and incubated overnight with different concentrations of Jag1-Fluc (range 50-400 $\mu\text{g}/\text{mL}$), then were imaged using a 10X objective. Due to the lower BL intensities and blurry signals only 200 and 400 $\mu\text{g}/\text{mL}$ concentration for 12 minutes of acquisition showed appreciable BL signal (**Fig 7.4A-C** and **7.4D-F**).

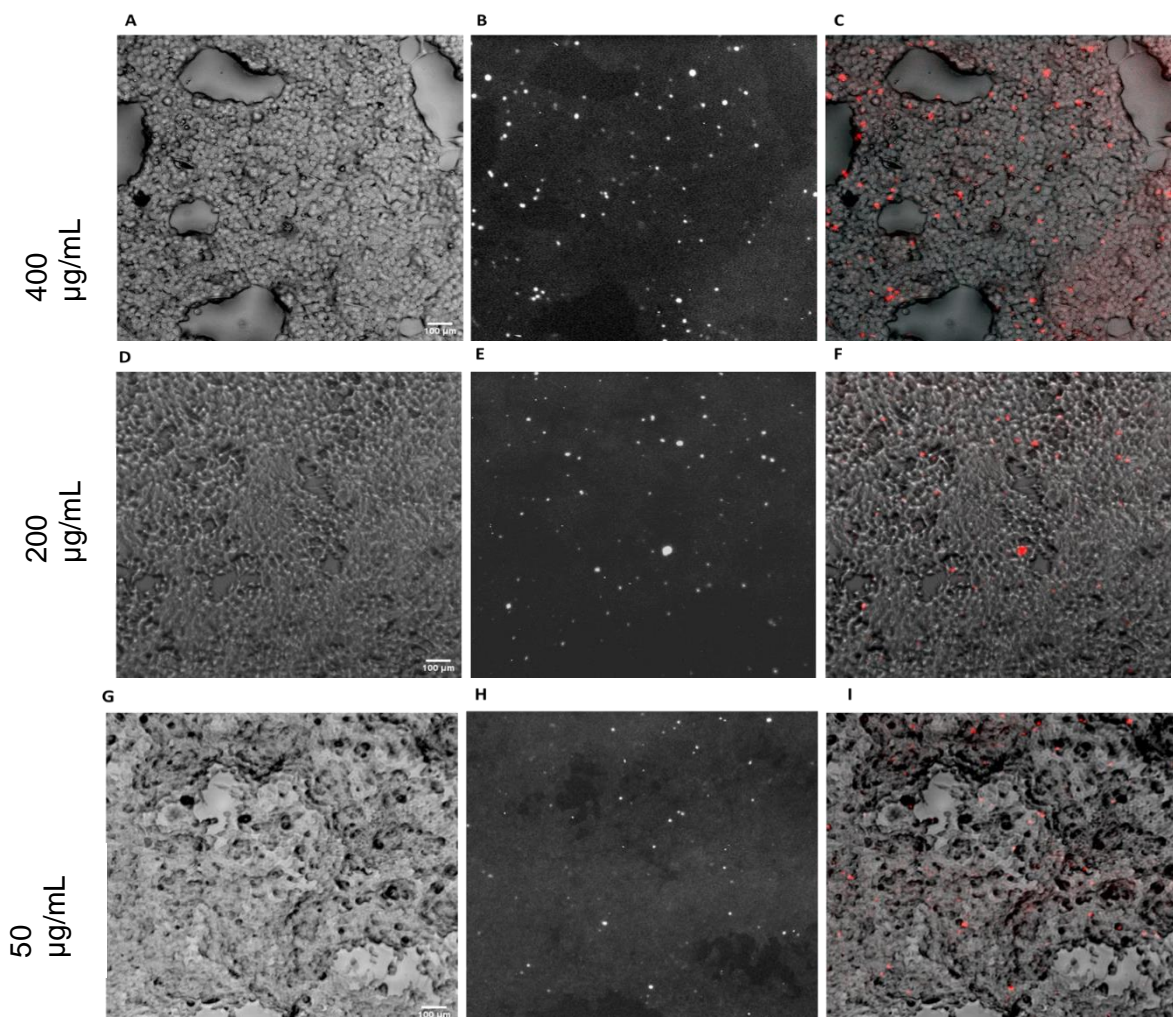


Figure 7.4: *A,D,G) Bright-field, B,E,H) bioluminescence and C,F,I) pseudocolor overlay images of Caco2 cells (10X objective, 12 min acquisition) incubated overnight with Jag1-Fluc (400-200-50 $\mu\text{g}/\text{mL}$).*

The output from BL imaging of Caco-2 cells incubated with Jag1-Fluc (400-200-50 $\mu\text{g}/\text{mL}$) is shown in **figure 3A–I**.

7.3.5 Ex vivo BLI: Jag1-Fluc binding on human tissue

To apply the potential Jag1-Fluc as a diagnostic tool on human tissue, we evaluated its binding to specimens obtained from one patient with colorectal cancer, since we expected an overexpression of the Notch pathway at this stage of the pathology [32,33]. After deparaffinization and rehydration, the biopsies were incubated overnight with Jag1-Fluc at 50 $\mu\text{g}/\text{mL}$. Tissues were imaged in the IVIS imager at different times (1, 10, 20, 30, 40, 50, 60, 120 sec) after the substrate addition. A strong BL signal was detected from the sample after just 1 sec of acquisition while the negative control gave no BL signal (**Fig. 7.5**). Further experiments will be performed on the other biopsies derived from subjects with hyperplastic polyps, adenomas (low and high grade) and CRC, in order to understand how the binding of Jag1 with Notch receptors is associated to and predictive of CRC progression.

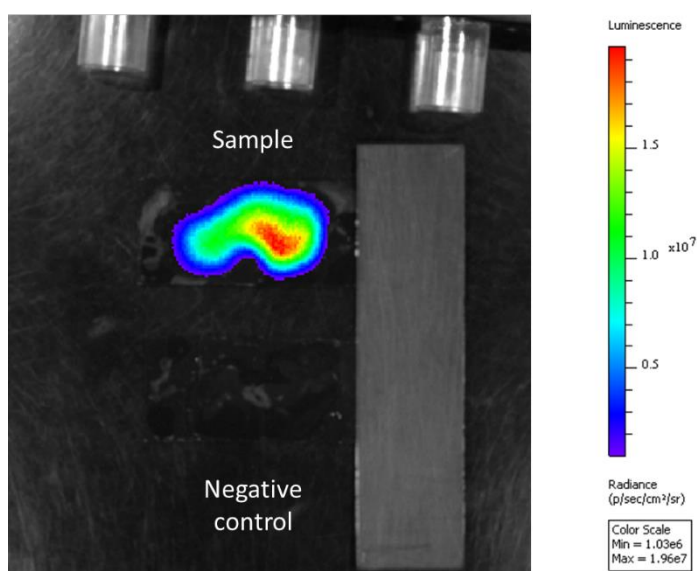


Figure 7.5: *Bioluminescence imaging of human biopsies of a single patient with colorectal cancer in the presence or not (negative control) of Jag1- FLuc 50 $\mu\text{g}/\text{mL}$ at IVIS imager with an exposure time of 1s.*

7.4 Conclusions

Since CRC incidence and mortality rates are expected to grow in the near future, understanding the molecular and cellular mechanisms underlying CRC becomes pivotal for better diagnostics, therapy, and prevention. In this work, we report the development of a new bioluminescent recombinant protein Jag1-Fluc and its characterization for the detection of ECD Notch receptors in human colorectal adenocarcinoma cells (Caco-2). Due to its involvement in both physiological cellular processes as well as in numerous disease states, the opportunity to fully understand the existing roles and interactions between Jag1 and Notch receptors in CRC progression is critically important [24,34]. Thus, we successfully demonstrated the feasibility of using the bioluminescent Jag1-Fluc protein for quantifying and imaging Notch expression of Caco-2 cells. This bioassay is simple to perform and at the same time very sensitive. In addition, thanks to the good results obtained on human tissue sections, Jag1-Fluc will be soon validated *ex vivo* on human biopsies derived from intestinal tumor lesions (dysplastic and benign/hyperplastic polyps, and cancer lesions), to understand how the binding of Jag1 with Notch receptors is representative and predictive for CRC progression. Indeed, Jag1-Fluc could represent an important new tool to improve the early detection and diagnosis of pre-neoplastic and neoplastic lesions and also effective CRC related therapies. In the near future, the integration of liquid biopsy [35] with imaging techniques [36] may prove useful for a better prediction of patient outcomes and for better-tailored treatment.

7.5 References

- [1] Cancer Today-Global Cancer Observatory-IARC., "https://gco.iarc.fr/today/data/factsheets/cancers/10_8_9 -Colorectum-fact-sheet.pdf".
- [2] M. de ROSA *et al.*, "Genetics, diagnosis and management of colorectal cancer (Review)," *Oncol Rep*, vol. 34, no. 3, pp. 1087–1096, Sep. 2015, doi: 10.3892/or.2015.4108.
- [3] R. Fodde, "The APC gene in colorectal cancer," *Eur J Cancer*, vol. 38, no. 7, pp. 867–871, May 2002, doi: 10.1016/S0959-8049(02)00040-0.
- [4] H.-H. Oh and Y.-E. Joo, "Novel biomarkers for the diagnosis and prognosis of colorectal cancer," *Intest Res*, vol. 18, no. 2, pp. 168–183, Apr. 2020, doi: 10.5217/ir.2019.00080.
- [5] S. G. Patel, J. J. Karlitz, T. Yen, C. H. Lieu, and C. R. Boland, "The rising tide of early-onset colorectal cancer: a comprehensive review of epidemiology, clinical features, biology, risk factors, prevention, and early detection," *Lancet Gastroenterol Hepatol*, vol. 7, no. 3, pp. 262–274, Mar. 2022, doi: 10.1016/S2468-1253(21)00426-X.
- [6] M. W. Saif and E. Chu, "Biology of Colorectal Cancer," *The Cancer Journal*, vol. 16, no. 3, pp. 196–201, May 2010, doi: 10.1097/PPO.0b013e3181e076af.
- [7] E. N. Kontomanolis *et al.*, "The Notch Pathway in Breast Cancer Progression," *The Scientific World Journal*, vol. 2018, pp. 1–11, Jul. 2018, doi: 10.1155/2018/2415489.
- [8] A. Tyagi, A. K. Sharma, and C. Damodaran, "A Review on Notch Signaling and Colorectal Cancer," *Cells*, vol. 9, no. 6, p. 1549, Jun. 2020, doi: 10.3390/cells9061549.
- [9] C. K. Jain, S. Bhargava, I. Jain, and S. Varshney, "Targeting Notch Pathway in Cancer Diagnostics and Therapeutics: An Emerging Approach," *Recent Pat Anticancer Drug Discov*, vol. 17, no. 3, pp. 244–252, Aug. 2022, doi: 10.2174/1574892816666210607092350.
- [10] A. Pannuti *et al.*, "Targeting Notch to Target Cancer Stem Cells," *Clinical Cancer Research*, vol. 16, no. 12, pp. 3141–3152, Jun. 2010, doi: 10.1158/1078-0432.CCR-09-2823.

- [11] B. Zhou *et al.*, “Notch signaling pathway: architecture, disease, and therapeutics,” *Signal Transduct Target Ther*, vol. 7, no. 1, p. 95, Mar. 2022, doi: 10.1038/s41392-022-00934-y.
- [12] M. Katoh and M. Katoh, “Notch signaling in gastrointestinal tract (review).,” *Int J Oncol*, vol. 30, no. 1, pp. 247–51, Jan. 2007.
- [13] T. J. Kohut, M. A. Gilbert, and K. M. Loomes, “Alagille Syndrome: A Focused Review on Clinical Features, Genetics, and Treatment.,” *Semin Liver Dis*, vol. 41, no. 4, pp. 525–537, Nov. 2021, doi: 10.1055/s-0041-1730951.
- [14] L. W. Ellisen *et al.*, “TAN-1, the human homolog of the Drosophila Notch gene, is broken by chromosomal translocations in T lymphoblastic neoplasms,” *Cell*, vol. 66, no. 4, pp. 649–661, Aug. 1991, doi: 10.1016/0092-8674(91)90111-B.
- [15] J. C. Aster, W. S. Pear, and S. C. Blacklow, “The Varied Roles of Notch in Cancer,” *Annual Review of Pathology: Mechanisms of Disease*, vol. 12, no. 1, pp. 245–275, Jan. 2017, doi: 10.1146/annurev-pathol-052016-100127.
- [16] K. E. Vinson, D. C. George, A. W. Fender, F. E. Bertrand, and G. Sigounas, “The Notch pathway in colorectal cancer,” *Int J Cancer*, vol. 138, no. 8, pp. 1835–1842, Apr. 2016, doi: 10.1002/ijc.29800.
- [17] G. RALLIS *et al.*, “Association of Notch and Hedgehog Pathway Activation With Prognosis in Early-stage Colorectal Cancer,” *Anticancer Res*, vol. 39, no. 4, pp. 2129–2138, Apr. 2019, doi: 10.21873/anticancerres.13326.
- [18] T. Nakata *et al.*, “Indispensable role of Notch ligand-dependent signaling in the proliferation and stem cell niche maintenance of APC-deficient intestinal tumors,” *Biochem Biophys Res Commun*, vol. 482, no. 4, pp. 1296–1303, Jan. 2017, doi: 10.1016/j.bbrc.2016.12.031.
- [19] M. Pelullo *et al.*, “Notch3/Jagged1 Circuitry Reinforces Notch Signaling and Sustains T-ALL,” *Neoplasia*, vol. 16, no. 12, pp. 1007–1017, Dec. 2014, doi: 10.1016/j.neo.2014.10.004.
- [20] T.-M. STRATI *et al.*, “Prognostic Subcellular Notch2, Notch3 and Jagged1 Localization Patterns in Early Triple-negative Breast Cancer,” *Anticancer Res*, vol. 37, no. 5, p. 2334, May 2017, doi: 10.21873/anticancerres.11570.
- [21] V. C. Luca *et al.*, “Notch-Jagged complex structure implicates a catch bond in tuning ligand sensitivity,” *Science (1979)*, vol. 355, no. 6331, pp. 1320–1324, Mar. 2017, doi: 10.1126/science.aaf9739.

- [22] S. Dahan, K. M. Rabinowitz, A. P. Martin, M. C. Berin, J. C. Unkeless, and L. Mayer, "Notch-1 Signaling Regulates Intestinal Epithelial Barrier Function, Through Interaction With CD4+ T Cells, in Mice and Humans," *Gastroenterology*, vol. 140, no. 2, pp. 550–559, Feb. 2011, doi: 10.1053/j.gastro.2010.10.057.
- [23] C. M. Moon *et al.*, "Nonsteroidal anti-inflammatory drugs suppress cancer stem cells *via* inhibiting PTGS2 (cyclooxygenase 2) and NOTCH/HES1 and activating PPARG in colorectal cancer," *Int J Cancer*, vol. 134, no. 3, pp. 519–529, Feb. 2014, doi: 10.1002/ijc.28381.
- [24] A. Louvi and S. Artavanis-Tsakonas, "Notch and disease: a growing field.," *Semin Cell Dev Biol*, vol. 23, no. 4, pp. 473–80, Jun. 2012, doi: 10.1016/j.semcdb.2012.02.005.
- [25] Human Protein Atlas, "https://www.proteinatlas.org/ENSG00000074181-NOTCH3/cell+line#colorectal_cancer."
- [26] J. Yun *et al.*, "p53 Modulates Notch Signaling in MCF-7 Breast Cancer Cells by Associating With the Notch Transcriptional Complex Via MAML1," *J Cell Physiol*, vol. 230, no. 12, pp. 3115–3127, Dec. 2015, doi: 10.1002/jcp.25052.
- [27] A. G. Clementz, A. Rogowski, K. Pandya, L. Miele, and C. Osipo, "NOTCH-1 and NOTCH-4 are novel gene targets of PEA3 in breast cancer: novel therapeutic implications," *Breast Cancer Research*, vol. 13, no. 3, p. R63, Jun. 2011, doi: 10.1186/bcr2900.
- [28] G. Lan *et al.*, "Notch pathway is involved in the suppression of colorectal cancer by embryonic stem cell microenvironment," *Onco Targets Ther*, vol. Volume 12, pp. 2869–2878, Apr. 2019, doi: 10.2147/OTT.S199046.
- [29] E. E. Tchekneva *et al.*, "Determinant roles of dendritic cell-expressed Notch Delta-like and Jagged ligands on anti-tumor T-cell immunity," *J Immunother Cancer*, vol. 7, no. 1, p. 124, Dec. 2019, doi: 10.1186/s40425-019-0592-2.
- [30] M. Masuya *et al.*, "The Soluble Notch Ligand, Jagged-1, Inhibits Proliferation of CD34+ Macrophage Progenitors," *Int J Hematol*, vol. 75, no. 3, pp. 269–276, Apr. 2002, doi: 10.1007/BF02982040.
- [31] Q. T. Bui *et al.*, "Essential role of Notch4/STAT3 signaling in epithelial–mesenchymal transition of tamoxifen-resistant human breast cancer," *Cancer Lett*, vol. 390, pp. 115–125, Apr. 2017, doi: 10.1016/j.canlet.2017.01.014.
- [32] L. Zhou *et al.*, "NOTCH4 maintains quiescent mesenchymal-like breast

cancer stem cells via transcriptionally activating SLUG and GAS1 in triple-negative breast cancer,” *Theranostics*, vol. 10, no. 5, pp. 2405–2421, 2020, doi: 10.7150/thno.38875.

- [33] R. Jackstadt *et al.*, “Epithelial NOTCH Signaling Rewires the Tumor Microenvironment of Colorectal Cancer to Drive Poor-Prognosis Subtypes and Metastasis.,” *Cancer Cell*, vol. 36, no. 3, pp. 319-336.e7, Sep. 2019, doi: 10.1016/j.ccell.2019.08.003.
- [34] I. Espinoza and L. Miele, “Notch inhibitors for cancer treatment,” *Pharmacol Ther*, vol. 139, no. 2, pp. 95–110, Aug. 2013, doi: 10.1016/j.pharmthera.2013.02.003.
- [35] M. Chen and H. Zhao, “Next-generation sequencing in liquid biopsy: cancer screening and early detection.,” *Hum Genomics*, vol. 13, no. 1, p. 34, Aug. 2019, doi: 10.1186/s40246-019-0220-8.
- [36] F. T. Kurz and H.-P. Schlemmer, “Imaging in translational cancer research,” *Cancer Biol Med*, vol. 19, no. 11, pp. 1565–1585, Dec. 2022, doi: 10.20892/j.issn.2095-3941.2022.0677.

7.6 Supplementary materials

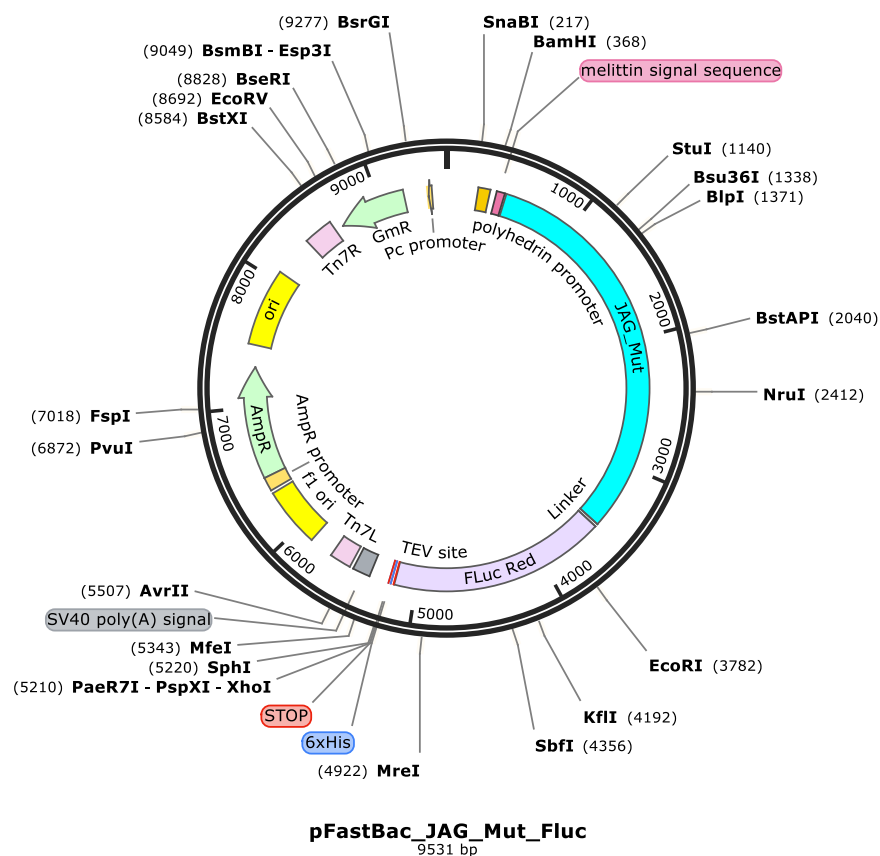
Supplementary Figure S1

Minigene sequence of JAG1_Mut_High_Affinity (ECD domain), 320 bp

```

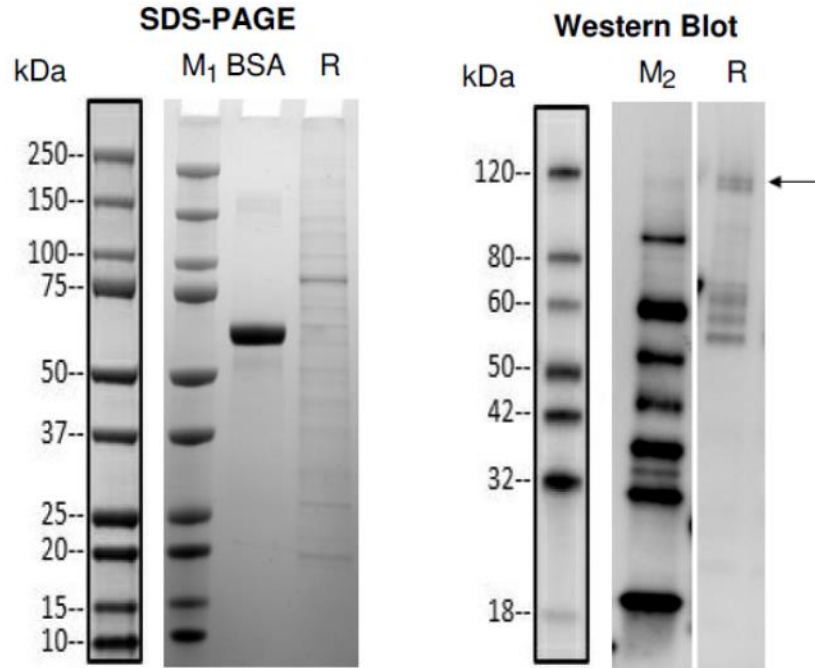
GTCTAGAGGATCCGGGGCCCTGGGTCAGTTCGAGTTGGAGATCCTGTCC
ATGCAGAACGTGAACGGGGAGCTGCAGAACGGGAAGTCTGCGGCGGC
GCCCGGAACCCGGGAGACCGCAAGTGCACCGGTGACGAGTGTAAACAT
ACTTCAAAGTGTGCCTCAAGGAGTATCAGTCCCGCGTCCGTGCCGGGGG
GCCCTGCAGCTTCGGCTCAGGGTCCACGCCTGTCATCGGGGGCAACACC
TTCAACCTCAAGGCCAGCCGCGGCAACGA
    
```

Supplementary Figure S2



Supplementary Figure S3

SDS-PAGE & Western blot Analysis:



Lane M₁: Protein Marker, Bio-rad, Cat. No. 1610374S, refer to annotated key on the left for size
 Lane M₂: Protein Marker, GenScript, Cat. No. M00521, refer to annotated key on the left for size
 BSA: 2.00 µg
 R: Reducing condition
 Primary antibody: Mouse-anti-His mAb (GenScript, Cat.No. A00186)

Supplementary Figure S4

Number of amino acids: 1609 Molecular weight: 175897.63 Theoretical pi: 5.59

MKFLVNVALVFMVYISYIYADRSALALGQFELEILSMQNVNDELQNGNCCGGARNPGRKCTGDECNTRYFKVCLKEYQSRVRAGGPCSFG
 SGSTPVIGGNTFNLKASRGNDRNRIVLPSFAWPRSYYLLVEAWDSSNDTVQPDSIIKASHSGMINPSRQWQTLKQNTGVAHFEYRIRVTC
 DDYYYGFGCNKFCRPRDDFFGHYACDQNGNKTCEMGWGMPECNRAICRQGCSPKHGSKCLPGDCRCQYGWQGLYCDKCIHPGCVH
 GICNEPWQCLCETNWGGQLCDKDLNYCGTHQPCLNNGGTCSENTGPKDYQCSCPEGYSGPNCEIAEHACLSDPCHNRGSKETSLSGFECE
 CSPGWTGPTCSTNIDDCSPNNCSHGTCQDLVNGFKVCPPQWTGKTCQLDANECEAKPCVNAKSKNLIASYYCDCLPGWGMQNCDI
 NINDCLGQCQNDASCRDLVNGYRNICPPGYAGDHCERDIDECASNPLNNGGHCQNEINRFQCLCPTGFSGNLQCLDIDYCEPNPCQNGAQ
 CYNRASDYFCKCPEDYEGKNCSHLKDHCRTTPCEVIDSCTVAMASNDTPEGVRYISSNVCGPHGKCKSQSGGKFTCDCNKGFTGTTCHE
 NINDCESNPCRNGGTCIDGVNSYKICSDGWEGAYCETNINDCSQNPCHNGGTCRDLVNDYCDCKNGWKGTCHSRDSQCDEATCNN
 GGTCYDEGDAFKCMCPGGWEGTTCNIARNSSCLPNPCHNGGTCVNVGESFTCVCKEGWEGPICAQNTNDCSPHPCYNSTGTCVDGDNW
 YRCEAPGFAGPDCRININEQSSPCAFGATCVDEINGYRCVCPGHSAGKQCEVSGRPCITMGSVIPDGAKWDDDCNTCQCLNGRIACS
 KVVWCGPRPCLLHKHGHSECPGQSCIPILDDQCFVHPCTGVGECRSSSLQPVKTKCTSDSYQDNCANITFTFNKEMMSPGLTTEHICSELR
 NLNILKNVSAEYSIYIACEPSPSANNEIHVAISAEDIRDDGNPIKEITDKIIDLVSKRDGSLAAGAMENMENDENIVVGPKPFYPIEESAGTQLR
 KYMERYAKLGAIAFTNAVTGVDYSYAEYLEKSCCLGKALQNYGLVVDGRIALCSENCEFFIPVIAGLFIGVGVAPTNEIYTLRELVHSLGISKP
 TIVFSSKKGLDKVITVQKTVTTIKTIVILDSKVDIRGYOCLDTFIKRNTPPGFQASSFKTVEVDRKEQVALIMNSSGSTGLPKGVQLTHEENTVT
 RFSHARDPIYGNQVSPGTAULTVVPFHGHGFMFTTLGYLICGFRVVMLTKFDEETFLKTLQDYKCTYVILVPTLFAILNKSELLNKYDLSNLV
 EIASGGAPLSKEVGEAVARRFNLPGVRQGYGLTETTSIIITPEGDDKPGASGKVVPLFKAKVIDLDTKSLGPNRRRGEVCKVGPMLMKGYV
 NNPEATKELIDEEGWLHTGDIGYYDEEKHFFIVDRLLKSLIKYKGYQVPPAELESVLLQHPISFDAGVAGVDPVAGELPGAVVVLESKNMTE
 KEVMDYVASQVSNKRLRGGVRFVDEVPKGLTGKIDGRAIREILKPKVAKMKGENLYFQG**HHHHHH**

Supplementary Figure S5

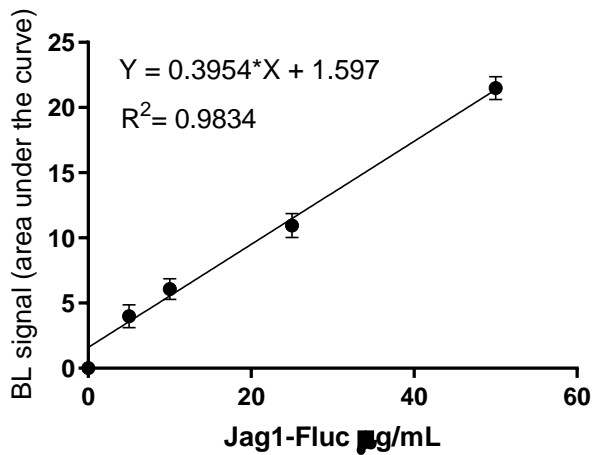


Figure S5: Calibration curve of Jag1-FLuc (range 5–50 $\mu\text{g/ml}$) obtained by analyzing BL signals after 90 min upon substrate addition in fixed Caco2 cells (1×10^5 cells well⁻¹).

Supplementary Figure S6

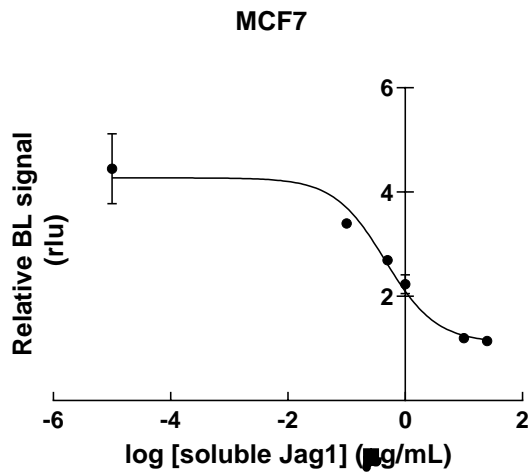


Figure S6: IC₅₀ graph of fixed MCF-7 cell line (1×10^5 cells well⁻¹) treated with the human soluble Jag1 chimera (range 0, 1–25 $\mu\text{g/mL}$) and Jag1-Fluc at fixed concentration (50 $\mu\text{g/mL}$).